

# Multi-modal, mobile microscopy for visualization of biological agents

Sara Kheireddine

Bioengineering Department

McGill University, Montreal

December 2020

A thesis submitted to McGill University in partial fulfillment of the  
requirements of the degree of Doctor of Philosophy in Biological and  
Biomedical Engineering

© Sara Kheireddine 2020

# Abstract

Biological and biomedical research is often contingent upon microscopy techniques for observation and studying of biological features and processes, and subsequent analysis. For many applications, it is necessary that the selected imaging system provide high spatial resolution and large field-of-view, in order to be able to visualize individual biological structures or agents within the sample, while capturing an area large enough, where meaningful analysis, such as particle tracking, could be performed within a single frame. Various lens-based and lens-free imaging platforms, each with their own sets of advantages and disadvantages, offer different imaging modalities suitable for different specimens and applications, but they all suffer from a main limitation: the trade-off between spatial resolution and field-of-view. This competition cannot be eliminated but could be optimized, based on the chosen imaging system specifications. This work addresses the restrictive trade-off, and introduces a mobile phone-based illumination-imaging platform that maximizes the attainable field-of-view at high resolution, and expands the use of phone screen illumination to a lens-free platform.

The thesis transitions from a broad introduction to microscopy in the biological and biomedical fields into a general protocol for identification of imaging system requirements for a targeted application, modelled after a specific example for imaging of a biocomputational microfluidic device that utilizes microorganisms as exploratory problem-solving agents. The following chapters introduce the aforementioned dual-phone system, which uses a phone camera with an external lens for imaging, to achieve a spatial resolution of at least  $2\mu\text{m}$ , and a large field-of-view of  $3.6 \times 2.7\text{mm}$ . For illumination, it uses the screen of another phone to project multi-modal illumination patterns, including but not limited to bright-field, dark-field, Rheinberg illumination, point illumination, fluorescence, and differential phase contrast. Put together, this illumination-imaging system forms a novel, inexpensive, compact, portable, and versatile microscope for use in low-resource environments. It could be used in research, medical, educational, and environmental settings for both qualitative and quantitative imaging of cells, microorganisms, and other micron-sized objects. The adaptability of phone screen illumination allows it to be further integrated into lens-free imaging platforms, as well as conventional microscopes.

# Résumé

La recherche biologique et biomédicale est souvent tributaire des techniques de microscopie pour l'observation et l'étude des caractéristiques et des processus biologiques, et l'analyse subséquente. Pour de nombreuses applications, il est nécessaire que le système d'imagerie choisi offre une résolution spatiale élevée et un champ de vision étendu, afin de pouvoir visualiser des structures biologiques ou des agents individuels à l'intérieur de l'échantillon, tout en capturant une zone suffisamment grande pour permettre une analyse significative, comme le suivi des particules, à l'intérieur d'une seule image. Différentes plates-formes d'imagerie avec ou sans objectif, chacune avec ses propres avantages et inconvénients, offrent différentes modalités d'imagerie adaptées à différents spécimens et applications, mais elles souffrent toutes d'une limitation majeure: le compromis entre la résolution spatiale et le champ de vision. Cette concurrence ne peut être éliminée, mais elle peut être optimisée en fonction des spécifications du système d'imagerie choisi. Ces travaux abordent le compromis restrictif et introduisent une plateforme d'illumination-imagerie basée sur un téléphone mobile qui maximise le champ de vision atteignable à haute résolution et étend l'utilisation de l'éclairage d'écran de téléphone à une plateforme sans objectif.

La thèse passe d'une introduction générale à la microscopie dans les domaines biologique et biomédical à un protocole général pour l'identification des besoins du système d'imagerie pour une application ciblée, modélisé d'après un exemple spécifique pour l'imagerie d'un dispositif microfluidique biocomputationnel qui utilise des microorganismes comme agents exploratoires de résolution de problèmes. Les chapitres qui suivent présentent le système dual-phonique susmentionné, qui utilise une caméra téléphonique avec un objectif externe pour l'imagerie, pour obtenir une résolution spatiale d'au moins  $2\ \mu\text{m}$  et un champ de vision de  $3.6 \times 2.7\ \text{mm}$ . Pour l'éclairage, il utilise l'écran d'un autre téléphone pour projeter des motifs d'éclairage multimodal, y compris, sans s'y limiter, champ clair, champ sombre, éclairage Rheinberg, éclairage ponctuelle, fluorescence et contraste de phase différentiel. Ensemble, ce système d'illumination-imagerie forme un microscope novateur, peu coûteux, compact, portable et polyvalent pour les environnements à faibles ressources. Il pourrait être utilisé dans des contextes de recherche, de médecine, d'éducation et d'environnement

pour l'imagerie qualitative et quantitative de cellules, de microorganismes et d'autres objets de la taille du micron. L'adaptabilité de l'éclairage d'écran de téléphone permet de l'intégrer davantage aux plates-formes d'imagerie sans objectif, ainsi qu'aux microscopes conventionnels.

# Acknowledgements

I would like to formally thank my supervisors, **Sebastian Wachsmann-Hogiu** and **Dan V. Nicolau**, for providing me with this great opportunity to learn, grow, and prove to them and to myself how fulfilling the fruit of perseverance and hard work can be. When days were rough, you helped guide me back onto the right path and regain my discipline. For that, and for your invaluable mentorship, I thank you. Additionally, I would also like to thank my co-supervisor, **Sylvain Martel**, and my Ph.D. committee members for their precious guidance on my work and future steps. Lastly, I would like to express my gratitude towards the Faculty of Engineering for awarding me the McGill Engineering Doctoral Award (MEDA), which helped fund my stipend for the duration of my studies.

I would like to thank my mom and dad, **Nada** and **Nadim**, for their moral support from overseas, my uncle and his wife, **Fadi** and **Sanaa**, for all the love and care they have shown me during my time in Montreal, and my friends, both local and abroad. Having you in my life provided me with a warm cushion to fall back on in times of hardship. More specifically, I would like to thank **Ayca**, **Dilek**, and more recently **Atagün** for being my go-to group of cinema buddies. Your company during our almost-weekly movie nights and afterwards has helped me decompress many a time. Of course, there are multiple people whose friendship I am grateful for, but I will be unable to name all of you; if you are reading this, you know who you are!

At the start of my Ph.D. journey, there were no older students in my group to learn from, look up to, or share the burden with. Thus, I decided to be that supportive, senior student for those who joined after me, and let me tell you, it was great! I helped them adjust and feel like there is someone they could rely on when things got tough, and it was definitely a two-way street. Looking back, I could not imagine my daily Ph.D. life without them! To **Mona** and **Juanjuan**, I sincerely thank you for sharing my joys and sorrows, for enjoying infinite amounts of coffee and tea with me, and more importantly, for being there through it all. I owe you ladies a lot. Fast-forward a year and a half, **Mira** joined our lab and brought much joy along with her, with her beautiful smile and personality. I am tremendously happy to have met all of you and gotten to know your lovely selves. Moreover,

as a teaching assistant, I also found inspiration in my undergraduate students, and I hope to have likewise motivated them to find value and fulfilment through the pursuit of science, and helping influence our world for the better.

Of course, there were also other people behind the scenes who helped me on numerous occasions or simply made life in the lab immensely better. To **Ayyappa**, thank you for bringing much-needed order, stability, and experience to the lab, and for our many many talks over lunch! Your presence helped transform our workspace for the better. To **Haruka**, **Abdulla**, and **Newsha**, thank you for providing me with cells for my experiments and tailoring them towards my seemingly strange experimental setups, and for the invaluable advice when I needed it. To the lab ladies: **Mahsa**, **Linda**, **Jackie** and the rest, thank you for many outings, Secret Santas, and wonderful brunches. Cheers to you, fellow ladies-in-science! I may not have mentioned all the names I have in mind, but my feelings are all the same. Some of you have left to pursue better things, and some of you only joined us right before I moved, but you all left a positive impact on me in your wake. I would also like to thank **Loïc** for the fun optical trapping experiments we did together. Lastly, I would also like to express my appreciation towards our lab manager, **Xavier**, for all his help and support. All of you were there for me in more ways than you could ever know!

During the later chapter of my Ph.D., I was quite lucky to receive a priceless opportunity to gain work experience in the industry as part of the Marie Skłodowska-Curie Actions fellowship program, as an Early Stage Researcher (ESR) at LaVision BioTec GmbH in Bielefeld, Germany. I am the confident, knowledgeable person I am today because of these people, and others, who aided me in navigating this challenging period of balancing company work, Ph.D. work, and social and personal life, through encouragement and pushing me out of my comfort zone, when necessary. For this, I would like to thank **Ingrid** and **Alexander** for hosting me when I first came to Bielefeld and treating me like a daughter, **Judith** for bearing with me through all our flights, layovers, meetings, conferences, etc. and always having a smile on her face and supporting me like a mother as well, **Martin Schütte** and **Martin Ruoff** for their guidance, mentorship, and project accommodations, **Ewa** for always going the extra mile for me, **Simon** for his unrelenting willingness to always lend a hand, and many many others at our lovely company. Finally, I would also like to send a shout-out to all the other ESRs in the program: you guys make all this worth it; I have made thirteen new lifelong friends! I am eternally grateful to **Prof. Thomas Huser**, at Bielefeld University, who recruited me as the final ESR for this project. I hope I prove myself worthy of this choice!

I would also like to extend my thanks to some of my friends by name: to **Ramsey**, you have proven to me over and over that he will always have my back, including but not limited

to endless Chicago-Montreal/Europe trips; to **John**, for always being a ray of sunshine and innocence in my life; to **Rafah**, we ultimately bonded after my latest move to Germany, but I believe this friendship transcends time and space - you mean to me more than you will ever know; to **Farhat**, words fail to explain how much I value you, your empathy, and your advice - I have so much love and respect for you; to **Hiba**, no matter how far away we are, I know I can always come to you for support and sympathy, without any judgement; to **Ola**, we may not talk often, but I just wanted to let you that I believe you have such a beautiful soul.

To **Lama**: we might as well be twins at this point, had it not been for our massive age difference. Thank you for being the constant rock in my life. I hope I can be the great sister you are to me, my gorgeous cheerleader, inside and out! And lest I forget, to my brother, **Hani**, for his cute hugs and our frustrating, but rewarding conversations. May you continue to grow and learn, and I am blessed to watch you blossom into an honourable man.

To **Ribal**, my partner through thick and thin, I can guarantee that I could not have done this without you. Thank you for your immeasurable and unwavering support. I love you! The ability to come home to your warm self every day is one of life's greatest pleasures. You help me become a better person. Also, to my handsome grey cat, **Gandalf**, who brings me joy every day through his warm existence. He is indeed a dapper feline gent (see below).

Last but not least, I leave you with one of my favourite quotes: "*All we have to decide is what to do with the time that is given to us.*" - **Gandalf the Grey**. P.S. For context, watch **Lord of the Rings**!

# Contribution to original knowledge

In chapters 2 and 3, I will be using text and figures that have been taken directly and in full from manuscripts where I am the first author. During the course of my Ph.D., I also made research contributions to two manuscripts as a co-author, and I partially integrated some of this work into the introduction and discussion chapters of this dissertation. As such, my contribution to original knowledge in terms of peer-reviewed publications is stated below:

- **First author**

1. S. Kheireddine, A. S. Perumal, Z. J. Smith, D. V. Nicolau, and S. Wachsmann-Hogiu, “**Dual-phone illumination-imaging system for high resolution and large field of view multi-modal microscopy,**” *Lab on a Chip*, vol. 19, no. 5, pp. 825–836, 2019.

This paper introduces a practical mobile phone-based illumination-imaging platform that allows for the multi-modal imaging of microorganisms, cells, and microfluidic channels. It uses the camera of one phone for imaging at high spatial resolution and large field-of-view, and the screen of another to generate illumination modalities, including bright-field, dark-field, Rheinberg illumination, point illumination, and fluorescence microscopy.

2. S. Kheireddine, Z. J. Smith, D. V. Nicolau, and S. Wachsmann-Hogiu, “**Simple adaptive mobile phone screen illumination for dual phone differential phase contrast (DPDPC) microscopy,**” *Biomedical Optics Express*, vol. 10, no. 9, p. 4369, 2019.

This paper extends the capabilities of the dual-phone illumination-imaging system described above to include differential phase contrast imaging. This is achieved via screen illumination of the sample with complementary semicircular patterns,

where the images are mathematically combined using a normalized difference to attain phase contrast images.

- **Co-author**

1. F. C. Van Delft, G. Ipolitti, D. V. Nicolau Jr, A. Sudalaiyadum Perumal, O. Kašpar, S. Kheireddine, S. Wachsmann-Hogiu, and D. V. Nicolau, “**Something has to give: scaling combinatorial computing by biological agents exploring physical networks encoding NP-complete problems,**” *Interface Focus*, vol. 8, no. 6, p. 20180034, 2018.

In this paper, we put together information regarding the spatial resolution and field-of-view capabilities of different lens-based and lens-free imaging systems, and delineated the biocomputational microfluidic device sizes that can be imaged using each technique, depending on the size of the biological agent used. This approach could similarly be used to identify appropriate imaging platforms for other applications.

2. M. Imanbekova, A. Sudalaiyadum Perumal, S. Kheireddine, D. V. Nicolau, and S. Wachsmann-Hogiu, “**Lensless, reflection-based dark-field microscopy (RDFM) on a CMOS chip,**” *Biomedical Optics Express*, vol. 11, no. 9, p. 4942-4959, 2020.

This paper introduces a technique for direct, on-chip dark-field microscopy via reflection-based oblique illumination on a lens-free imaging platform. In the manuscript, the system uses a single LED as a light source, but I replace the LED setup with phone screen ring illumination to further simplify this modality.

# Contribution of authors

- **Dual-phone illumination-imaging system for high resolution and large field of view multi-modal microscopy**

S.K. performed experiments, image and data analysis, and prepared the figures and the manuscript. A.S.P. helped with some preliminary imaging as well as fluorescence microscopy experiments. Z.J.S. contributed to corrections and additions to the manuscript. D.V.N. coordinated the project. S.W.-H. conceived the project idea, aided in experimental planning, and supervised and coordinated the project. All authors contributed to work planning, to data interpretation, to writing the manuscript and gave final approval for publication.

- **Simple adaptive mobile phone screen illumination for dual phone differential phase contrast (DPDPC) microscopy**

S.K. performed experiments, image and data analysis, and prepared the figures and the manuscript. Z.J.S. contributed fig. 3.6 as well as corrections and additions to the manuscript. D.V.N. helped coordinate the project. S.W.-H. conceived the project idea, aided in experimental planning, and supervised and coordinated the project. All authors contributed to work planning, to data interpretation, to writing the manuscript and gave final approval for publication.

- **Something has to give: scaling combinatorial computing by biological agents exploring physical networks encoding NP-complete problems**

F.C.M.J.M.v.D. conceived the run mode scaling models, the read-out nomograms and Tag & Trace. G.I. programmed and carried out numerical scaling simulations. D.V.N. Jr conceived the SSP bio-computing method from mathematical principles. A.S.P. collected data concerning bacterial motility and energy consumption. O.K. modelled parallel networks and created three-dimensional drawings. S.K. modelled stitching methods for optical microscopy readout. S.W.-H. collected data concerning microscopy methods, field-of-view and resolution. D.V.N. calculated energy consumption, initiated and coordinated the project. All

authors contributed to work planning, to data interpretation, to writing the manuscript and gave final approval for publication.

- **Lensless, reflection-based dark-field microscopy (RDFM) on a CMOS chip**

M.I. and A.S.P. performed experiments, image and data analysis, and prepared the figures and the manuscript. S.K. performed preliminary experiments with the CMOS-based lens-free microscopy setup, in addition to experiments with combining direct CMOS imaging with mobile phone screen illumination (not included in the manuscript), wrote part of the manuscript introduction, and contributed to corrections and additions to the manuscript. D.V.N. helped coordinate the project. S.W.-H. conceived the project idea, aided in experimental planning, and supervised and coordinated the project. All authors contributed to work planning, to data interpretation, to writing the manuscript and gave final approval for publication.

# Contents

|          |   |           |
|----------|---|-----------|
| <b>1</b> | <b>An introduction to lens-based and lens-free microscopy techniques for visualization of biological agents</b>                   | <b>1</b>  |
| 1.1      | Background . . . . .  | 1         |
| 1.1.1    | Microscopy in biology . . . . .   | 2         |
| 1.1.2    | Relevant optical parameters . . . . .   | 4         |
| 1.1.2.1  | Spatial resolution . . . . .  | 4         |
| 1.1.2.2  | Field-of-view . . . . .   | 7         |
| 1.1.2.3  | Other parameters . . . . .  | 8         |
| 1.1.2.4  | Optical aberrations and corrections . . . . .   | 9         |
| 1.1.3    | Lens-based microscopy approaches . . . . .  | 10        |
| 1.1.4    | Lens-free microscopy approaches . . . . .   | 10        |
| 1.1.5    | Image processing and analysis . . . . .   | 12        |
| 1.2      | Rationale . . . . .   | 13        |
| 1.3      | Identification of imaging system requirements . . . . .   | 16        |
| 1.3.1    | Introduction . . . . .  | 16        |
| 1.3.2    | Biological agent, biocomputational device, and optical technology size and parameter considerations . . . . .                     | 17        |
| 1.3.3    | Image stitching parameter considerations . . . . .  | 19        |
| 1.3.4    | Mathematical modelling of SSP biocomputational device dimensions based on biological agent size and problem cardinality . . . . . | 22        |
| 1.3.5    | Conclusion . . . . .  | 26        |
|          | References . . . . .  | 28        |
| <b>2</b> | <b>Dual-phone illumination-imaging system for high resolution and large field of view multi-modal microscopy</b>                  | <b>33</b> |
| 2.1      | Preface . . . . .   | 33        |
| 2.2      | Manuscript details . . . . .  | 34        |
| 2.3      | Authors and affiliations . . . . .  | 34        |

|       |   |    |
|-------|---|----|
| 2.4   | Abstract . . . . .  | 34 |
| 2.5   | Introduction . . . . .  | 35 |
| 2.6   | Results and discussion . . . . .  | 38 |
| 2.6.1 | Description of the imaging platform . . . . .   | 38 |
| 2.6.2 | Description of the illumination system . . . . .  | 40 |
| 2.6.3 | System characterization for spatial resolution, field-of-view (FOV) and working distance (WD) . . . . . | 41 |
| 2.6.4 | Application to imaging of microorganisms in microfluidic devices . . . . .                              | 43 |
| 2.6.5 | Application to imaging cells with different illumination patterns . . . . .                             | 44 |
| 2.6.6 | Application to quantitative analysis of microorganism motility . . . . .                                | 47 |
| 2.6.7 | Application to fluorescence microscopy . . . . .  | 49 |
| 2.7   | Experimental . . . . .  | 50 |
| 2.7.1 | Imaging . . . . .   | 50 |
| 2.7.2 | Illumination . . . . .  | 51 |
| 2.7.3 | Fluorescence imaging . . . . .  | 51 |
| 2.7.4 | Microfluidics . . . . .   | 52 |
| 2.7.5 | Microorganisms . . . . .  | 52 |
| 2.7.6 | Cell lines . . . . .  | 53 |
| 2.8   | Conclusion . . . . .  | 53 |
| 2.9   | Conflicts of interest . . . . .   | 54 |
| 2.10  | Acknowledgements . . . . .  | 54 |
|       | References . . . . .  | 55 |

**3 Simple adaptive mobile phone screen illumination for dual phone differential phase contrast (dpDPC) microscopy 59**

|       |   |    |
|-------|---|----|
| 3.1   | Preface . . . . .   | 59 |
| 3.2   | Manuscript details . . . . .  | 60 |
| 3.3   | Authors and affiliations . . . . .  | 60 |
| 3.4   | Abstract . . . . .  | 60 |
| 3.5   | Introduction . . . . .  | 61 |
| 3.6   | Results and discussion . . . . .  | 63 |
| 3.6.1 | Description of the imaging and illumination platforms . . . . .                           | 63 |
| 3.6.2 | Generation of differential phase contrast (DPC) images . . . . .                          | 65 |
| 3.6.3 | Application of the mobile phone-based imaging system to DPC microscopy of cells . . . . . | 68 |

|          |  |           |
|----------|--|-----------|
| 3.6.4    | Application of the phone illumination to DPC microscopy of cells using a low-cost microscope . . . . .                   | 70        |
| 3.7      | Conclusion . . . . .   | 72        |
| 3.8      | Experimental . . . . .   | 73        |
| 3.8.1    | Imaging . . . . .  | 73        |
| 3.8.2    | Illumination . . . . .   | 74        |
| 3.8.3    | Image analysis . . . . .   | 74        |
| 3.8.4    | Samples . . . . .  | 74        |
| 3.9      | Acknowledgements . . . . .   | 75        |
| 3.10     | Funding . . . . .  | 75        |
| 3.11     | Disclosures . . . . .  | 75        |
|          | References . . . . .   | 76        |
| <b>4</b> | <b>Discussion</b>  | <b>80</b> |
| 4.1      | Identification of system requirements . . . . .  | 80        |
| 4.2      | Dual-phone illumination-imaging system for high resolution and large field of view multi-modal microscopy . . . . .      | 81        |
| 4.3      | Simple adaptive mobile phone screen illumination for dual phone differential phase contrast (dpDPC) microscopy . . . . . | 82        |
| 4.4      | Translation of phone screen illumination to lens-free microscopy . . . . .   | 83        |
| 4.5      | Outlook and future perspectives . . . . .  | 85        |
|          | References . . . . .   | 86        |
| <b>5</b> | <b>Conclusion</b>  | <b>88</b> |

**Bibliography**

**Appendix A Addendum to chapter 2 following thesis review**

**Appendix B Addendum to chapter 3 following thesis review**

# Chapter 1

## An introduction to lens-based and lens-free microscopy techniques for visualization of biological agents

### 1.1 Background

This thesis discusses the importance of light microscopy in the biomedical and biological engineering fields, describes the significance and advantages of employing microscopy systems with high spatial resolution and large fields-of-view (FOVs), and introduces low-cost, adaptive, user-friendly, versatile, and portable lens-based and lens-free illumination-imaging microscopy systems for multi-modal imaging of micrometer-sized objects, biological or otherwise, with potential applications in biology, education, and the environment. More specifically, observation of biological agents, such as microorganisms and cells, within confined spaces, such as microfluidic devices, is of particular importance for studying motility patterns of microorganisms as well as for performing biological computations and simulations.

Throughout the body of this manuscript-based thesis, every chapter contains a standalone introduction with corresponding literature review for the manuscript at hand. In chapter 2, I introduce a mobile phone-based multi-modal illumination-imaging system capable of bright-field, dark-field, point illumination, Rheinberg illumination, and fluorescence microscopy, with applications in imaging of microorganisms and cells in confined spaces. This work is further developed in chapter 3 to perform differential phase contrast microscopy. Finally, in section 4.4 of chapter 4, I briefly discuss the potential application of phone screen illumination to a lens-free imaging platform, to achieve reflection-based dark-field illumination for imaging of biological agents.

In this chapter, I provide a general introduction with relevant background information and theoretical definitions, which serves to establish the rationale and motivation behind my Ph.D. work and give a framework to the thesis overall. Section 1.3 of this introduction identifies the necessary specifications that an imaging system must meet in order to be able to visualize microorganisms within specific biocomputational microfluidic networks. This same logic could be expanded to virtually any imaging system, depending on the application at hand.

### 1.1.1 Microscopy in biology

In biology, the most commonly used microscopy types are light, electron, scanning probe, and to a lesser extent, acoustic microscopy [1]. Electron microscopy is mainly used to image thin tissue sections, and allows for spatial resolution in the range of ångströms but requires expensive equipment, intensive sample preparation, and specialized training to operate. Scanning probe microscopy is used to map surface topography down to the atomic level, going below the diffraction limit through the use of a cantilever. Different probe scanning devices and mechanisms exist, with the most common one being the Atomic Force Microscope (AFM), which uses a piezoelectric cantilever tip, and can be used for molecular probing of protein aggregates [2], for instance.

Conversely, light microscopy, utilizing visible light, is delimited by the relatively longer wavelengths used for imaging, which in turn imposes a limit on the spatial resolution. With widefield microscopy, where the entire sample is illuminated, we would expect a high-magnification, high-numerical-aperture (NA) objective to provide a spatial resolution close to 200 nm using green (550 nm) light. Super-resolution techniques could further improve this resolution limit through selective sample illumination and image post-processing, and typically require more complex hardware, specialized or customizable software as well as advanced image manipulation and processing. In principle, for an image to be formed using a light microscope, light has to be diffracted by the sample under observation. This diffracted light is then redirected by the objective lens and detection-side optics to form an image through constructive and destructive interference. A clearly observable image relies on having stark contrast between its elements, and as such, contrast in the final image can be changed through the manipulation of how light interacts with the sample in the first place [3].

Due to its relative simplicity, light microscopy can be used for multitudes of biological applications, such as observation of prokaryotic or eukaryotic cell morphology and behaviour, immunohistochemistry, cell counting, live cell imaging, determination of cell culture conflu-

ence, and many more. Additionally, by varying the illumination, sample contrast could be enhanced, and different aspects of the sample could be highlighted, resulting in different imaging modalities. Bright-field illumination is the most straightforward, where all parts of the sample are illuminated, and the resulting image is formed by the absorption interactions of light with different parts of the sample having different optical densities. Denser areas would absorb more incident light, resulting in lower amplitude of emitted light, and thus appear darker in the final image, and vice versa. Bright-field microscopy can be used for stained biological tissue, coloured or translucent samples, and samples with high contrast, such as polystyrene microspheres.

Point illumination reduces background or out-of-focus light via the introduction of a spatial pinhole, such as in confocal microscopy, and illuminating smaller regions within the sample for imaging, as opposed to flooding the sample with light as in the case of bright-field illumination, resulting in better contrast. Furthermore, for samples that require enhanced contrast, such as unstained epithelial tissue, dark-field imaging provides sharper images through the use of oblique illumination or ring illumination, whereby only diffracted light from the sample is collected by the objective, as opposed to bright-field, where both diffracted and non-diffracted background light reach the objective. A special instance of dark-field illumination is Rheinberg illumination, where instead of illuminating the sample with a ring of white light against a dark background, a coloured ring is juxtaposed against a background of a different colour. The colour combination is chosen in such a way so as to underscore certain parts of the sample, such as specific cell organelles, to allow for better observation.

Another more complex modality to use for imaging transparent samples is phase-contrast microscopy. Since theoretically in a transparent sample no incident light is absorbed, and light amplitude passes through the sample unperturbed, no amplitude-based image can be formed. Instead, a phase-based image is formed due to differences in refractive index within different parts of the sample, where regions with higher refractive index result in larger phase delays of the incident light. Since phase differences cannot be visually observed, a system of aligned annular and phase rings translate these to observable amplitude differences in the final image, by introducing delays to the background light, such that it can interfere constructively or destructively with the delayed light emitted from the specimen, resulting in an amplitude image.

Fluorescence microscopy is another modality that highlights the sample region-of-interest via fluorescent labelling of the relevant structures, where different moieties are labelled with fluorophores of different excitation and emission wavelengths. The sample is then illuminated with a laser of an appropriate wavelength for excitation of the bonded fluorophore of interest,

which in turn will emit a longer wavelength of light that forms the final image. The emitted light is filtered through to make sure that only the correct emission bandwidth is detected, and eliminate any cross-talk of fluorophores. Fluorescence microscopy is typically used for live/dead stains, differentiation of various cell types in tissue, and cell and reaction tracking.

### 1.1.2 Relevant optical parameters

To characterize an optical system, several parameters have to be taken into consideration, the most prominent of which are spatial resolution, field-of-view (FOV), magnification, and working distance (WD). It is also important to consider the physical limitations of the system components, including but not limited to, chromatic and spherical aberrations, and their corresponding applicable corrections.

#### 1.1.2.1 Spatial resolution

Spatial resolution determines the fineness of structures that the imaging system can visualize. More specifically, it indicates the minimum separation between two adjacent structures in a specimen, whereby these structures can still be visualized or resolved as two separate entities. If the distance between them is smaller than the resolution limit of the imaging system, they would not be resolved and would appear as a single structure instead.

Typically, the spatial resolution of a microscope is assessed via imaging small, point-like objects, such as nanospheres, which have a known uniform size, well below the theoretical resolution limit of the system in question. When a point object with these criteria is illuminated, an image of a diffraction pattern is formed due to light interference, which comprises a central diffraction spot or disk, surrounded by a series of diffraction rings. The bright rings indicate points of constructive interference (maxima), and the dark regions in between represent destructive interference (minima). This observed pattern is known as an Airy pattern and the radius of the central disk specifies the lateral  $(x, y)$  resolution of the system, and is directly dependent on the light wavelength ( $\lambda$ ) used, and the numerical aperture (NA) of the used objective, as is shown in the following equation, proposed by Ernst Abbe:

$$\text{Lateral resolution } (x, y) = \frac{\lambda}{2\text{NA}} \quad (1.1)$$

where  $\lambda$  is the average wavelength of transmitted light in widefield mode, or the excitation bandwidth in fluorescence mode, and

$$\text{NA} = n \sin \theta \quad (1.2)$$

where  $n$  is the refractive index of the imaging medium, and  $\theta$  is the half-angle of the cone of light that can enter the objective aperture. For most biological applications, the axial ( $z$ ) resolution is also of interest for imaging of  $z$ -stacks for 3D image reconstruction. Given that the Airy pattern formed along  $z$ , which collectively with the lateral Airy pattern is known as the point-spread function (PSF), is elliptical in nature, the disk radius is larger, which in turn leads to worse axial resolution, as compared to lateral, in accordance with the following equation:

$$\text{Axial resolution } (z) = \frac{2\lambda}{\text{NA}^2} \quad (1.3)$$

Theoretically, based on the equations above, improving spatial resolution can be achieved by using a shorter wavelength for illumination, enlarging the NA, or using a medium with a higher refractive index. However, due to physical limitations in terms of the glass transmission spectrum and NA enhancement, a light microscope with even the best specifications is still limited to a lateral resolution of around 200 nm, thus rendering such widefield systems diffraction-limited. Realistically, the practical spatial resolution of an imaging system is generally worse than the theoretical value due to background noise, sample autofluorescence, and other light interactions, which make distinguishing the object PSF from the unwanted noise difficult in the first place.

Ideally, for two adjacent point objects to be resolved, they should be positioned far apart enough such that their PSFs do not overlap. In practice, samples rarely contain perfect objects and instead usually have fully or partially overlapping objects. Whereas fully overlapping objects cannot be resolved, as their PSFs would be merged into one, in order for two partially overlapping point objects to be resolved by the imaging system as two separate entities, there exists an acceptable limit of diffraction pattern overlap, beyond which the objects cannot be distinguished individually anymore. There are multiple mathematical criteria that vary in their accuracy and applicability depending on PSF geometry, such as the Sparrow limit, the full width at half maximum (FWHM), or the Rayleigh criterion.

The Rayleigh criterion states that for two overlapping point objects to be resolved, the principal maximum (central Airy disk) of the PSF of one must coincide with the first minimum of that of the other (first dark region around central disk). As such, given these parameters, the achievable resolution limit is as follows, where any adjacent image PSFs with a distance equal to or larger than this value can be readily resolved, and vice versa [3]:

$$\text{Rayleigh resolution criterion } (x, y) = \frac{0.61\lambda}{\text{NA}} \quad (1.4)$$

Mathematically speaking, an image (I) of an object or specimen can be described as a

convolution between the spatial light distribution (illumination and emission/transmission) (S) of the object and its corresponding PSF that had been generated by the objective, along all three dimensions:

$$I(x, y, z) = S(x, y, z) * \text{PSF}(x, y, z) \quad (1.5)$$

Translating this complex mathematical operation from the time domain into the frequency (Fourier) domain shifts convolution to simple multiplication, and spatial position/location data into corresponding spatial frequencies (sines and cosines with multiple frequencies), as portrayed below, with higher frequencies indicating finer detail in the specimen, and vice versa [4]:

$$I(f) = S(f) \cdot \text{PSF}(f) \quad (1.6)$$

Consequently, it can be deduced that microscopy systems that allow higher frequencies to pass through, before the frequency cut-off imposed by the resolution limit is reached, can provide finer detail and thus higher spatial resolution overall, where essentially the cut-off frequency and the resolution criterion (e.g. Rayleigh) are two sides of the same coin. In other words, the latter is described in terms of spatial separation of PSFs in micrometres, and the former in terms of spatial frequency in reciprocal micrometres. Moreover, the larger the frequency bandwidth, the more information about the object that can be acquired and represented in the image. As such, the Fourier transform of the object PSF, denoted by  $\text{PSF}(f)$ , can be thought of as a transfer function of which frequencies of the original sample are transferred into the microscope image of the sample, known as the optical transfer function (OTF), and indicates the efficiency of the optical system performance [3] as well as the contrast information present in the image.

Experimentally, when assessing the spatial resolution capabilities of an imaging system, it follows that the larger the number of object spatial frequencies sampled, the closer the assessment is to reality, and the more accurate it is. However, the more thorough the sampling, the larger the size of the resulting data is, and the more time it takes to process it for image parameter extraction. Since there is a feasibility limit in terms of available data storage and required post-processing, it makes sense to only record enough information for a reasonable evaluation. This limit, as dictated by the Nyquist sampling theorem [5], requires an optical pixel size  $\approx 3$  times smaller than the theoretical value of the spatial resolution of the objective in question [6].

In order to establish an accurate PSF measurement in practice, one must choose a complementary combination of objective lens parameters (lateral resolution, total magnification)

and camera sensor pixel size, with a nanosphere object size ideally equal or below the diffraction limit ( $\approx 200$  nm) and well below the objective theoretical lateral resolution, so that the objects have sufficient high spatial frequency components. In order to determine the optical pixel size of such a system, the actual sensor pixel size should be divided by the total magnification of the optical components contributing to the image, as shown below, whereby to adhere to the Nyquist criterion, the optical pixel size needs to be at least three times smaller than the Abbe resolution of the used objective:

$$\text{Optical pixel size} = \frac{\text{Sensor pixel size}}{\text{Total system magnification}} \quad (1.7)$$

After taking multiple 3D stacks of the bead samples, the lateral and axial spatial resolution values can be approximated by examining line/area profiles across the individual bead PSFs, fitting them with a Gaussian function, and determining the FWHM, which would correspond to the Abbe resolution limit. Other criteria than the FWHM can also be used, depending on the optical setup used and the expected accuracy. For instance, optical nanoscopy or super-resolution microscopy systems offer better localization of point objects, which renders the object PSFs smaller overall; therefore, frequency cut-off values as small as  $\frac{1}{7}$  can be tolerated while maintaining the ability to resolve the individual object PSFs [7].

Diffraction gratings could also be used as objects for imaging system analysis in lieu of beads, but instead of observing PSFs, the modulation transfer function (MTF) values would be calculated directly from the contrast values extracted from the image, plotted versus spatial frequency, and the spatial resolution determined by choosing an appropriate frequency cut-off value. Furthermore, a method based on Fourier ring correlation (FRC), known as decorrelation analysis, can be used to estimate the spatial resolution through running an algorithm on two identical images of a real sample, captured at two different time points [8].

### 1.1.2.2 Field-of-view

The field-of-view (FOV) of an optical system is defined as the maximum specimen area that can be observed or imaged when looking through the objective. Provided that the camera has a sensor area large enough to capture the full FOV, and that there are no other limiting factors in the optical path of the imaging system, the FOV is typically determined by the objective itself, and is denoted as a diameter. When describing the FOV in terms of the camera image sensor, it can be denoted as a diagonal of a square or rectangular region.

For biological samples, it is important not only to have sufficient spatial resolution for visualization of cellular or subcellular structures, and optical sectioning in 3D stacks, but

also large enough FOV to capture meaningful biological data such as for statistical studies of cellular populations [9], developmental biology [10], neuronal mapping [11], and cell tracking [12]. However, in lens-based microscopy, there typically exists a trade-off between spatial resolution and FOV, such that it is possible to capture either a macroscopic view (low resolution with large FOV) of the specimen, or a zoomed-in view (small FOV) at high resolution. Whereas image stitching of multiple high-resolution FOVs could be done, it comes with its own set of limitations in terms of image seamlessness, and would be problematic for applications requiring live imaging [13].

### 1.1.2.3 Other parameters

Depending on the thickness of the sample to be measured, and the level of detail necessary for imaging, it is important to consider the working distance (WD) of the objective, and its magnification, respectively, whereby the latter goes hand in hand with the objective NA. The WD is defined as the distance between the outermost part of the objective and the top of the sample when the image is in focus. In general, the WD decreases with increasing magnification and NA, and vice versa [4]. Since there is typically a finite space for the specimen in the sample holder, an objective with a shorter WD could impose a restriction on the coverslip thickness to be used.

So far, the parameters mentioned in section 1.1.2 have been primarily described in relation to the specifications of the used objectives. Nevertheless, some parameters, such as spatial resolution and FOV, could also be influenced by the specifications of the camera sensor used for image capture. Even if the microscope comprises high quality objectives, sensor pixel size and area can delimit the spatial resolution and FOV, respectively, whereby smaller pixel size and larger sensor area contribute to better image quality in theory. However, it is also important to take into consideration the contributions of noise inherent to the sensor, based on sensor type and specifications as well as the sample, and illumination properties.

The principal noise types involved in sensor image capture are photon (shot) noise, read noise, and dark (thermal) noise. Shot noise stems from illumination and optical properties of the sample, and it is a statistical occurrence derived from the nature of photons, which follows a Poisson distribution. Shot noise cannot be avoided, but can be reduced by using longer exposure times and binning. Readout and thermal noise are both sensor-related, where the former comes from the photon-electron conversion fundamental to the signal readout process, and the latter is dependent on the temperature of the image sensor. Read noise is denoted as a root mean square (RMS) of electrons, and only appears relatively significant at low image signals. Dark noise, like shot noise, follows a Poisson distribution, and can be minimized by cooling the sensor chip [3], [4].

A digital image consists of both the wanted signal emitted from the specimen and unwanted noise, and this is represented in the recorded intensity values of each pixel. When the noise is significant relative to the signal, it becomes difficult to distinguish the signal-of-interest from the noisy background, and this is portrayed visually as artefacts and/or a loss of contrast in the image, and numerically as a low signal-to-noise (SNR) ratio. A number of factors, including but not limited to optics, camera, illumination, sample, system/component alignment, and potential aberrations, could affect image quality, which is the reason why a real system generally cannot match its theoretical specifications exactly. As such, it is crucial to optimize imaging system parameters for the application at hand, while keeping in mind that some compromise might be necessary.

#### 1.1.2.4 Optical aberrations and corrections

Simple lenses, by virtue of their material, shape, design, and manufacturing process suffer from optical aberrations, which could distort the resulting image. They can be broadly classified into on-axis and off-axis aberrations, where the former are spherical and chromatic aberrations, and the latter include, but are not limited to, astigmatism and field curvature [4]. Such aberrations could contribute to added noise and misalignment in the optical system, which in turn would worsen the spatial resolution and introduce unwanted artefacts.

Owing to their typical spherical shape, lenses refract light rays passing through the top and bottom edges of the lens more strongly than the rays that are passing closer to the optical axis, which leads to their having slightly different focal points along the optical axis of the lens. This results in a poorly defined image plane that appears blurry. Since spherical aberration cannot be completely eliminated, it can be corrected by using a compound system of positive and negative lenses with varying thickness, to allow more light rays to converge at a single focal point. Similarly, chromatic aberration stems from light rays with different wavelengths intersecting the optical axis at different focal points, due to each wavelength travelling at a different speed through the lens medium. The outcome is a blurry image with coloured edges, and chromatic magnification differences, which could be corrected using achromatic compound lenses.

On the other hand, astigmatism occurs because light rays from the object, passing through the horizontal and vertical diameters of the lens, are focused at two different focal planes, resulting in the image PSF of a point object having a nearly elliptical shape, as opposed to the typical disk shape. Field curvature is an aberration that leads a flat object to have a spherical-looking image, whereby only certain parts of the object could be brought into sharp focus at any one time, instead of having uniform sharpness across the FOV. This is typically due to the curved shape of lenses, but is also exacerbated by the flatness of the

image sensor, where the central part of the exposed sensor area receives light at a right angle, whereas the sensor pixels at the edges receive light at an angle.

This not only leads to poorer focus along the edges of the image, and thereby uneven image resolution, but also contributes to another process known as light fall-off, or vignetting, which results in darker image edges compared to the image center. Once again, compound lens systems with various specifications can be combined to correct such unwanted effects, but image post-processing could further improve this through the use of techniques such as flat-field correction [14] to combat field curvature and vignetting.

### 1.1.3 Lens-based microscopy approaches

Classical microscopy approaches utilize systems of lenses (objectives) to magnify the specimen to be examined, in addition to other components such as diaphragms, condensers, mirrors, and filters, to redirect and reshape light beams along the optical path, from the illumination source to the detection unit. Each microscope component partially contributes to some of the optical parameters mentioned in section 1.1.2, and therefore has to be chosen with compatible specifications for the overall imaging system requirements. Moreover, precise alignment of all these components has to be performed, in order to maximize system performance. Despite their ubiquity, and given the nature of lens-based platforms, they are typically limited by the trade-off between spatial resolution and FOV.

Aside from microscope-based assemblies, standalone imaging devices such as cameras, mobile phones, and flatbed scanners could also be used as lens-based imaging platforms for biological samples. Cameras would provide low spatial resolution and large FOV, and mobile phones would achieve higher spatial resolution at the expense of a smaller FOV. With flatbed scanners, the spatial resolution depends on the scanner type (contact image sensor (CIS), or charge-coupled device (CCD)), and the FOV can be as large as that of an A4 paper. In spite of their limitations compared to traditional microscopes, these imaging devices have the added advantage of portability, where mobile phones could even be used as point-of-care devices, complete with image data analysis and transmission. In many cases, such devices would need to be modified or adapted according to the application at hand, as mentioned in the introduction of chapter 2.

### 1.1.4 Lens-free microscopy approaches

Lens-free microscopy approaches allow for a better compromise between spatial resolution and FOV than lens-based platforms, since they can make use of the full potential of the image sensor, without being limited by lens specifications. To be able to achieve high spatial

resolution and a large FOV, it is crucial to use an image sensor (CCD or complementary metal-oxide-semiconductor (CMOS)) with small pixel size and a large active area. In lens-free imaging, the sample sits either at a certain distance away from the image sensor or directly on the sensor surface, without the need for other optical components in between, and the illumination can range from a simple light-emitting diode (LED) to a more complex setup, depending on the application at hand. Image information is then transmitted from the sensor to a computer for reconstruction and processing.

Lens-free microscopy can be broadly classified into two categories: contact-mode or direct on-chip imaging and sensing, and diffraction-based lens-free imaging [15]. In the former, the sample is placed directly on the chip surface, and the distance between the specimen and the active sensor area is quite small, which means that the sensor records shadows cast directly beneath the sample due to transmission, and any potential diffraction could be neglected [16]. Similar setups have been used for biological applications such as characterizing individual cell types on microscope slides [17], and within microfluidic devices [18], studying the behaviour of *C. elegans* [19], and detecting cells exhibiting chemiluminescence [20]. Diffraction-based imaging, as the name suggests, records diffraction and interference patterns emanating from the object. The sample is placed at a distance away from the sensor, and then the recorded interference patterns, which include amplitude and phase information, are digitally reconstructed to form an image using computer algorithms [21], [22].

Diffraction-based lens-free microscopy could in turn be further sub-classified according to sample distance from the image sensor, and illumination type, into digital inline holography (DIH), and shadow imaging. In DIH, the specimen is illuminated by spherical waves from a coherent point source of light, with the sample placed at a distance from the sensor. The scattered light from the sample interferes with itself and with unscattered background light, which results in a hologram of the object being recorded by the sensor chip. The reconstruction of the image from the hologram is then performed using computational algorithms. Such systems have been used for imaging of biological samples [23]–[29], and nanoparticles [30], [31]. On the other hand, shadow imaging uses partially coherent light for illumination of the sample, and has been used for various in-vitro cellular applications [32]–[36]. The specimen is placed at a closer distance to the sensor, as compared to DIH. Moreover, by having a shorter sample-to-sensor distance than the illumination-to-sample distance, this setup simplifies the subsequent image reconstruction because the illumination wave can be considered planar as opposed to spherical [37].

Whereas diffraction-based shadow imaging leads to lower noise being recorded by the sensor relative to DIH, the spatial resolution is still limited by the sensor pixel size in both cases. This can be overcome by sub-pixel shifting of the sample or illumination source, whereby

images of the sample are taken at different positions, and then stitched together to form the final image [38]–[41]. However, this can be quite computationally demanding. Overall, with microscopy, a trade-off exists between certain parameters. For instance, whereas diffraction-based lens-free microscopy requires heavy post-processing for image production compared to contact-mode lens-free platforms, it allows for 3D imaging of samples, due to its ability to capture samples at different z-positions, whereas the latter does not. Furthermore, when it comes to the bigger picture, lens-free approaches get rid of the bulky and expensive optics that comprise lens-based platforms, but in return require heavy post-processing of recorded object data, which could be mathematically and computationally taxing, thus shifting the mass of the imaging process from hardware to software.

### 1.1.5 Image processing and analysis

Post-processing of microscopy images is generally necessary for subsequent analysis, and extraction of qualitative and quantitative image information. Images imported to the computer from the camera/image sensor are saved as integer matrices of pixel intensity values, with the range of values depending on the sensor design, image type, and software used. A pixel intensity matrix could also be represented as an image histogram, indicating the relative pixel distribution over the range of intensity values. Converting the native image to other image formats, or adjusting image brightness or contrast alters the native image histogram, and this transformation between old and new values is applied with the help of a look-up table (LUT). The LUT could be appended to the image as part of the metadata, such that the native pixel values could be retained and not overwritten.

Image processing serves as an intermediary between the native image captured by the camera sensor, and the extraction of desired information from the image via analysis. One such technique that simplifies feature identification, for instance, is background subtraction. This can be done by recording the image of interest, capturing a similar image with the exact same parameters but without the specimen, and then subtracting the latter from the former. Depending on the image in question, how strongly the features of interest blend into the background, and the type of background signal, background subtraction might not always be successful. In chapter 2, figure 2.6, background subtraction was performed prior to microorganism trajectory tracing, to highlight the paths more clearly, thus leading to more accurate measurements.

A more thorough approach is to apply flat-field correction, previously referred to in section 1.1.2.4, where three images are recorded and combined mathematically, resulting in a corrected image. As with background subtraction, the image of interest (Native), and an

image with identical settings but without the sample (Flat) should be recorded. Additionally, a third image, similar to the flat image but with the illumination source turned off (Dark) is also captured, and the corrected image is generated from these three images as shown in the equation below:

$$\text{Flat-field correction} = \frac{\text{Native} - \text{Dark}}{\text{Flat} - \text{Dark}} \quad (1.8)$$

where the flat image mainly captures the noise due to optical aberrations in the used microscope setup, and the dark image represents noise produced by the sensor [4]. With mathematical image combinations, the final image is generated through arithmetic manipulation of the matrices of the corresponding images. An example of image arithmetic performed with Fiji software is shown in chapter 3, figure 3.1, resulting in a differential phase contrast (DPC) image.

Image analysis is useful in biological and biomedical imaging for distinguishing cell types, assessing cell viability, health, and growth, characterizing cell morphology, performing cell (particle) counts, measuring lateral (and axial, in the case of 3D image acquisition) dimensions of cells, microorganisms, and biological features therein as well as performing cell tracking, and speed calculations. Moreover, pixel intensity (line or area) profiles measured across cells are necessary for contrast calculations, which could be useful for optimization of imaging parameters for optimal visualization of the biological specimen. Contrast is typically quantified using the following standard contrast transfer function (CTF):

$$\text{CTF} = \frac{I_{\max} - I_{\min}}{I_{\max} + I_{\min}}, \quad (1.9)$$

where  $I_{\max}$  is the maximum intensity value detected within the region of interest in the raw or processed images, and  $I_{\min}$  is the lowest [42]. Lastly, as mentioned in section 1.1.2.1, nanospheres are typically used to evaluate the spatial resolution of the microscopy system, and whereas they are not biological samples, they are necessary for accurate system assessment, which in turn is crucial for high-quality biological imaging, leading to more precise subsequent measurements.

## 1.2 Rationale

Biological and biomedical imaging generally requires high spatial resolution in combination with a large FOV for application areas such as cell culture and assays, histopathology, embryology and developmental biology, and neuroscience, as previously mentioned in section 1.1.2.2. Imaging in such fields necessitates having sufficient spatial resolution for identifi-

cation of individual cells and microorganisms, their morphology, and subcellular structures, while simultaneously having a FOV large enough for surveying expansive regions of the sample in one shot or frame. However, as discussed at length in the previous sections, microscopy suffers from a compulsory trade-off between resolution and FOV, and as such, depending on the application at hand, it is essential to achieve the most suitable compromise that would cater for it, such that undesirable losses are minimized.

Typically, a sample is mounted onto a glass slide, where it is sealed onto the glass with a coverslip, and then placed on the microscope stage for imaging. Specifically for live imaging, this creates a confined environment for observation of cells or microorganisms under different conditions, by varying the suspension media, stage temperature, and other stimuli. The advent of microfluidics introduced even more customizable systems, where microchannels and reservoirs could be microfabricated with multiple geometries, and used to expose cells to various environmental conditions, for instance, while cellular response can be monitored with the aid of a microscope [43]. In such systems where real-time or live motion needs to be surveyed, the active area of the microfluidic device should be ideally captured in one FOV, where individual cells could be resolved.

Similarly, microfluidic platforms could also be used for observation of microorganisms, where channels or plazas of such devices could provide valuable data about their behaviour. Depending on the device design, different aspects of the microorganism can be studied. Straight channels of various widths could provide information about microorganism movement trajectory, velocity, cell division, and growth. Microfluidic devices that have microfabricated pillars could be used for traffic control, and observation of group motility behaviour. Moreover, wide areas with borders, such as plazas, could provide an idea of the affinity of microorganisms for walls or corners, and could also be used to observe motion trajectory, and perform agent counts, and dimension measurements [44], [45].

Motility of microorganisms depends on both the species of the microorganism in question, and the surrounding environment. While some microorganisms are inherently non-motile and others motile, the motility pattern can change due to chemotaxis [46], where the microorganism would swim along or against a chemical gradient, depending on whether the chemical at hand is an attractant or a repellent, respectively [47]. As such, observation and characterization of motility patterns of microorganisms could have potential applications in classification of pathogens present in drinking water [48], for example, where a primary sorting of pathogens present in a water sample could be done, which could then be followed by classical microbial culture for more accurate identification.

Furthermore, microfluidic devices could also be used for biocomputation, where mathematical problems are encoded graphically into the physical chip design, and and for bio-

logically guided simulations, whereby the chip design is modelled after the map of a city, structure, or location, such that traffic patterns could be studied and adapted accordingly. In both cases, microorganisms are allowed to traverse the network freely, and generate computational solutions in the former, and traffic information in the latter. For such networks, it is important to be able to view the whole device area in one shot, since it is fundamental to monitor the movement of the biological agent within the network in real time, in order to generate density maps of the network, and track the movements of the microorganisms where necessary.

Figure 1.1 shows the computational region of a biocomputational microfluidic device that encodes an instance of the Subset Sum Problem (SSP). This chip was fabricated based on the design in [49], where each exit represents a potential solution. When bacteria are allowed to traverse the chip for a sufficient amount of time, a density map can be generated, which would show that network exits with higher concentrations of bacteria indicate the correct solutions for this particular problem. As for biologically guided simulations, biological agents explore these networks freely, simulating areas of high and low traffic through gathering and dispersion, respectively, and potential bottlenecks through aggregation, owing to their inherent space-searching capabilities [50].

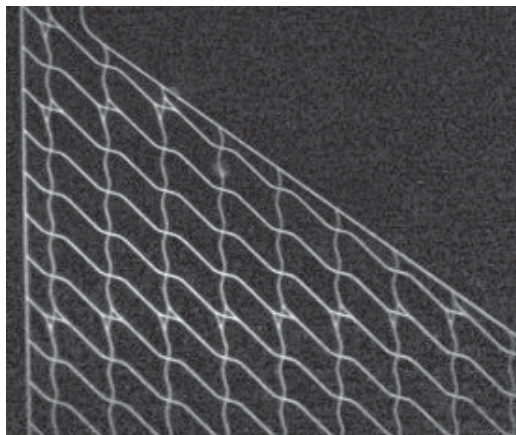


Figure 1.1: A biocomputational microfluidic device that encodes an instance of the Subset Sum Problem.

In conclusion, observation of biological agents within confined spaces provides valuable data, and is requisite of an imaging system with simultaneously high spatial resolution and large FOV, for many biological and biomedical applications, such as high throughput screening [51], and particularly for ones that require agent tracking [52]. Accordingly, in the course of this dissertation, I present four research papers: one that discusses system requirements, in terms of spatial resolution and FOV, for observation of biological agents within microfluidic devices, two that describe a mobile-phone based illumination-imaging system that allows

for visualization of biological agents using numerous microscopy modalities, and one that introduces a contact-mode lens-free platform for imaging of micron-sized objects. Both of these platforms optimize the resolution-FOV trade-off for their relevant applications, and establish novel microscopy capabilities via integration of pre-existing systems.

## 1.3 Identification of imaging system requirements

While microfluidic devices performing biocomputation only require microorganisms to function, the outcome cannot be read or utilized without pairing it with a suitable optical system. As such, to get an idea of appropriate imaging platforms for different sizes of the Subset Sum Problem (SSP) microfluidic device, we put together information regarding the spatial resolution and field-of-view (FOV) capabilities of different lens-based and lens-free imaging systems, and delineated the SSP chip sizes that can be imaged using each technique, depending on the size of the biological agent used. In general, such microscopy system requirements need to be assessed on a case-by-case basis, and could vary in complexity depending on how complicated the application in question is.

This section is based partially on research contributions I made as a co-author to a published manuscript [53], and introduces the different SSP complexity scenarios to be considered, the pertaining imaging challenges, in addition to the feasibility of each. It then discusses the regions of operation of different optical technologies in terms of spatial resolution and FOV, with the aim of pairing SSP devices that have various sizes and use diverse biological agents to the most fitting imaging platform. For biocomputational chips with large areas that could require image stitching, time and hardware constraints are discussed for situations of high and low biological agent density. Finally, a predictive mathematical model for device dimensions based on agent size and SSP cardinality is presented. Overall, a similar or a simpler version of this approach could be used for identification of imaging system requirements for other applications.

### 1.3.1 Introduction

To be able to accurately solve the SSP using biocomputation, the physical coordinates of every biological agent within the microfluidic device should be reported, and if that is not feasible, then at least the sequence of junctions each agent passes through should be known. In practice, implementation of such a system requires technological innovation, and until such a time this could be achieved, optical microscopy is the most pragmatic approach, as long as the agent positions could be recorded with enough spatial and temporal precision,

such that agent location history is documented with minimal to zero error.

In order to approach such precision, agent trajectories should be ideally captured in a single shot, within one FOV, at a spatial resolution that allows for resolving individual agents. However, if the device area is too large to visualize within a single FOV, and image stitching is to be performed at a later stage, different regions of the device, where the agent motion can be observed, would need to be recorded, and the switching frequency between regions would need to be high enough to avoid confusing agent identity or localization. To express this problem in more practical terms, traffic considerations could be split into three scenarios, listed in order of decreasing complexity:

1. biological agents are able to cross over one another axially (along the z-plane) within the microfluidic channel, in such a way so as to appear as one agent when observed in the x-y cross-section;
2. biological agents are able to pass or overtake one another only laterally (within the x-y plane) within the channel; and
3. biological agents are only able to move in single file along the channels, without any crossing, passing, or overtaking.

For computational device fabrication purposes, reducing the channel widths and heights to less than twice the agent width would prevent overtaking, yet, the possibility of agent clogging would be very large, and as such, channels with widths and heights approximately four-times the agent width should be fabricated, for smoother functioning of the device. Consequently, scenario three is virtually unattainable. Moreover, realistically speaking, since optical agent tracking can only be done in the x-y plane, the first scenario cannot be recorded and analysed without errors, given that agent cross-over occurs axially, which is why error-free agent tracking would require an innovative agent tagging system. Finally, for scenario two, an imaging system capable of resolving objects smaller than the agent width, and length would be necessary for reliable agent localization information.

### **1.3.2 Biological agent, biocomputational device, and optical technology size and parameter considerations**

Figure 1.2 shows the expected SSP biocomputational chip size as a function of the biological agent width, for multiple prime number SSP cardinalities. The horizontal black dashed lines in the figure delineate the standard semiconductor industry silicon wafer sizes of 4-, 6-, and 8-inches diameter, which are used for fabrication of SSP microfluidic devices. The vertical

blue bars depict biological agent width, where average widths of molecular motor-driven cytoskeletal filaments, i.e. actin-myosin (AM) and microtubule-kinesin (MK) complexes, and microorganisms, i.e. *Escherichia coli* (*E. coli*), and *Euglena viridis* (*E. viridis*) are shown. Due to the existing trade-off between spatial resolution and FOV, the active device area should be imaged at a spatial resolution, denoted as the maximum usable pixel size (MUPS), capable of resolving individual agents, as previously mentioned.

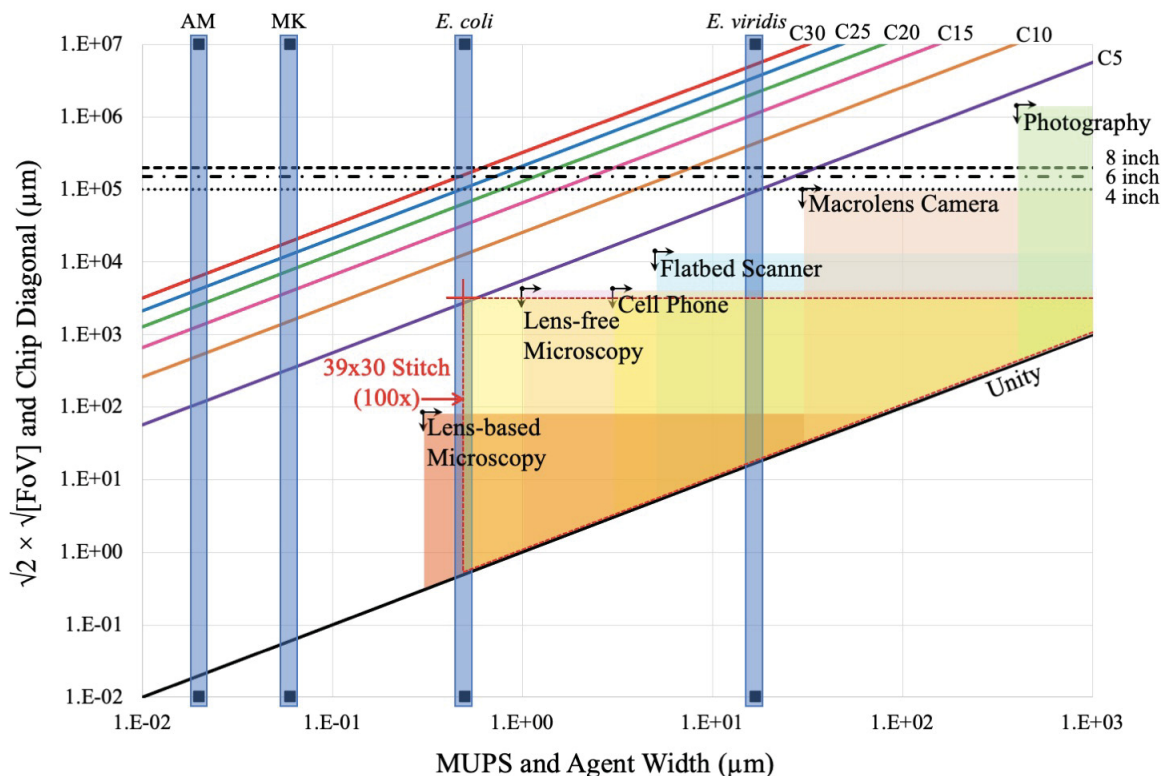


Figure 1.2: **Device size vs. agent width, and field-of-view (FOV) vs. maximum usable pixel size (MUPS).** The triangular regions denote the usable optical range for various microscopy techniques. An example of an enlarged usable region via image stitching is denoted by a red cross.

Each pair of crossed black arrows delimits a triangular region for the imaging technology under consideration, which represents the intersection of the maximum attainable FOV (denoted as  $\sqrt{2} \times \text{FOV}$ , which is equivalent to the diagonal of a rectangular FOV), and the minimum pixel size (or maximum achievable spatial resolution) of the system. As shown in the figure, each triangle is bounded by the ‘unity’ black diagonal line, which indicates the points where the FOV and pixel size are equal, beyond which any values would be infeasible. As such, these coloured triangular regions denote the usable optical range per technology. In principle, to efficiently utilize the available FOV for biocomputational imaging, the agent

width should be as close as possible to the spatial resolution limit of the system.

Whenever the point of intersection of a blue bar and an SSP cardinality line lies within a technologically achievable triangular area, that imaging technology can be used to record the active area of that particular SSP problem in a single FOV, while being able to resolve that specific biological agent used for solving the problem. Subsequently, based on the figure, actin and microtubule filaments cannot be optically resolved, given the technologies in question, and therefore cannot be monitored for SSP biocomputation. Moreover, individual *E. coli* agents could be resolved with lens-based microscopy, but the full size of the smallest-mentioned SSP device cannot be covered in one FOV without additional image stitching. As indicated by the red cross in the figure, a 100x objective lens could be used for resolving *E. coli*, and  $39 \times 30$  individual images would have to be captured by the microscope within a specific time frame, in order to capture the full SSP device area. As for *E. viridis*, the FOV and spatial resolution of a flatbed scanner would allow the capture of  $3 \times 3$  unit cells in one FOV.

### 1.3.3 Image stitching parameter considerations

Whenever the area to be imaged is larger than the FOV of the imaging system, image stitching can be used to overcome this, but at the expense of losing some spatial and temporal information. It follows that this loss could be minimised by using faster switching speeds between the imaged sectors, but this in turn is limited by the mechanical capabilities of the microscope stage. To perform these calculations, the following factors should be taken into account:

- Speed of biological agent used
- Exposure time of each partition of the image

For the sake of simplifying our sample calculations, we are assuming no horizontal or vertical image overlap, negligible exposure times (which in reality can go as low as 1 - 10 ms for bright field imaging and as high as 500 ms for fluorescence imaging), perfect functioning of pass and split junctions in our SSP networks, and unidirectional movement of our biological agents with no U-turns. Factoring in the density of the agents necessitates choosing the optimal switching speed based on dependency on body length in case of high agent density, and based on distance between adjacent junctions in case of low agent density.

For the scenarios described below, numerical examples are shown for *E. coli* K-12, where body width (BW) =  $0.5 \mu\text{m}$ , body length (BL) =  $2.5 \mu\text{m}$ , and speed  $v = 10 \mu\text{m/s}$ . Vertical and Diagonal Junction Distances (i.e. between two adjacent junctions) for the subset sum

problem network (SSP) fabricated with 2  $\mu\text{m}$ -width channels for *E. coli*, are 60  $\mu\text{m}$  (VJD) and 100  $\mu\text{m}$  (DJD), respectively.

- In the case of high agent density (scenario where more accurate tracking is required)
  1. Speed of agent:  $v = 10 \mu\text{m/s}$
  2. Speed  $v_b$  of agent in body lengths per second:  $v_b = \frac{v}{\text{BL}} = 4 \frac{\text{bl}}{\text{s}}$
  3. Time period to return to original image partition (in case we wish the agent to have moved only  $\frac{1}{2}$  a body length):  $t_r = 0.5 \frac{\text{BL}}{v} = \frac{0.5 \text{ bl}}{v_b} = 125 \text{ ms}$
  4. The average switching time between partitions  $t_s$  is determined by  $t_s = \frac{t_r}{nm}$ , where  $n$  and  $m$  are the number of partitions in x and y respectively (e.g.  $2 \times 2$ ,  $3 \times 4$ ). Hence, for a  $2 \times 2$  stitching mode,  $t_s = \frac{125 \text{ ms}}{4} = 31.25 \text{ ms}$
- In case of low agent density (scenario where less accurate tracking is acceptable)
  1. Speed of agent:  $v = 10 \mu\text{m/s}$
  2. Speed of agent ( $v_v$  or  $v_d$ ) in vertical- or diagonal junction steps per second:  $v_v = \frac{v}{\text{VJD}} = 0.17 \frac{\text{vjs}}{\text{s}}$  and  $v_d = \frac{v}{\text{DJD}} = 0.1 \frac{\text{djs}}{\text{s}}$
  3. Time period to return to original image partition (in case we want the agent to have moved by 1 vjs or 1 djs):  $t_v = \frac{\text{VJD}}{v} = \frac{1 \text{ vjs}}{v_v} = 6 \text{ s}$  and  $t_d = \frac{\text{DJD}}{v} = \frac{1 \text{ djs}}{v_d} = 10 \text{ s}$
  4. The average vertical switching time between partitions  $t_{sv}$  is given by  $t_{sv} = \frac{t_v}{nm}$ , where  $n$  and  $m$  are the number of partitions in x and y respectively (e.g.  $2 \times 2$ ,  $3 \times 4$ ); the average diagonal switching time between partitions  $t_{sd}$  is given by  $t_{sd} = \frac{t_d}{nm}$ . Hence, for a  $2 \times 2$  stitching mode  $t_{sv} = \frac{6 \text{ s}}{4} = 1.5 \text{ s}$  and  $t_{sd} = \frac{10 \text{ s}}{4} = 2.5 \text{ s}$

The calculations shown above describe two extreme cases in terms of agent density, and as a result the necessary corresponding tracking accuracy. However, in real-life situations, we will mostly have intermediate scenarios that fall between both, and it would be up to our discretion to choose the appropriate values to use.

As such, the overall parametric equation to calculate switching time ( $t_s$ ) can be described as:  $t_s = \frac{t_r}{nm} = \frac{d}{v^* nm}$ , where  $t_s$  is the switching time between image partitions,  $t_r$  is the time period to return to original image partition,  $n$  is the number of image partitions in the form ' $n \times m$ ',  $d$  is the displacement we would like our agent to have moved by the time we

return to the original image partition expressed in terms of BL/VJD/DJD etc., and  $v^*$  is the agent speed expressed in terms of BL/VJD/DJD etc. rather than in unit length per second.

The switching time ( $t_s$ ) encompasses two values, namely translation time ( $t_t$ ) and exposure time ( $t_e$ ), where  $t_t$  can be expressed as:  $t_t = \text{FOV} / v_{ss}$  where FOV is the diagonal field-of-view of the system, and  $v_{ss}$  is the speed of the scanning microscope stage. Moreover,  $t_e$  is dependent on illumination technique (e.g. bright field), system magnification (inversely proportional), and when using fluorescence, the fluorophore used. It follows from this that  $t_s \geq t_t + t_e$  in order to achieve the required agent tracking accuracy.

In terms of what the current technology can offer, the fastest motorised translational stage, to the best of our knowledge, offers a maximum speed of 250 mm/s, with an accuracy  $< 3 \mu\text{m}$ . This stage utilises a servo motor as its actuator, and is available from Thorlabs Inc.

Once again, using two extreme scenarios for the FOV can help shed light on what this system could help us achieve. If we use a 100x objective (NA = 1.4), which gives us a FOV  $\approx 60 \mu\text{m}$ , we get  $t_t = 240 \mu\text{s}$ . When pairing this with a reasonably low  $t_e$ , one can achieve high accuracy with a large number of partitions, and a high resolution ( $\approx 0.5 - 1 \mu\text{m}$ ), but the overall FOV covered would be quite small. On the other hand, if we use a 2x objective (NA = 0.3), with FOV  $\approx 1.5 \text{ cm}$ , we get  $t_t = 60 \text{ ms}$ . Based on our previous calculations, regardless of the  $t_e$  used, we will not be able to use this system to scan even the smallest ( $2 \times 2$ ) partition matrix for the most accurate tracking scenario ( $t_s \leq 31.25 \text{ ms}$ ). However, we can still use this for a slightly less accurate tracking scenario while covering a larger overall FOV with a fairly good resolution ( $\approx 3 - 5 \mu\text{m}$ ).

Typically, for observing *E. coli* in the SSP chip, we use a 4x objective (NA = 0.16) under fluorescence, with  $t_e = 500 \text{ ms}$ . In order to observe the largest chip we have with cardinality 30 (C30), which has an area of  $\approx 13 \times 10 \text{ cm}$ , and using the same 4x objective with FOV  $\approx 1 \text{ cm}$ , we would need  $13 \times 10$  partitions. For this set-up, and using the more accurate tracking approach, we would need a  $t_s = \frac{125 \text{ ms}}{13 \times 10} = 0.962 \mu\text{s} = \approx 1 \text{ ms}$ , which is unattainable given the large  $t_e$  requirement. Moreover, using the less accurate tracking approach, we would need a  $t_s = \frac{10 \text{ s}}{13 \times 10} = \approx 0.077 \text{ s} = 77 \text{ ms}$ , which once again is infeasible. If, however, we disregard  $t_e$ , we would need a  $v_{ss} = 10 \text{ m/s}$ , and  $v_{ss} = \approx 13 \text{ cm/s}$  respectively. Since the SSP device has a triangular profile, and only half of the rectangular partition grid will be traversed by the moving stage, the calculated  $t_s$  should be multiplied by 2, which would result in half the speed requirement. This, even with the improved requirements, is nowhere near feasible given the current available technology. While ignoring  $t_e$  is unrealistic for tracking *E. coli*, it could potentially work for bacterial species that provide good contrast, such as cocci.

Table 1.1 shows which chips can be observed with image stitching using the specific objectives available on an Olympus IX83 microscope. This comparison was made using

appropriate exposure times for each magnification, in addition to the translation time using the stage speed available (13 mm/s).

It shows that, with stitching, up to C15 can be observed with a 10x objective and up to C20 with a 4x objective, compared to C4 and C11 respectively without stitching (i.e. one FOV). However, just to relax to speed requirements and other elements that were not taken into account (such as areas of image overlap, precision issues, etc.), the limit will be more likely at C15 when using the 4x objective.

| Objective | NA   | Resolution<br>( $\mu\text{m}$ ) | FOV<br>( $\mu\text{m}$ ) | Cardinality<br>(1 FOV) | Stitching<br>limits | Cardinality<br>(stitched FOV) |
|-----------|------|---------------------------------|--------------------------|------------------------|---------------------|-------------------------------|
| 2x        | 0.3  | 5                               | 15000                    | 11                     | $4 \times 3$        | 21                            |
| 4x        | 0.16 | 3                               | 10000                    | 9                      | $6 \times 4$        | 20                            |
| 10x       | 0.4  | 2                               | 2000                     | 4                      | $14 \times 11$      | 15                            |
| 20x       | 0.75 | 2                               | 1000                     | 3                      | $24 \times 18$      | 14                            |
| 40x       | 0.96 | 2                               | 500                      | $27 \times 20$         | 11                  |                               |
| 60x       | 1.35 | 1                               | 200                      | $32 \times 24$         | 8                   |                               |
| 100x      | 1.4  | 0.5                             | 60                       | $39 \times 30$         | 5                   |                               |

Table 1.1: SSP chips that can be observed with image stitching using the specific objectives available on an Olympus IX83 microscope

### 1.3.4 Mathematical modelling of SSP biocomputational device dimensions based on biological agent size and problem cardinality

Based on our current geometrical design of the SSP network, we can derive formulae for predicting the corresponding dimensions of the SSP device for different channel widths. The design rules and spatial relationships for all chips were inferred from the 16@3 SSP chips with  $2\mu\text{m}$  channel widths that we have available.

The chip sizes mentioned throughout this document refer to the main computational part of the chip delineated by the lines in Figure 1.3. Given that the computational part comprises the bulk of the chip, and that there is no standard design strategy to be followed in designing the inlet and outlet areas of the chip, we chose to exclude these regions from our size calculations. Since the inlets and outlets would have to be designed differently for different organisms, and a number of factors would have to be taken into account, predicting these measurements would be difficult without prior knowledge of the design to be used.

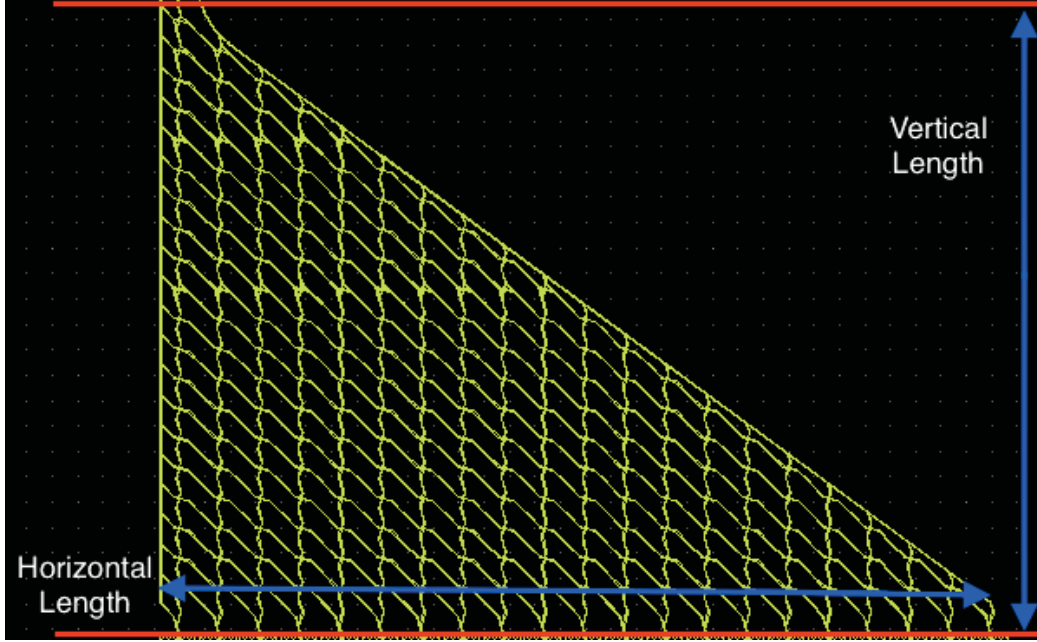


Figure 1.3: Computational region of SSP chip.

From Figure 1.3, we can see that the layout of the channels throughout the computational region follows both vertical and diagonal alignments. We could then deduce that with a change in channel width, the corresponding change in vertical length would be due to the vertical projection of the diagonal channels, and the corresponding change in horizontal length would be due to the horizontal projection of the diagonal channels, in addition to the vertical channels. Consequently, the equations for the vertical and horizontal lengths have 1 and 2 factors corresponding to the change in channel width, respectively. This explains why the horizontal length of the chip will always be larger than the vertical length.

$$l_{v1} = \frac{w(n+1)}{\sqrt{2}} \quad (1.10)$$

$$l_{h1} = w(n+1) + \frac{w(n+1)}{\sqrt{2}} = w(n+1) \left[ 1 + \frac{1}{\sqrt{2}} \right] \quad (1.11)$$

where  $l_{v1}$  is the vertical length corresponding only to a change in channel width,  $l_{h1}$  is the horizontal length corresponding only to a change in channel width,  $w$  is the channel width, and  $n$  is the number of nodes.

We could also do this calculation in an incremental manner, where the new chip size will be the size of the original  $2\mu\text{m}$  chip, plus the change in size of the respective dimension (i.e. vertical or horizontal length). However, since the size of the original  $2\mu\text{m}$  chip becomes in-

significant when we are dealing with much larger chips, we decided not to do the calculations in this way.

Moreover, an additional factor needs to be added to both equations to account for the distance between adjacent nodes. Since the larger designs are simple overall enlargements of the original 2  $\mu\text{m}$  chip, the distance between adjacent nodes follows the same enlargement factor; e.g. a chip with a channel width of 4  $\mu\text{m}$  has a channel width that is double that of the original 2  $\mu\text{m}$  chip, and therefore the distance between adjacent nodes is also double that of the original chip. As such, because the distance between adjacent nodes in the original chip is 50  $\mu\text{m}$ , which is 25 times the channel width of 2  $\mu\text{m}$ , we could use this factor as a rule of thumb for other chips as well.

$$l_v = 25w(n + 1) + \frac{w(n + 1)}{\sqrt{2}} = w(n + 1) \left[ 25 + \frac{1}{\sqrt{2}} \right] \quad (1.12)$$

$$l_h = 25w(n + 1) + w(n + 1) \left[ 1 + \frac{1}{\sqrt{2}} \right] = w(n + 1) \left[ 26 + \frac{1}{\sqrt{2}} \right] \quad (1.13)$$

where  $l_v$  is the overall vertical length,  $l_h$  is the overall horizontal length,  $w$  is the channel width, and  $n$  is the number of nodes.

Nevertheless, it is good to keep in mind the organism we are dealing with. In case the body length of an organism is much larger than its width, we would have to account for that by allowing for a larger distance between adjacent nodes, to make sure no extensive crowding of organisms takes place between nodes. This way we could ensure that individual organisms could still maintain a certain direction or change it freely, without any biases from its environment or from other organisms.

Finally, based on the 16@3, 20@4, and the 42@7 SSP chips with 2  $\mu\text{m}$  channel widths that we have, we can see that the 20@4 chip is 1.25 (or  $\frac{20}{16}$ ) times larger than the 16@3 in terms of vertical and horizontal lengths, and that the 42@7 chip is 2.1 (or  $\frac{42}{20}$ ) times larger than the 20@4. This can also be deduced from the fact that when we say 20@4, we mean that we have 20 nodes both on the vertical and horizontal edges of the chip. Hence, when we have a 42@7, we can automatically know that the number of nodes on each dimension will approximately double, which gives us an overall doubling in vertical and horizontal lengths. The number of elements in the set (primes or otherwise) is irrelevant in this case.

As such, for any other channel width, one can simply predict the corresponding size of the 16@3 chip using the aforementioned equations, and then scale up accordingly to chips of equal channel width with a larger number of nodes from there, without having to do the calculations from scratch.

Table 1.2 depicts the predicted chip dimensions for a number of different organisms. The predictions were done following the previously described procedure. The SSP chip sizes are written in the format:  $l_v \times l_h$ . Furthermore, the average body widths of the organisms are mentioned in Table 1.3, along with their respectively chosen SSP channel widths.

We typically choose a slightly larger channel width than the actual width of the organism to make certain that the organisms have just enough space to move along the channels freely, without allowing them to perform u-turns or to have two organisms moving side-by-side within the channels. Besides, this also accounts for the size of the bacterial flagella, which can be quite large. Lastly, keep in mind that ants would not be appropriate for biocomputation since their group dynamics might influence their individual exploration of the network, but they were mentioned here for the sake of size comparison.

| Organism \ SSP               | 16@3                   | 20@4                   | 42@7                    |
|------------------------------|------------------------|------------------------|-------------------------|
| <b>Escherichia coli</b>      | $1 \times 1.3$ mm      | $1.23 \times 1.65$ mm  | $2.55 \times 3.43$ mm   |
| <b>Pseudomonas putida</b>    | $1 \times 1.3$ mm      | $1.23 \times 1.65$ mm  | $2.55 \times 3.43$ mm   |
| <b>Magnetococcus marinus</b> | $1.75 \times 1.82$ mm  | $2.19 \times 2.28$ mm  | $4.59 \times 4.78$ mm   |
| <b>Euglena gracilis</b>      | $1.75 \times 1.82$ cm  | $2.19 \times 2.27$ cm  | $4.59 \times 4.77$ cm   |
| <b>Paramecium bursaria</b>   | $4.81 \times 4.99$ cm  | $6.01 \times 6.24$ cm  | $12.62 \times 13.11$ cm |
| <b>Ant</b>                   | $1.31 \times 1.36$ m   | $1.64 \times 1.70$ m   | $3.44 \times 3.58$ m    |
| <b>Dog</b>                   | $131.1 \times 136.2$ m | $163.9 \times 170.3$ m | $344.2 \times 357.6$ m  |
| <b>Cow</b>                   | $502.6 \times 522.1$ m | $628.2 \times 652.7$ m | $1.32 \times 1.37$ km   |

Table 1.2: Organism used vs. projected SSP chip size

|                              | Average Body Width | SSP Channel Width |
|------------------------------|--------------------|-------------------|
| <b>Escherichia coli</b>      | 0.5 $\mu$ m        | 2 $\mu$ m         |
| <b>Pseudomonas putida</b>    | 0.5 $\mu$ m        | 2 $\mu$ m         |
| <b>Magnetococcus marinus</b> | 1 $\mu$ m          | 4 $\mu$ m         |
| <b>Euglena gracilis</b>      | 30 $\mu$ m         | 40 $\mu$ m        |
| <b>Paramecium bursaria</b>   | 100 $\mu$ m        | 110 $\mu$ m       |
| <b>Ant</b>                   | 2 mm               | 3 mm              |
| <b>Dog</b>                   | -                  | 30 cm*            |
| <b>Cow</b>                   | -                  | 115 cm**          |

\* this value denotes the average door opening width for a large dog such as a German Shepherd or a Golden Retriever

\*\* this value denotes the average stall width for a 600-kg cow

Table 1.3: Average organism body width and chosen SSP channel width

### 1.3.5 Conclusion

In this section, I explained the considerations to be taken into account for visualization of biological agents within a specific microfluidic network, namely the SSP biocomputational network. The chosen imaging technology would need to provide spatial resolution that is good enough to distinguish individual biological agents used in the network, and a FOV large enough to take in the full device area in a single frame. This approach could be translated onto any other application, whereby the geometrical and temporal constraints are known in advance. Of course, the SSP problem happens to be a complex one, where device areas ranging from  $1\text{ mm}^2$  to  $1\text{ m}^2$ , with channel widths from  $2\text{ }\mu\text{m}$  to  $110\text{ }\mu\text{m}$ , need to be imaged. Hence, for more straightforward applications, such an extensive analysis might not be necessary, and a usable imaging system with appropriate parameters could be readily found and used.

In the following chapters, the proposed imaging technologies are restricted to primarily mobile-phone-based, lens-based, and lens-free platforms, as signified by the shaded red region in Figure 1.4. The introduced systems will be used for imaging of microorganisms and cells within open and confined spaces, and will operate within the span of spatial resolution and FOV indicated by the region boundaries.

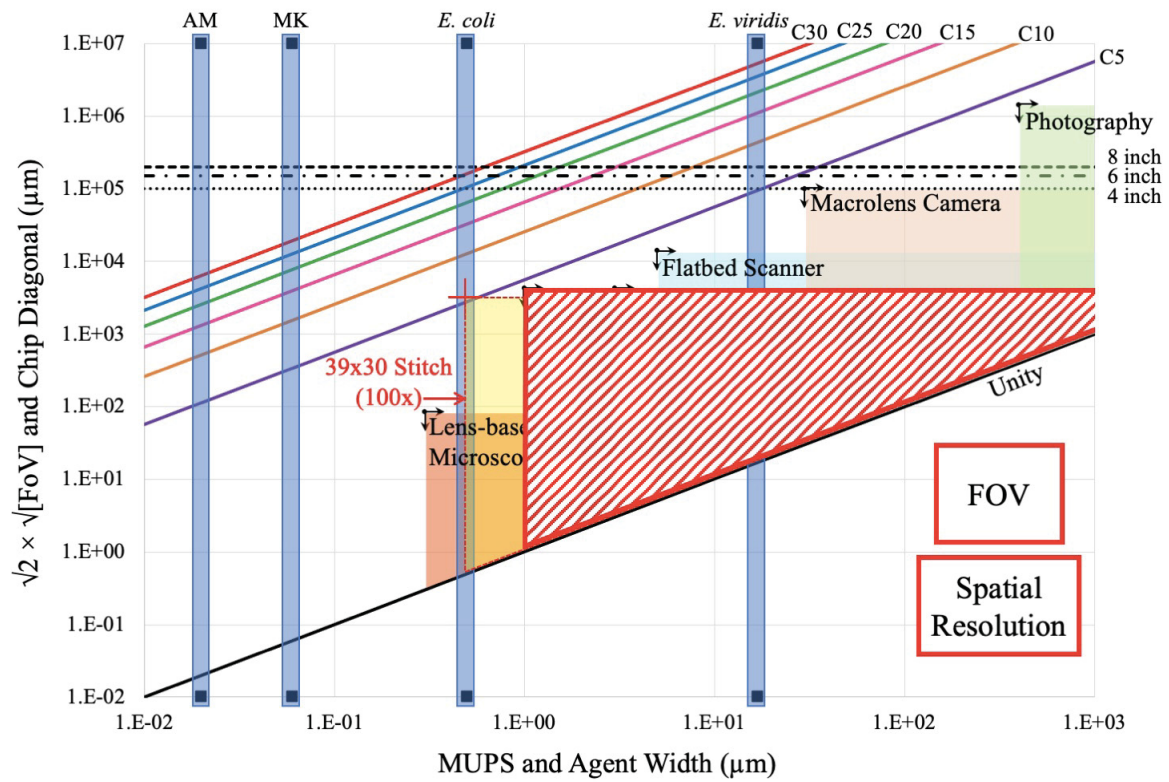


Figure 1.4: The area marked in red delineates the window of spatial resolution and FOV that the imaging platforms described in the following chapters operate within.

## References

- [1] W. J. Croft, *Under the microscope: a brief history of microscopy*. World Scientific, 2006, vol. 5.
- [2] Y. D. Ivanov, T. O. Pleshakova, I. D. Shumov, A. F. Kozlov, I. A. Ivanova, A. A. Valueva, V. Y. Tatur, M. V. Smelov, N. D. Ivanova, and V. S. Ziborov, “Afm imaging of protein aggregation in studying the impact of knotted electromagnetic field on a peroxidase,” *Scientific Reports*, vol. 10, no. 1, pp. 1–9, 2020.
- [3] J. Sanderson, *Understanding light microscopy*. John Wiley & Sons, 2019.
- [4] D. B. Murphy, *Fundamentals of light microscopy and electronic imaging*. John Wiley & Sons, 2002.
- [5] H. Nyquist, “Certain topics in telegraph transmission theory,” *Transactions of the American Institute of Electrical Engineers*, vol. 47, no. 2, pp. 617–644, 1928.
- [6] R. W. Cole, T. Jinadasa, and C. M. Brown, “Measuring and interpreting point spread functions to determine confocal microscope resolution and ensure quality control,” *Nature protocols*, vol. 6, no. 12, pp. 1929–1941, 2011.
- [7] R. P. Nieuwenhuizen, K. A. Lidke, M. Bates, D. L. Puig, D. Grünwald, S. Stallinga, and B. Rieger, “Measuring image resolution in optical nanoscopy,” *Nature methods*, vol. 10, no. 6, pp. 557–562, 2013.
- [8] A. C. Descloux, K. S. Grussmayer, and A. Radenovic, “Parameter-free image resolution estimation based on decorrelation analysis,” *Nature Methods*, vol. 16, no. ARTICLE, pp. 918–924, 2019.
- [9] I. de Kernier, A. Ali-Cherif, N. Rongeat, O. Cioni, S. Morales, J. Savatier, S. Monneret, and P. Blandin, “Large field-of-view phase and fluorescence mesoscope with microscopic resolution,” *Journal of biomedical optics*, vol. 24, no. 3, p. 036 501, 2019.
- [10] Y. Wan, K. McDole, and P. J. Keller, “Light-sheet microscopy and its potential for understanding developmental processes,” *Annual review of cell and developmental biology*, vol. 35, pp. 655–681, 2019.
- [11] J. N. Stirman, I. T. Smith, M. W. Kudenov, and S. L. Smith, “Wide field-of-view, multi-region, two-photon imaging of neuronal activity in the mammalian brain,” *Nature biotechnology*, vol. 34, no. 8, pp. 857–862, 2016.

- [12] S. Eom, S. Sanami, R. Bise, C. Pascale, Z. Yin, S.-i. Huh, E. Osuna-Highley, S. N. Junkers, C. J. Helfrich, P. Y. Liang, *et al.*, “Phase contrast time-lapse microscopy datasets with automated and manual cell tracking annotations,” *Scientific data*, vol. 5, no. 1, pp. 1–12, 2018.
- [13] J. Chalfoun, M. Majurski, T. Blattner, K. Bhadriraju, W. Keyrouz, P. Bajcsy, and M. Brady, “Mist: Accurate and scalable microscopy image stitching tool with stage modeling and error minimization,” *Scientific reports*, vol. 7, no. 1, pp. 1–10, 2017.
- [14] P. Kask, K. Palo, C. Hinnah, and T. Pommerenke, “Flat field correction for high-throughput imaging of fluorescent samples,” *Journal of microscopy*, vol. 263, no. 3, pp. 328–340, 2016.
- [15] A. Greenbaum, W. Luo, T.-W. Su, Z. Göröcs, L. Xue, S. O. Isikman, A. F. Coskun, O. Mudanyali, and A. Ozcan, “Imaging without lenses: Achievements and remaining challenges of wide-field on-chip microscopy,” *Nature methods*, vol. 9, no. 9, pp. 889–895, 2012.
- [16] Z. Göröcs and A. Ozcan, “On-chip biomedical imaging,” *IEEE reviews in biomedical engineering*, vol. 6, pp. 29–46, 2012.
- [17] T.-W. Su, S. O. Isikman, W. Bishara, D. Tseng, A. Erlinger, and A. Ozcan, “Multi-angle lensless digital holography for depth resolved imaging on a chip,” *Optics express*, vol. 18, no. 9, pp. 9690–9711, 2010.
- [18] J. Kun, M. Smieja, B. Xiong, L. Soleymani, and Q. Fang, “The use of motion analysis as particle biomarkers in lensless optofluidic projection imaging for point of care urine analysis,” *Scientific reports*, vol. 9, no. 1, pp. 1–12, 2019.
- [19] X. Cui, L. M. Lee, X. Heng, W. Zhong, P. W. Sternberg, D. Psaltis, and C. Yang, “Lensless high-resolution on-chip optofluidic microscopes for caenorhabditis elegans and cell imaging,” *Proceedings of the National Academy of Sciences*, vol. 105, no. 31, pp. 10 670–10 675, 2008.
- [20] T. Tanaka, T. Saeki, Y. Sunaga, and T. Matsunaga, “High-content analysis of single cells directly assembled on cmos sensor based on color imaging,” *Biosensors and Bioelectronics*, vol. 26, no. 4, pp. 1460–1465, 2010.
- [21] J. Garcia-Sucerquia, W. Xu, S. K. Jericho, P. Klages, M. H. Jericho, and H. J. Kreuzer, “Digital in-line holographic microscopy,” *Applied optics*, vol. 45, no. 5, pp. 836–850, 2006.
- [22] M. Kanka, R. Riesenberger, and H. Kreuzer, “Reconstruction of high-resolution holographic microscopic images,” *Optics letters*, vol. 34, no. 8, pp. 1162–1164, 2009.

- [23] A. Ozcan and U. Demirci, “Ultra wide-field lens-free monitoring of cells on-chip,” *Lab on a Chip*, vol. 8, no. 1, pp. 98–106, 2008.
- [24] G. Stybayeva, O. Mudanyali, S. Seo, J. Silangcruz, M. Macal, E. Ramanculov, S. Dandekar, A. Erlinger, A. Ozcan, and A. Revzin, “Lensfree holographic imaging of antibody microarrays for high-throughput detection of leukocyte numbers and function,” *Analytical chemistry*, vol. 82, no. 9, pp. 3736–3744, 2010.
- [25] Y. Zhang, H. C. Koydemir, M. M. Shimogawa, S. Yalcin, A. Guziak, T. Liu, I. Oguz, Y. Huang, B. Bai, Y. Luo, *et al.*, “Motility-based label-free detection of parasites in bodily fluids using holographic speckle analysis and deep learning,” *Light: Science & Applications*, vol. 7, no. 1, pp. 1–18, 2018.
- [26] T.-W. Su, A. Erlinger, D. Tseng, and A. Ozcan, “Compact and light-weight automated semen analysis platform using lensfree on-chip microscopy,” *Analytical chemistry*, vol. 82, no. 19, pp. 8307–8312, 2010.
- [27] R. Delacroix, S. N. A. Morel, L. Hervé, T. Bordy, J.-M. Dinten, M. Drancourt, and C. Allier, “Cerebrospinal fluid lens-free microscopy: A new tool for the laboratory diagnosis of meningitis,” *Scientific reports*, vol. 7, no. 1, pp. 1–8, 2017.
- [28] W. Xu, M. Jericho, I. Meinertzhagen, and H. Kreuzer, “Digital in-line holography for biological applications,” *Proceedings of the National Academy of Sciences*, vol. 98, no. 20, pp. 11 301–11 305, 2001.
- [29] A. F. Coskun, T.-W. Su, and A. Ozcan, “Wide field-of-view lens-free fluorescent imaging on a chip,” *Lab on a Chip*, vol. 10, no. 7, pp. 824–827, 2010.
- [30] O. Mudanyali, E. McLeod, W. Luo, A. Greenbaum, A. F. Coskun, Y. Hennequin, C. P. Allier, and A. Ozcan, “Wide-field optical detection of nanoparticles using on-chip microscopy and self-assembled nanolenses,” *Nature photonics*, vol. 7, no. 3, p. 247, 2013.
- [31] F. Kazemzadeh and A. Wong, “Laser light-field fusion for wide-field lensfree on-chip phase contrast microscopy of nanoparticles,” *Scientific reports*, vol. 6, no. 1, pp. 1–6, 2016.
- [32] T. Aidukas, R. Eckert, A. R. Harvey, L. Waller, and P. C. Konda, “Low-cost, sub-micron resolution, wide-field computational microscopy using open-source hardware,” *Scientific reports*, vol. 9, no. 1, pp. 1–12, 2019.
- [33] G. Jin, I.-H. Yoo, S. P. Pack, J.-W. Yang, U.-H. Ha, S.-H. Paek, and S. Seo, “Lens-free shadow image based high-throughput continuous cell monitoring technique,” *Biosensors and Bioelectronics*, vol. 38, no. 1, pp. 126–131, 2012.

- [34] A. Greenbaum, Y. Zhang, A. Feizi, P.-L. Chung, W. Luo, S. R. Kandukuri, and A. Ozcan, “Wide-field computational imaging of pathology slides using lens-free on-chip microscopy,” *Science translational medicine*, vol. 6, no. 267, 267ra175–267ra175, 2014.
- [35] M. Roy, D. Seo, C.-H. Oh, M.-H. Nam, Y. J. Kim, and S. Seo, “Low-cost telemedicine device performing cell and particle size measurement based on lens-free shadow imaging technology,” *Biosensors and Bioelectronics*, vol. 67, pp. 715–723, 2015.
- [36] A. Shanmugam and C. D. Salthouse, “Lensless fluorescence imaging with height calculation,” *Journal of Biomedical Optics*, vol. 19, no. 1, p. 016 002, 2014.
- [37] M. Roy, D. Seo, S. Oh, J.-W. Yang, and S. Seo, “A review of recent progress in lens-free imaging and sensing,” *Biosensors and Bioelectronics*, vol. 88, pp. 130–143, 2017.
- [38] W. Bishara, T.-W. Su, A. F. Coskun, and A. Ozcan, “Lensfree on-chip microscopy over a wide field-of-view using pixel super-resolution,” *Optics express*, vol. 18, no. 11, pp. 11 181–11 191, 2010.
- [39] W. Bishara, U. Sikora, O. Mudanyali, T.-W. Su, O. Yaglidere, S. Luckhart, and A. Ozcan, “Holographic pixel super-resolution in portable lensless on-chip microscopy using a fiber-optic array,” *Lab on a Chip*, vol. 11, no. 7, pp. 1276–1279, 2011.
- [40] G. Zheng, S. A. Lee, Y. Antebi, M. B. Elowitz, and C. Yang, “The epetri dish, an on-chip cell imaging platform based on subpixel perspective sweeping microscopy (spsm),” *Proceedings of the National Academy of Sciences*, vol. 108, no. 41, pp. 16 889–16 894, 2011.
- [41] A. C. Sobieranski, F. Inci, H. C. Tekin, M. Yuksekkaya, E. Comunello, D. Cobra, A. Von Wangenheim, and U. Demirci, “Portable lensless wide-field microscopy imaging platform based on digital inline holography and multi-frame pixel super-resolution,” *Light: Science & Applications*, vol. 4, no. 10, e346, 2015.
- [42] C. S. Williams and O. A. Becklund, *Introduction to the optical transfer function*. SPIE Press, 2002, vol. 112.
- [43] H.-C. Shih, T.-A. Lee, H.-M. Wu, P.-L. Ko, W.-H. Liao, and Y.-C. Tung, “Microfluidic collective cell migration assay for study of endothelial cell proliferation and migration under combinations of oxygen gradients, tensions, and drug treatments,” *Scientific reports*, vol. 9, no. 1, pp. 1–10, 2019.
- [44] R. Rusconi, M. Garren, and R. Stocker, “Microfluidics expanding the frontiers of microbial ecology,” *Annual review of biophysics*, vol. 43, pp. 65–91, 2014.

- [45] M. Binz, A. P. Lee, C. Edwards, and D. V. Nicolau, “Motility of bacteria in microfluidic structures,” *Microelectronic Engineering*, vol. 87, no. 5-8, pp. 810–813, 2010.
- [46] J. Taktikos, H. Stark, and V. Zaburdaev, “How the motility pattern of bacteria affects their dispersal and chemotaxis,” *PloS one*, vol. 8, no. 12, e81936, 2013.
- [47] H. C. Berg, *Random walks in biology*. Princeton University Press, 1993.
- [48] G. Saxena, R. N. Bharagava, G. Kaithwas, and A. Raj, “Microbial indicators, pathogens and methods for their monitoring in water environment,” *Journal of water and health*, vol. 13, no. 2, pp. 319–339, 2015.
- [49] D. V. Nicolau, M. Lard, T. Korten, F. C. van Delft, M. Persson, E. Bengtsson, A. Månsson, S. Diez, and H. Linke, “Parallel computation with molecular-motor-propelled agents in nanofabricated networks,” *Proceedings of the National Academy of Sciences*, vol. 113, no. 10, pp. 2591–2596, 2016.
- [50] A. Tero, S. Takagi, T. Saigusa, K. Ito, D. P. Bebbler, M. D. Fricker, K. Yumiki, R. Kobayashi, and T. Nakagaki, “Rules for biologically inspired adaptive network design,” *Science*, vol. 327, no. 5964, pp. 439–442, 2010.
- [51] G. Du, Q. Fang, and J. M. den Toonder, “Microfluidics for cell-based high throughput screening platforms—a review,” *Analytica chimica acta*, vol. 903, pp. 36–50, 2016.
- [52] L. Eamer, R. Nosrati, M. Vollmer, A. Zini, and D. Sinton, “Microfluidic assessment of swimming media for motility-based sperm selection,” *Biomicrofluidics*, vol. 9, no. 4, p. 044113, 2015.
- [53] F. C. Van Delft, G. Ipolitti, D. V. Nicolau Jr, A. Sudalaiyadum Perumal, O. Kašpar, S. Kheireddine, S. Wachsmann-Hogiu, and D. V. Nicolau, “Something has to give: Scaling combinatorial computing by biological agents exploring physical networks encoding np-complete problems,” *Interface focus*, vol. 8, no. 6, p. 20180034, 2018.

# Chapter 2

## Dual-phone illumination-imaging system for high resolution and large field of view multi-modal microscopy

### 2.1 Preface

Given the **trade-off between spatial resolution and field-of-view (FOV)**, and the physical limitations in terms of aberrations that are constituent to lens-based systems, a combination of small sensor pixel size, large sensor area, and appropriate lens specifications can yield an imaging system that provides high spatial resolution with a large FOV. Moreover, with the use of practical systems such as mobile phones, imaging, as well as illumination could be simplified.

This chapter introduces a practical **mobile phone-based illumination-imaging platform** that allows for the **multi-modal imaging** of microorganisms, cells, and microfluidic channels. It uses the camera of one phone for imaging at high resolution and large FOV, and the screen of another to generate illumination modalities, including **bright-field, dark-field, Rheinberg illumination, point illumination, and fluorescence microscopy**. The manuscript describes the microscopy setup in detail, highlighting both its qualitative and quantitative imaging capabilities, as well as its potential applications within the lab and out in the field. The figures show bright-field images of microorganisms within microfluidic devices of various geometries, images of cells with bright-field, dark-field, and Rheinberg illumination, and a facile method for agent speed calculations using long-exposure images.

---

This chapter was taken in full from the following paper:

S. Kheireddine, A. S. Perumal, Z. J. Smith, D. V. Nicolau, and S. Wachsmann-Hogiu, “**Dual-phone illumination-imaging system for high resolution and large field of view multi-modal microscopy**,” *Lab on a Chip*, vol. 19, no. 5, pp. 825–836, 2019.

## 2.2 Manuscript details

Title: “**Dual-phone illumination-imaging system for high resolution and large field of view multi-modal microscopy**”

Journal: *Lab on a Chip*

Published online: January 30, 2019

DOI: <https://doi.org/10.1039/C8LC00995C>

URL: <https://pubs.rsc.org/en/content/articlelanding/2019/lc/c8lc00995c>

## 2.3 Authors and affiliations

Sara Kheireddine <sup>a</sup>, Ayyappasamy Sudalaiyadum Perumal <sup>a</sup>, Zachary J. Smith <sup>b</sup>, Dan V. Nicolau <sup>\*a</sup> and Sebastian Wachsmann-Hogiu <sup>\*ac</sup>

\* Corresponding authors

<sup>a</sup> Department of Bioengineering, McGill University, Montreal, Quebec, Canada

**E-mail:** [dan.nicolau@mcgill.ca](mailto:dan.nicolau@mcgill.ca), [sebastian.wachsmannhogiu@mcgill.ca](mailto:sebastian.wachsmannhogiu@mcgill.ca)

<sup>b</sup> Department of Precision Machinery and Precision Instrumentation, University of Science and Technology of China, Hefei, China

<sup>c</sup> Department of Pathology and Laboratory Medicine, University of California Davis, Davis, CA, USA

## 2.4 Abstract

In this paper we present for the first time a system comprised of two mobile phones, one for illumination and the other for microscopy, as a portable, user-friendly, and cost-effective microscopy platform for a wide range of applications. Versatile and adaptive illumination is made with a Retina display of an Apple mobile phone device. The phone screen is used to

project various illumination patterns onto the specimen being imaged, each corresponding to a different illumination mode, such as bright-field, dark-field, point illumination, Rheinberg illumination, and fluorescence microscopy. The second phone (a Nokia phone) is modified to record microscopic images about the sample. This imaging platform provides a high spatial resolution of at least  $2\ \mu\text{m}$ , a large field-of-view of  $3.6 \times 2.7\ \text{mm}$ , and a working distance of  $0.6\ \text{mm}$ . We demonstrate the performance of this platform for the visualization of microorganisms within microfluidic devices to gather qualitative and quantitative information regarding microorganism morphology, dimension, count, and velocity/trajectories in the x-y plane.

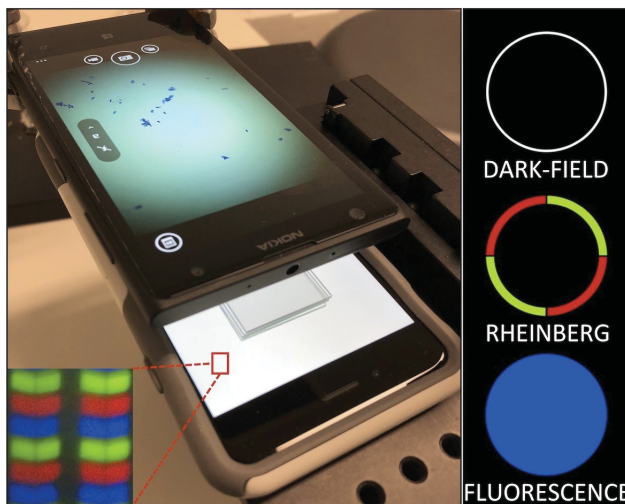


Figure 2.1: Graphical abstract

## 2.5 Introduction

There is a compelling need for an imaging system that can provide simultaneously high spatial resolution and large field of view (FOV) at a moderate cost. This need manifests itself in biomedical application areas such as reading well plates for colorimetric assays or cell cultures, where high spatial resolution is required for observing cell morphology and subcellular structures. In addition, a large FOV is required to survey large sample areas for high throughput screening [54], histopathology [55], embryology, where phenotypic screening in transgenic mice is performed by monitoring of embryo organogenesis [56], and developmental biology [57]. Moreover, in neuroscience, brain sectioning is used as a means to identify specific brain networks involved in behaviours or functions via reconstruction of neural wiring diagrams [58], which also requires a large FOV for accurate reconstruction and high spatial resolution for precise identification of these paths.

Lens-based imaging approaches are faced with a trade-off between resolution and field-of-view (FOV). Generally, the greater the resolvable detail in a sample, the smaller the FOV we can observe. To delineate this, in a totally incoherent imaging system (such as in fluorescence microscopy), a 100x microscope objective lens with numerical aperture (NA) of 1.4 offers a theoretical resolution of  $0.25\ \mu\text{m}$ , with a FOV diameter of  $\approx 60\ \mu\text{m}$ , whereas a typical 2x objective with NA of 0.05 provides a theoretical resolution of  $6\ \mu\text{m}$ , with a FOV diameter of 1.5 cm. While low magnification, large NA objectives are available, they typically have large costs and may lead to pixel-limited rather than optically limited performance due to their high space-bandwidth products. Furthermore, beyond fluorescence imaging, in a partially coherent system such as in Bright-Field or phase imaging, both the NA of the objective and the NA of the condenser need to be taken into consideration. The resolving power of the microscope in this case is determined by:

$$D = \frac{1.22\lambda}{(\text{condenser NA} + \text{objective NA})} \quad (2.1)$$

where  $D$  is the minimum resolved distance in  $\mu\text{m}$ , and  $\lambda$  is the wavelength in  $\mu\text{m}$ . Consequently, spatial resolution, and therefore image quality, is not only dependent on the specifications of the lens system in use, but also on the illumination [4].

Due to this imposed trade-off between resolution and field of view, at high resolutions, the sample would have to be imaged in sections and then the image mosaic-assembled via stitching techniques. Image stitching or mosaicking includes two steps: image registration and image merging, with the latter adjusting for non-uniform brightness within the images and blending the images in a way that ensures uniform transitions from one tile to the next [59]. Merging the individual partitions into a large FOV in this manner, however, takes a long time and often results in a checkboard-like pattern in the final mosaic because of differences in illumination in adjacent images, with the inhomogeneities being most apparent at the edges of the stitched images, as well as image focus errors within parts of the sample having various depths, as is common in biological samples [56]. While low-cost three-dimensional microscope systems have been reported, their increased complexity presents a barrier to adoption [60]. Flatbed scanners have also been used to achieve ultra-widefield imaging at high resolution [61]–[67], but often require extensive post-purchase modification, and have slow scanning speeds. This is particularly relevant for applications that require recording image sequences or real-time tracking where partitioning the FOV would lead to loss of valuable data.

On the other hand, lens-free approaches allow for better resolution and larger FOV than lens-based ones since they can make use of the full potential of the image sensor,

without being limited by lens specifications. As such, using an image sensor with a large area and a small pixel size is crucial for large FOV and high resolution, respectively. Lens-free microscopy also offers cost-effectiveness, portability, and depth-resolved three-dimensional (3D) imaging [68]. This approach is particularly useful for applications that require heavy statistical analysis. Moreover, the lens-free system design can also be adapted for a number of applications, such as fluorescence imaging [29], and imaging *S. pombe* yeast cells [69] and *C. elegans* [19] within microfluidic devices. However, they require extensive data post-processing and complex reconstruction methods that may present a barrier for non-experts.

Cameras of mobile phones, meanwhile, create a lens-based platform that is more than the sum of its parts – a standalone imaging system capable of data transmission, which in addition to being portable, makes it invaluable specifically in resource-limited settings. Consequently, mobile phone based imaging has been applied in areas related to health, the environment, and education [70]. In terms of biomedical applications, mobile phone imaging has been used as tool for partial blood counts [71], complete blood counts [72], fluorescence detection of *Giardia lamblia* water-borne protozoan parasites [73], and soil-transmitted helminths (*Ascaris lumbricoides*, *Trichuris trichiura*, and hookworm) in stool samples [74], as well as diagnosis of malaria [75], sickle cell anaemia [54], and dermatological disease [76]. As for environmental applications, a mobile phone based system was developed for imaging a plasmonic colorimetric assay that performs mercury(ii) detection in water samples [77]. Phone based systems have also been used for imaging microfluidic devices, such as for detection of Salmonella [78], and imaging microfluidic-based enzyme-linked immunosorbent assay (ELISA) used for the detection of a food contaminant [79]. Thus, mobile-phone microscopy might be seen as an intermediate point between traditional microscopy and lens-free methods. However, mobile phone microscopy has traditionally used simple LED illumination, generally optimized for a single imaging type, such as fluorescence, bright field, or dark field.

Illumination is often one of the most critical determinants of image quality in microscopy, and may need to be dynamically adapted based on the requirements of the sample. Unstained mammalian cells, for instance, can be more clearly distinguished using dark-field (DF) or phase-contrast (PC) illumination, rather than using bright-field (BF) illumination. Other samples may find certain wavelengths phototoxic, or require narrow-band excitation to provide greater contrast. In general, such illumination modes require additional microscopy hardware such as condenser annuli in multiple sizes to accommodate objectives with different numerical apertures (NAs), and specialized PC objectives, which makes such setups relatively restrictive in how adaptive they can be. To overcome this, programmable light-emitting diode (LED) arrays have been used as adaptive illumination sources that offer more imaging flexibility [80]. These arrays have also been adapted to allow for real-time acqui-

sition of image sequences using time-multiplexed LED illumination [81]. Moreover, specific modifications of the LED illumination allows for extracting quantitative phase information via differential phase contrast (DPC) [82].

In this paper, we demonstrate for the first time that two mobile phones can be combined to create a simple microscopy platform with high resolution, large field-of-view, and dynamically adaptive illumination. For our imaging system, we used the Retina display of an Apple device (iPhone 6) as a versatile illumination source. The screen, which is composed of high density RGB LEDs, is used to project various illumination patterns onto the specimen being imaged, each corresponding to a different illumination mode, with a second phone (a Nokia Lumia 1020) capturing the resulting image. The patterns include BF, DF, point illumination (PI), Rheinberg illumination (RI), and fluorescence microscopy. Not only does this illumination setup allow for design and projection of a variety of patterns with ease, but it permits creativity in terms of production and testing of novel illumination patterns or structures, and merging multiple illumination modes together, and is overall simpler to control and use than an LED array.

We use a Nokia Lumia 1020 mobile phone as a portable, user-friendly, and cost-effective imaging platform with high spatial resolution and large FOV. As such, our system presents great potential to cater for a wide range of applications. We show that, in contrast with traditional microscopy, for an objective lens with a comparable FOV, the Nokia phone offers better resolution. Moreover, the system can capture standard (720p) or full (1080p) high-definition (HD) image sequences (videos) at rates of 24, 25, and 30 frames per second (fps), in addition to images at long exposure times of up to 4 seconds.

## 2.6 Results and discussion

### 2.6.1 Description of the imaging platform

To build an imaging system that is capable of high spatial resolution and a large FOV, we used the Nokia Lumia 1020, which has a 41.3-megapixel (MP) image sensor with a pixel size of  $1.12\ \mu\text{m}$ , and attached an external lens (iPhone 5 lens:  $\text{NA}=0.23$ ,  $f2.2$ ) for an overall 2x magnification and a theoretical spatial resolution of  $1.3\ \mu\text{m}$ . We assembled this system to image biological specimens in free space or confined in microfluidic devices. For imaging, we place the sample in between the Nokia-lens system (Fig. 2.2(a)) and the illumination source, as shown in the sketch of the optical setup (Fig. 2.2(b)). Fig. 2.2(c) shows the imaging system in use with halogen lamp illumination, and Fig. 2.2(d) and 2.2(e) show the imaging system in use with Retina display illumination.

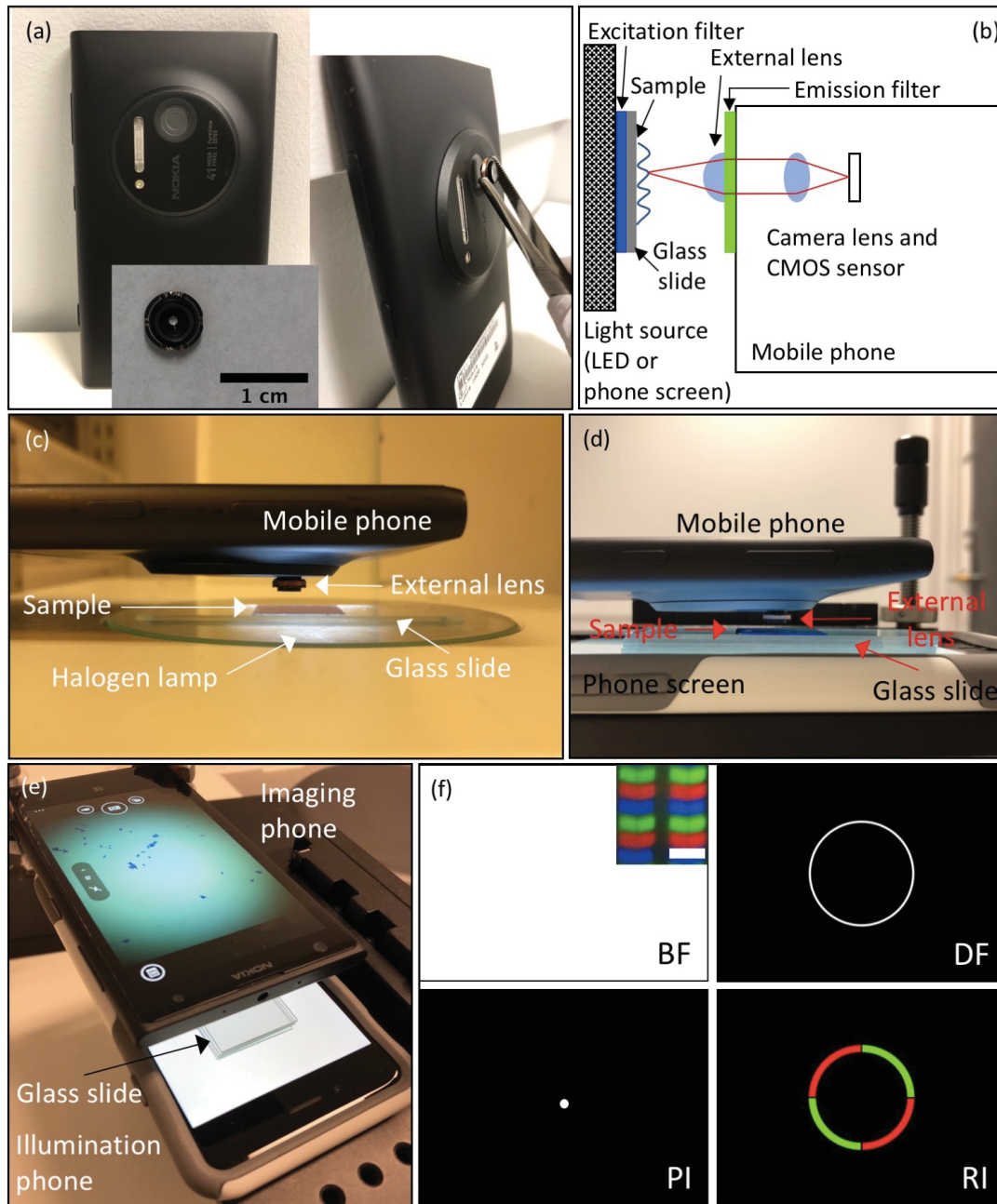


**Figure 2.2: Description of the system and components.** (a) Photograph of the Nokia Lumia 1020 mobile phone, the external lens, and their assembly to form a microscopy system. (b) Sketch of the overall optical setup of the imaging system and the illumination system. (c) Side-view photograph of the imaging phone with external lens assembly with a halogen lamp as an illumination source. (d) Similar arrangement as in (c) but with the Retina display of a second phone used as an illumination source instead. (e) Photograph from a different angle of the arrangement in (d) showing the sample image on the Nokia phone screen obtained with Bright-Field illumination on the Retina display of the bottom phone. (f) Examples of different illumination patterns created on the Retina display, each corresponding to a different illumination mode, such as Bright-Field (BF), Dark-Field (DF), Point Illumination (PI), and Rheinberg Illumination (RI) (coloured-quarters pattern). The inset within the BF illumination pattern shows a microscopic image of the LED pixels on the Retina display obtained with the Nokia microscope, with the scale bar indicating the pixel width of  $\approx 78 \mu\text{m}$ . The RGB patterns of each illumination pixel are clearly resolved.

While the imaging phone-lens system is held in place by a clamp, the sample along with the illumination phone are able to be moved in 3D via a translation stage. More specifically, to image microfluidic devices, we place them onto a glass slide, which in turn is placed directly onto the screen of the illumination phone. For imaging thin samples such as diatoms, *E. gracilis*, or human epithelial cheek cells (HECC), we placed the specimen on a glass slide underneath a cover slip, we need to add three extra glass slides between the slide carrying the sample and the illumination phone screen to provide the necessary distance such that the screen is not in the focus of the imaging system.

## 2.6.2 Description of the illumination system

Microsoft PowerPoint was used to generate various illumination patterns to be displayed on an Apple Retina display as shown in Fig. 2.2(f). For the BF imaging mode, we project a white screen, at the highest screen brightness, where the sample receives uniform illumination throughout. In addition, we designed patterns for PI, DF, and RI. PI was achieved by creating a very small white full circle on a black background. For DF illumination, on the other hand, we drew a ring of a size just outside the NA of the imaging lens. We created single (DF-single), double (DF-double), and triple (DF-triple) ring illumination patterns by drawing concentric white rings on a black background.

RI is similar to DF, but whereas DF relies on a ring of white light contrasted against a dark specimen background, the RI utilizes a ring of coloured light contrasted against a specimen background of a different color. These contrasting colors are specimen-dependent, and are typically chosen to maximally enhance the specimen image without the need for specimen staining. RI also includes rings that have multiple colors (two-sector or four-sector patterns) against a dark specimen background. We designed RI patterns where we used coloured rings, and coloured the area inside the ring as well. We also sectioned rings into halves or quarters to make two- or four-sector patterns.

Retina display illumination allows for ease of pattern design without any limitations in terms of the shape, size, or color. Since multiple shapes can be created with PowerPoint, virtually endless patterns can be generated and tested with different samples. This makes our illumination platform more versatile than an LED array. Moreover, this platform is just as portable as our imaging system and thus this combined setup can be tested in various settings outside the laboratory, which makes it particularly useful in low-resource environments.

Whereas the patterns we used in screen illumination were mostly classic illumination patterns, this platform provides the option for simple experimentation with a variety of creative patterns, as well as combinations of multiple patterns. For example, Zheng et al.

recently developed a method of obtaining large FOV, high-resolution intensity and phase images from stained and unstained samples, using a computation method dubbed Fourier Ptychography Microscopy (FPM) [83]–[86]. Critically, the illumination must come from sets of LEDs turned on and off by an LED array. The method could be easily adapted to the dynamic illuminator described here, substantially simplifying implementation of FPM for applications in low-resource settings.

Similarly, Tian and Waller recently described the use of an LED array to create a quantitative phase imaging system with rather high image quality [87]. Again, by replacing the LED array requiring an external microcontroller with a simple phone screen that can be controlled through an app, the implementation of their method in low-resource settings where trained experts may be lacking could be a substantial benefit.

### **2.6.3 System characterization for spatial resolution, field-of-view (FOV) and working distance (WD)**

We determined the spatial resolution of the Nokia phone-lens system under different illumination conditions by mounting the external lens onto the Nokia phone camera, and imaging a 1951 USAF resolution test chart, once using halogen lamp illumination (Fig. 2.3(c)), and another time using the Retina display illumination (Fig. 2.3(d)). The Nokia-lens system was held in place by a clamp, and we placed the resolution chart, along with the illumination phone, if applicable, onto a translation stage. We then moved the stage until the line pairs on the chart were in focus, and took the images.

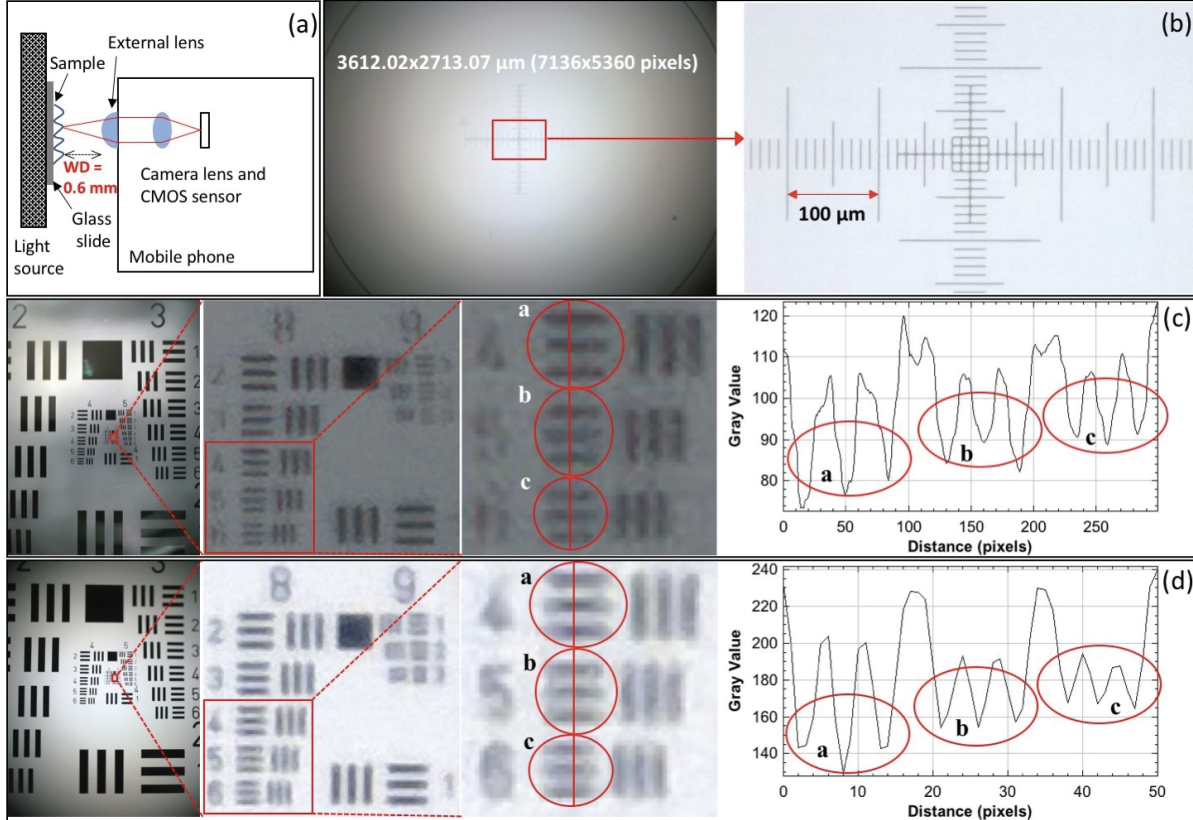


Figure 2.3: **System characterization for spatial resolution, field-of-view (FOV) and working distance (WD).** (a) Optical setup indicating the working distance (WD) of the system. (b) Image of the stage micrometer that was used to determine the FOV. (c) Image of the 1951 USAF resolution test chart taken with the phone-lens system using halogen lamp illumination. From left to right, subsequent insets are shown with the image on the right providing a cross-section of the circles highlighting the lowest resolved groups (group 8, elements 4, 5, and 6). These cross sections are used to determine the spatial resolution of the system. (d) Similar photograph, with Retina display illumination in Bright-Field mode (white screen).

Fig. 2.3 also shows a plot of intensity profiles of the line pairs in the resulting images generated by using the Fiji (ImageJ) software. We observed that our system is capable of spatially resolving 406.4 line pairs per millimetre (lp/mm) (group 8, element 5) with halogen lamp illumination (Fig. 2.3(c)), and 362.0 lp/mm (group 8, element 4) with Retina display illumination (Fig. 2.3(d)); therefore, both illumination approaches provide us with a comparable spatial resolution of below  $2\ \mu\text{m}$ . If the spatial resolution were assessed qualitatively, however, up to element 1 of group 9 can be resolved by eye in both cases, which corresponds to a spatial resolution of 512.0 lp/mm. Moreover, we used a stage micrometer and Fiji (ImageJ) software to measure the FOV, as shown in Fig. 2.3(b), and determined it to be  $\approx 3.6 \times 2.7\ \text{mm}$ . Furthermore, we characterized the WD to be 0.6 mm in air (Fig. 2.3(a)).

Given the low magnification in our system (2x), the system requires small pixels in order to Nyquist sample the optical point spread function. Therefore, to achieve high resolution

with large FOV, a system with a large number of small pixels is required. In terms of system hardware, the image sensor of the Nokia Lumia 1020 is currently one of the largest on the market (41.3 MP), that in combination with a 1.12  $\mu\text{m}$  pixel size provides both high spatial resolution and large FOV.

#### 2.6.4 Application to imaging of microorganisms in microfluidic devices

As a potential application, we imaged multiple microorganisms in various microfluidic structures under different illumination conditions. We chose to image two species: *E. gracilis* and *E. coli*. Since *E. gracilis* have relatively large physical dimensions ( $\approx 15 \mu\text{m}$  width), this makes them a good sample for testing the image quality of the microscopy system. Moreover, because these microorganisms are pigmented, and their bodies scatter light well, they serve as an ideal sample for use in testing the DF and RI capabilities of the imaging system. On the other hand, in the case of *E. coli*, because of their small physical dimensions ( $\approx 0.5 \mu\text{m}$  width), they are a good candidate for demonstrating the high spatial resolution of the system.

These organisms are studied in complex environments to learn about their motility and behaviour. In this article, we show that our illumination-imaging system can be used to observe them in confined spaces, such as channels or plazas of microfluidic devices, to provide valuable data about their behaviour. Depending on the device design, different aspects of the microorganism can be studied. For instance, we used devices with straight channels of various widths ranging from 50 to 450  $\mu\text{m}$  that provide information about the movement trajectory of microorganisms. We also used for our experiments microfluidic devices that have micro-fabricated pillars (50  $\mu\text{m}$  pillar diameter), which are typically used for observing traffic and group motility behaviour in microorganisms. Moreover, we imaged a microfluidic device with 2  $\mu\text{m}$ -wide channels that was previously designed for parallel exploration by biological agents [53], [88]. Finally, wide areas with borders, such as plazas, provide an idea of the affinity of microorganisms for walls or corners, and can also be used to perform particle counts and dimension measurements.

Figure 2.4 shows microscopic images of these microorganisms in the microfluidic devices described before. In order to demonstrate the utility of the illumination with the Retina display, we show images of *E. gracilis* and *E. coli* with Retina display illumination (Fig. 2.4(a) - left) and halogen lamp illumination (Fig. 2.4(b) and 2.4(c)). We also compared images of *E. gracilis* in a microfluidic device with multi-sized channels taken with the phone imaging system (Fig. 2.4(a) - left) and with an Olympus IX83 microscope (4x magnification

with  $NA = 0.16$ ) (Fig. 2.4(a) - right). The results suggest that for a comparable FOV, the phone system demonstrates superior image quality compared with the traditional microscope (Fig. 2.4(a) - insets). We also took images of *E. gracilis* in a microfluidic device with pillars and were able to observe chloroplasts in individual *E. gracilis* (Fig. 2.4(b)). Moreover, we imaged *E. coli* within a microfluidic device. Our system was able to resolve intricate details within the device junctions (Fig. 2.4(c) - left), as well as individual *E. coli* in the plaza areas (Fig. 2.4(c) - right).

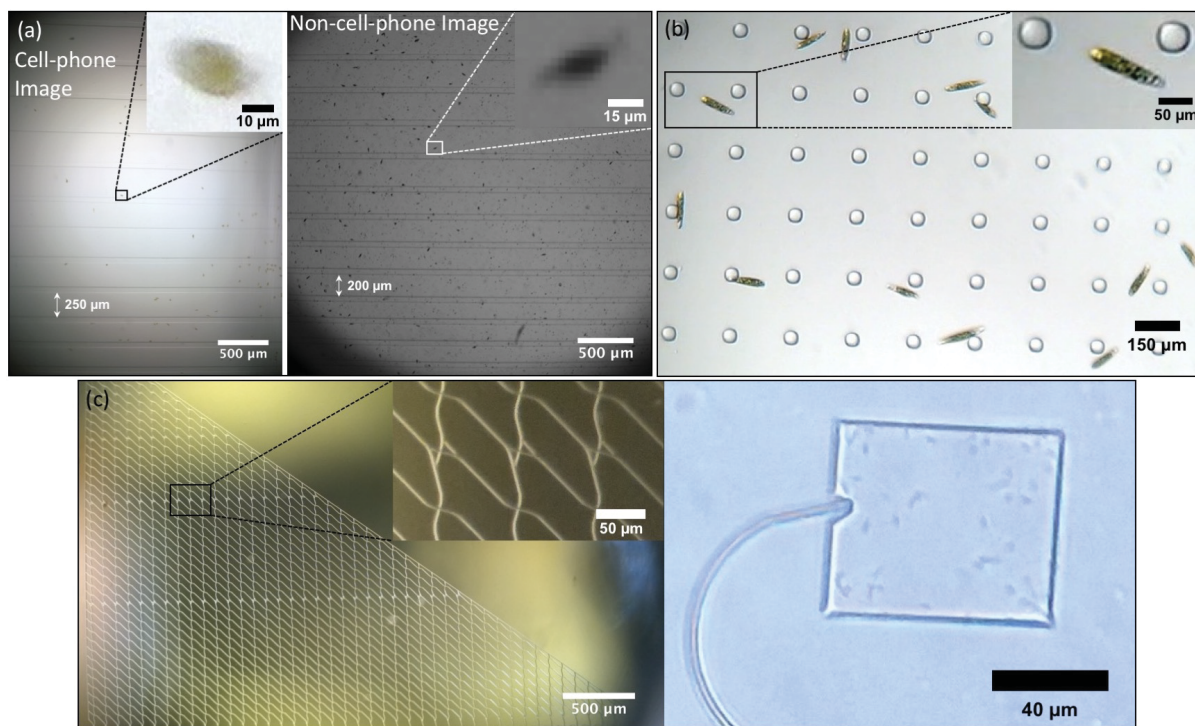


Figure 2.4: **Application to imaging of microorganisms in microfluidic devices.** (a) Comparison of images of *E. gracilis* in a microfluidic device with multi-sized channels taken with the Nokia phone-lens system (Retina display illumination) (left) and with the Olympus IX83 microscope (4x magnification with  $NA = 0.16$ ) (right). The insets show zoomed-in images of individual *E. gracilis*. (b) Image of *E. gracilis* in a microfluidic device with pillars (halogen lamp illumination). The inset shows a zoomed-in image of *E. gracilis*. (c) Image of a microfluidic device taken with the Nokia phone-lens system (halogen lamp illumination), where the inset shows a zoomed-in image of the device junctions (left). Image of the plaza region of the same device, where the inset shows a zoomed-in image of *E. coli* in the plaza (right).

## 2.6.5 Application to imaging cells with different illumination patterns

In the previous section we presented images of microorganisms in microfluidic devices with a Retina display illumination in BF mode and a Nokia phone microscope. In order to observe the range of capabilities of Retina display illumination, we used our microscopy-

illumination system with different types of cells, and imaged them under various illumination conditions. We imaged thin samples of diatoms, *E. gracilis*, and Human Epithelial Cheek Cells (HECC) under a cover slip. Diatoms were tested in powder form because they form highly variable and heterogeneous samples. HECC are particularly interesting because, as translucent mammalian cells, they are difficult to observe in BF mode. We used illumination patterns such as white screen (BF), single-, double-, and triple-rings (DF), and coloured rings encircling differently coloured backgrounds (RI), as well as two-sector or four-sector circles with multi-coloured sectors (RI). These contrasting colors in RI are chosen depending on the specimen being imaged to enhance the specimen-background contrast. The resulting images are shown in Figure 2.5.

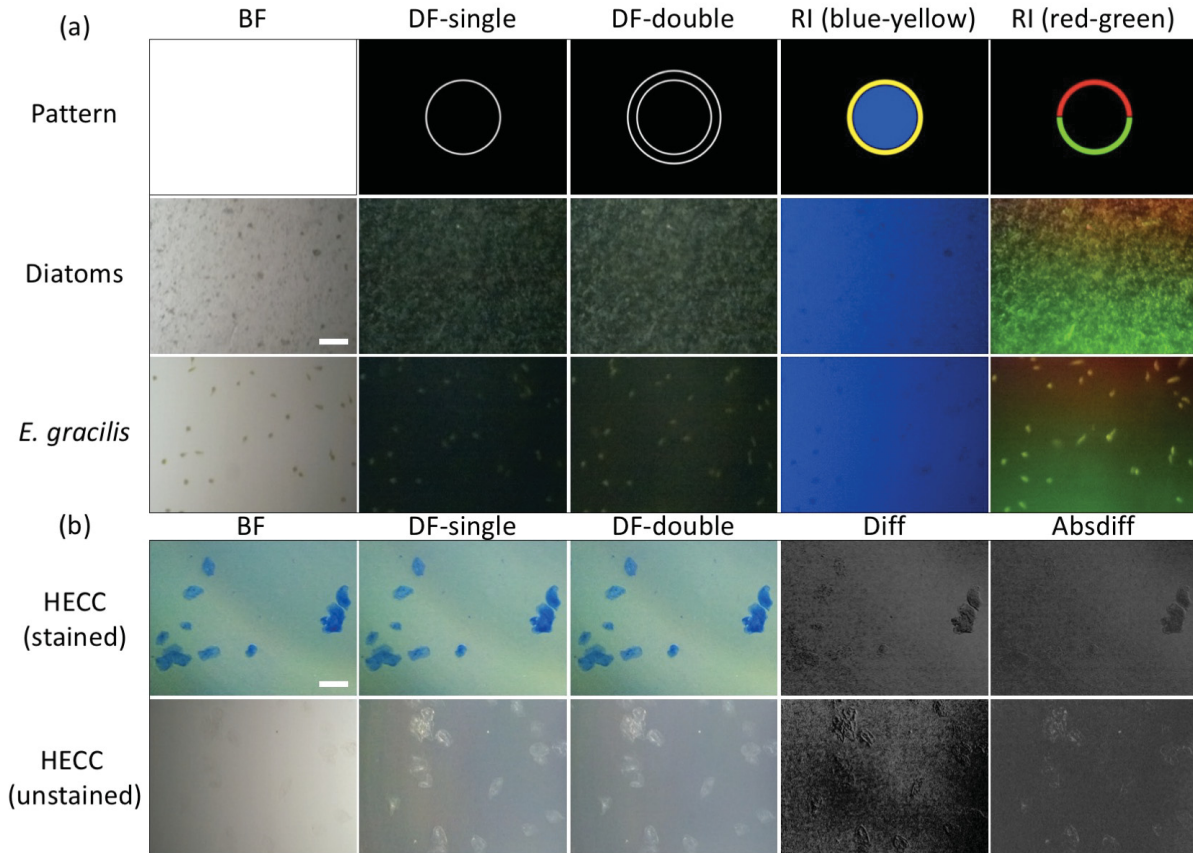


Figure 2.5: **Application to imaging cells with different illumination patterns.** (a) Zoomed-in and cropped images of diatoms, and *E. gracilis* under Bright-Field (BF), Dark-Field (DF) and Rheinberg (RI) illumination patterns (second and third rows). These illumination patterns were created with the Retina display and are shown in the top row. We used single Dark-Field (DF-single), and double Dark-Field (DF-double) ring illumination patterns (second and third columns). Different forms of RI were prepared: blue-yellow patterns (fourth column), and half-rings with multiple colors (red-green half-rings pattern) against a dark specimen background (fifth column). (b) Zoomed-in and cropped images of stained (methyl blue) and unstained Human Epithelial Cheek Cells (HECC) under Bright-Field (BF) and Dark-Field (DF) illumination patterns. Subtracted images formed with single Dark-Field (DF-single) illumination pattern (second column) from images formed with double Dark-Field (DF-double) ring illumination pattern (third column) using regular arithmetic difference (Diff) or absolute difference (Absdiff), which resulted in the images shown in the fourth and fifth columns respectively. These images show an effect similar to that of image embossing. Both scale bars indicate 125  $\mu\text{m}$ .

Figure 2.5(a) shows digitally zoomed and cropped images of diatoms and *E. gracilis* under BF, DF and RI illumination patterns (Fig. 2.5(a), second and third rows). The illumination patterns as projected on the Retina display are shown in the top row of the figure. We used single Dark-Field (DF-single), double Dark-Field (DF-double) ring illumination patterns (second and third columns). Moreover, we prepared different forms of RI: yellow ring with blue background (fourth column), and red-green half-rings pattern against a dark specimen background (fifth column). Figure 2.5(b) shows digitally zoomed and cropped images

of stained and unstained HECC under BF and DF illumination patterns. Images formed with single Dark-Field (DF-single) ring illumination pattern (Fig. 2.5(b), second column) were subtracted from images formed with double Dark-Field (DF-double) ring illumination pattern (Fig. 2.5(b), third column) in MATLAB using regular arithmetic difference (Diff) or absolute difference (Absdiff), which resulted in an effect similar to that of image embossing (Fig. 2.5(b), fourth and fifth columns).

Our choice of imaging samples was intended to test the extent of our system capabilities in terms of spatial resolution and contrast enhancement. In the case of *E. gracilis*, a qualitative assessment of the images shows that the microorganisms are easier to observe with the green pattern compared to the blue pattern. This can be attributed to the presence of chloroplasts in *E. gracilis*, which are green in color, and therefore reflect green light well. Moreover, with diatoms, the blue background highlighted the intact diatoms within the diatom powder mixture. Additionally, for HECC, DF images provided much better contrast than BF images, and the embossing-like effect that we achieved with subtraction of double- and single-ring DF images further enhances visual cell detection. These results verify the adaptability of our imaging-illumination system to different types of specimens with varying optical properties.

### 2.6.6 Application to quantitative analysis of microorganism motility

The still images we showed previously can provide us with qualitative information regarding cell/microorganism morphology, and quantitative information such as cell/microorganism dimensions and count. However, when it comes to calculating velocities of microorganisms, image sequences (videos) would have to be taken instead, and particle tracking would have to be done between successive video frames. Particle tracking is typically time consuming and can be particularly difficult in areas where there is a large number of microorganisms with overlapping trajectories. In order to overcome this, we took still images of motile specimens with long exposure times to help us determine their velocities and trajectories in the x-y plane. In a long-exposure image, the trajectory that a microorganism follows is highlighted over a predetermined period of time.

First, we took a DF image with the maximum exposure time of 4 seconds of the motile *E. gracilis* sample, and then converted it to 8-bit in Fiji (ImageJ) and performed background correction to better highlight the trajectories. Using the Simple Neurite Tracer plug-in [89] in the Fiji (ImageJ) software, we traced the microorganism trajectories semi-automatically, where we specified various beginning and end points for each trajectory, and the plug-in would then predict the overall trajectory from these points. After tracing several hundred

trajectories of *E. gracilis*, we exported the trace length values we got in pixels, converted these values to micrometers using the predetermined scale of our imaging system, and calculated the respective speeds by taking the exposure time used into account. We then plotted a histogram with the speed distributions of the microorganisms, with the error bars indicating the standard deviation from the mean trajectory length of all the analysed images per bin.

Figure 2.6(a) shows the DF image we took of *E. gracilis* with 4 s exposure time, where the microorganism trajectories can be observed. Fig. 2.6(b) shows the processed image after background correction and tracing of the *E. gracilis* paths, where the individual trajectories are highlighted in green. After using data from 10 different images and exporting 20 trajectories per image, we constructed a histogram of the speed distribution of *E. gracilis* using these 200 data points (Fig. 2.6(c)). The error bars in the histogram indicate the standard deviation from the mean of all the images per bin. As such, we determined the average speed of *E. gracilis* to be  $\approx 90 \mu\text{m/s}$ , with a standard deviation of  $\approx 24 \mu\text{m/s}$ , which is consistent with values previously reported in the literature [90].

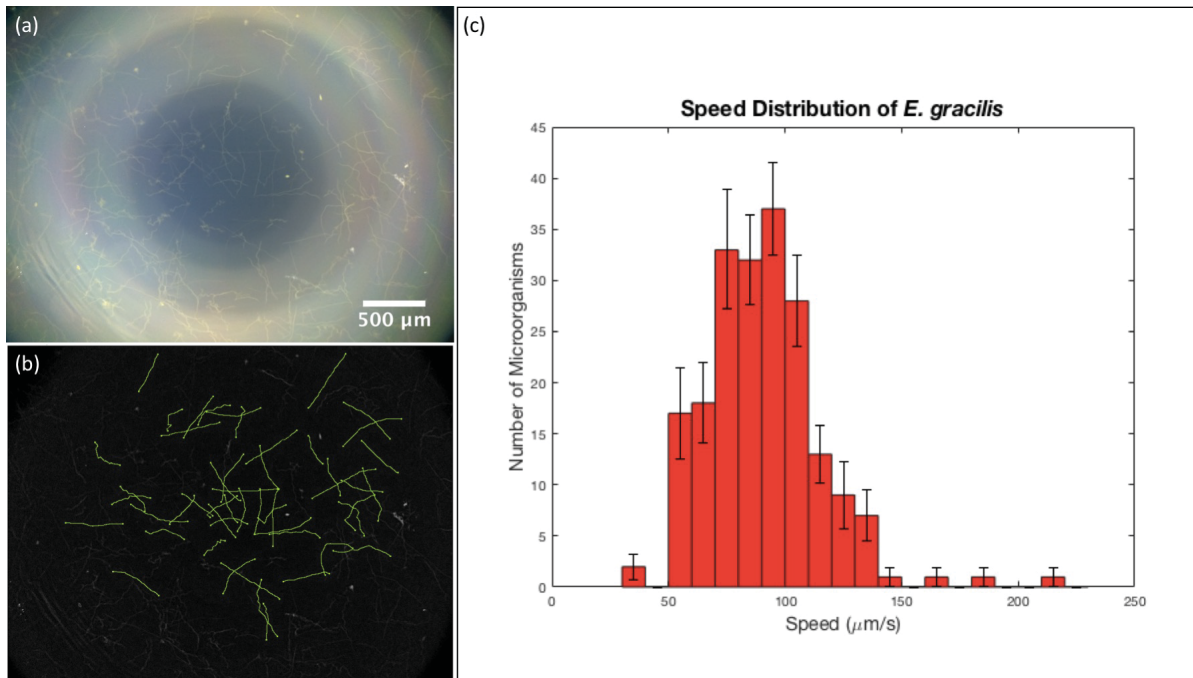


Figure 2.6: **Application to quantitative analysis of microorganism motility.** (a) DF image of *E. gracilis* with maximum exposure time (4 seconds), where the trajectories of the microorganisms can be observed. (b) Resulting image from (a) after image background correction and trajectory tracing using the Simple Neurite Tracer plug-in in Fiji (ImageJ) software, where the trajectories are highlighted in green. Here we show 50 trajectories. (c) Histogram of the speed distribution of *E. gracilis*, with the error bars indicating the standard deviation from the mean trajectory length of all the analysed images per bin (c). To construct this histogram, we used data from 10 images and exported 20 trajectories per image.

### 2.6.7 Application to fluorescence microscopy

Fluorescence is a valuable imaging technique for biological samples that can be used to determine cell viability and activity, to distinguish a specific cell type or multiple cell types within a mixture of cells, and to track cells. The addition of fluorescence capability to this simple and versatile phone illumination-imaging system will make this technique suitable for a range of applications in the field where fluorescence needs to be detected.

Here we demonstrate fluorescence imaging of both microfluidic structures and cells using the dual phone illumination-imaging system. The illumination is performed with a solid, blue-coloured 15 mm circle generated with the retina display screen. The luminance of a typical screen is in the order of hundreds of  $\text{cd}/\text{m}^2$ , and since we only use the blue emitters, the luminous intensity of the blue illumination circle is in the order of  $1 \times 10^{-2}$  cd. This allows us to use the Nokia phone microscope to record fluorescence images of a fluorescein dye solution inside microfluidic devices with varying channel shapes and sizes (Fig. 2.7(a) and 2.7(b)). In addition, we used the same system to record fluorescence images of CMFDA-stained HEK 293 cells and compared those with images obtained with an Olympus IX83 microscope (10x magnification with  $\text{NA} = 0.4$ ) (Fig. 2.7(c)).

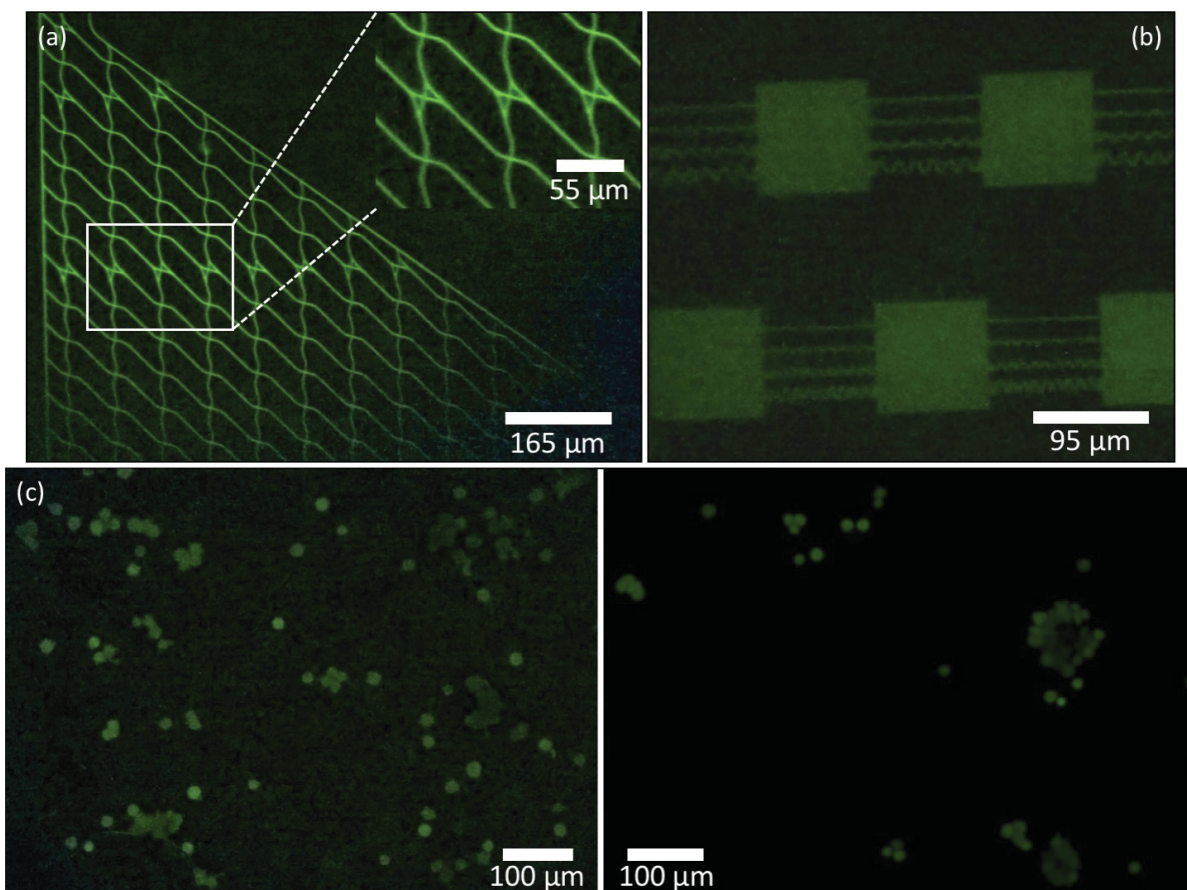


Figure 2.7: **Application to fluorescence microscopy.** (a) Zoomed-in and cropped fluorescence image of a microfluidic device taken with the Nokia phone-lens system (Retina display illumination) with fluorescein dye solution in the plaza regions and channels. The inset shows a zoomed-in image of the device junctions, similar to Fig. 2.4(c) - left. (b) Zoomed-in and cropped fluorescence image of a microfluidic device with fluorescein dye solution in plaza regions and multi-shaped channels (Retina display illumination). (c) Comparison of zoomed-in and cropped fluorescence images of CMFDA-stained HEK 293 cells taken with the Nokia phone-lens system (Retina display illumination) (left) and with the Olympus IX83 microscope (10x magnification with  $NA = 0.4$ ) (right).

## 2.7 Experimental

### 2.7.1 Imaging

For imaging, we used a Nokia Lumia 1020, which has a 41.3-megapixel (MP) image sensor with a pixel size of  $1.12\mu\text{m}$ , and attached an external lens (iPhone 5 lens:  $NA = 0.23$ ,  $f2.2$ , 2x magnification) to the camera to improve focus, which limits the theoretical spatial resolution of our system to  $1.3\mu\text{m}$ . For illumination, we used a 120 mm Retina display of an Apple device (iPhone 6), with a pixel density of 326 pixels per inch (PPI) which translates

to an RGB pixel size of  $\approx 78 \mu\text{m}$ . The imaging phone-lens system is held in place by a clamp, and the sample along with the illumination phone is placed onto an XYZ-translation stage (Thorlabs Inc.) for simple directional manipulation. The pictures were taken using the Lumia Camera application. Characterization of the phone system for spatial resolution was done using 1951 USAF resolution test chart (Edmund Optics). Characterization of FOV and WD was done using a stage micrometer (Motic) and cover slips (Fisherbrand,  $150 \mu\text{m}$  thickness), respectively.

### 2.7.2 Illumination

Patterns to be projected onto the Retina display are designed using the Microsoft PowerPoint application for iOS. Different patterns correspond to different imaging illumination modes. BF mode is attained by projecting a white screen, at the highest brightness, where the sample has uniform illumination throughout. DF illumination is typically achieved with ring illumination, where the ring lies just outside the NA of the objective lens. We created single (DF-single), double (DF-double), and triple (DF-triple) ring illumination patterns by drawing concentric white rings on a black background.

RI is similar to DF, but whereas DF relies on a ring of white light contrasted against a dark specimen background, RI utilizes a ring of coloured light contrasted against a specimen background of a different color. These contrasting colors are specimen-dependent, and are typically chosen to maximally enhance the specimen image without the need for specimen staining. RI also includes rings that have multiple colors (two-sector or four-sector patterns) against a dark specimen background. Designs can be expanded to include more coloured sectors per circle. PI can be accomplished by drawing and filling a small white circle on a black background.

### 2.7.3 Fluorescence imaging

To adapt the system for fluorescence, we used a fluorescence excitation filter (Chroma, 470/40 nm) inserted between the illumination phone screen and the sample, and a fluorescence emission filter (Chroma, 525/50 nm) between the imaging phone camera and the external lens.

For illumination of fluorescent samples, we prepared and used a blue-coloured filled circle with a diameter of approximately 15 mm on the illumination phone screen. To observe fluorescence within microfluidic devices, we added a 2.7 mM solution of fluorescein dye (Sigma-Aldrich) into the channels. As for cells, we used CellTracker<sup>TM</sup> Green CMFDA dye (Thermo Fisher Scientific) and followed the staining protocol for cells in suspension specified by the

manufacturer to stain HEK 293 cells. The final working concentration of the dye was 25  $\mu\text{M}$ . All fluorescence images were recorded with an exposure time of 4 s with the mobile phone and 10 ms with the Olympus IX83 microscope.

#### 2.7.4 Microfluidics

Our microfluidic devices are fabricated using soft lithography. Polydimethylsiloxane (PDMS) (Sylgard<sup>®</sup> 184) is mixed in a 10:1 polymer to crosslinker ratio, poured onto silica masters (designed and written at the Kavli Institute of Nanoscience Delft, The Netherlands), and cured overnight in an oven at 60 °C. The cured PDMS is then cut and peeled from the masters, and bonded to glass cover slips (Fisherbrand, 150  $\mu\text{m}$  thickness) using plasma treatment for 30 to 45 seconds. Next, the finished device is pre-wet with a medium suitable for the microorganism to be used, by adding 50 to 100  $\mu\text{L}$  of medium onto the cover slip of the device, and placing it in a vacuum chamber for 30 minutes. The device is then ready for use in experiments.

#### 2.7.5 Microorganisms

For the microorganisms that we used in testing our imaging system, namely *Escherichia coli* and *Euglena gracilis*, we acquired the *E. coli* 437 strain from Prof. Howard C. Berg's laboratory at Harvard University, and we purchased *E. gracilis* from Carolina Biological Supply Company (USA). We grow *E. coli* colonies on Luria-Bertani (LB)-agar Petri dishes at 37 °C and *E. gracilis* in liquid Provasoli's enriched seawater (PES) medium at room temperature. For using *E. coli* in experiments, we inoculate a single colony in 4–6 mL of LB and incubate it at 37 °C overnight. On the day of the experiment, the liquid culture can either be directly pipetted onto the microfluidic device, or if its optical density is too high, then it can be diluted in LB to a more suitable concentration. The diluted mixture should then be further incubated at 37 °C for anywhere between half an hour to three hours, depending on the concentration, until the bacteria regain their growth and motility. On the other hand, *E. gracilis* can be directly used in experiments by pipetting a few microliters of the microorganism from its liquid culture onto the microfluidic device. LB and PES media were prepared according to the protocols mentioned in the Handbook of Culture Media for Food and Water Microbiology [91].

### 2.7.6 Cell lines

To prepare unstained human epithelial cheek cell (HECC) samples, we pipette 50  $\mu\text{L}$  of Milli-Q water onto a glass slide (Globe Scientific Inc., 1.1 mm thickness), and place the cells directly onto the water drop, then add a cover slip on top. The HECC were harvested by swabbing the inside of the cheek using a toothpick. To prepare stained HECC samples, we follow the same procedure, but we use 50  $\mu\text{L}$  of methylene blue (Bio Basic Inc.) solution (0.1% W/V) instead of Milli-Q water. For diatoms and *E. gracilis*, we pipette 50  $\mu\text{L}$  from a diatom suspension in Milli-Q water (1% W/V) or from *E. gracilis* suspension in PES medium, respectively, directly onto a glass slide, and then add a cover slip on top. The HEK 293 cells we used for fluorescence imaging were obtained from Prof. Amine Kamen's laboratory at McGill University.

## 2.8 Conclusion

In this manuscript we report for the first time the combination of two mobile phones to provide a simple, versatile, and portable microscopy system that uses the screen of one phone for illumination and the camera of the other phone for imaging. While the phone screen illumination allows for facile generation of illumination patterns that can be used in different microscopy modalities, the imaging phone provides high spatial resolution and large FOV. With this system we demonstrate imaging of cells, microorganisms in microfluidic structures, as well as accurately determine their velocities. Overall, the design and construction of this system allows for substantial integration and miniaturization of the illumination-imaging components into a portable and user-friendly device.

The imaging system is based on a Nokia Lumia 1020 with an attached external lens (iPhone 5 lens: NA = 0.23, f2.2) yielding an overall 2x magnification and a theoretical spatial resolution limit of 1.3  $\mu\text{m}$ . This platform has an image sensor with 41.3 MP and 1.12  $\mu\text{m}$  pixel size, with a spatial resolution of at least 2  $\mu\text{m}$ , a field-of-view of  $3.6 \times 2.7$  mm, and a working distance of 0.6 mm. We used this device in combination with a Retina display (iPhone 6) illumination system to project multiple illumination patterns such as bright-field, dark-field, Rheinberg, and point illumination. To demonstrate the capabilities of this system, we imaged *E. gracilis* and *E. coli* within microfluidic devices, diatoms, and human epithelial cheek cells. We also measured the velocities of *E. gracilis* using images recorded with long exposure times, and determined that they agree with previously reported data. Finally, we demonstrated that with this simple screen illumination, fluorescence microscopy can be performed as well.

These results verify the aforementioned capabilities of our Nokia-lens imaging system with Retina display illumination and demonstrate a range of applications that this system can be used for. While our choice of phones was based on their specifications, other phones and combinations of phones can also be used. In particular, various patterns of illumination can be easily obtained with other smartphone displays as well, adding to the versatility of the microscopy platform. Obvious imaging applications for this platform include microfluidics, motility studies of microorganisms, and cell analysis. Based on the results we showed, potential applications for our systems could include blood counts, downstream cell analysis, and reading colorimetric assays. This last application may especially benefit from a well-controlled illuminator, as quantifying colorimetric assays depends critically on an illumination source with stable, well-calibrated color characteristics [92].

This new imaging-illumination microscopy system, by virtue of its portability and versatility, can complement or even replace heavy and complex microscopes, in addition to being relatively inexpensive and adaptive. Our system can serve as a platform for further development, where it can be adapted for other applications as well, and would be especially advantageous in low-resource settings.

## 2.9 Conflicts of interest

There are no conflicts to declare.

## 2.10 Acknowledgements

This work was financially supported by the Defense Advanced Research Projects Agency (DARPA) under Grant Agreement No. HR0011-16-2-0028 (to D. V. N.) and by the National Sciences and Engineering Research Council of Canada (NSERC), Discovery Grant RGPIN-2018-05675 (to S. W.-H.). S. K. acknowledges the McGill Engineering Doctoral Award (MEDA).

## References

- [4] D. B. Murphy, *Fundamentals of light microscopy and electronic imaging*. John Wiley & Sons, 2002.
- [19] X. Cui, L. M. Lee, X. Heng, W. Zhong, P. W. Sternberg, D. Psaltis, and C. Yang, “Lensless high-resolution on-chip optofluidic microscopes for caenorhabditis elegans and cell imaging,” *Proceedings of the National Academy of Sciences*, vol. 105, no. 31, pp. 10 670–10 675, 2008.
- [29] A. F. Coskun, T.-W. Su, and A. Ozcan, “Wide field-of-view lens-free fluorescent imaging on a chip,” *Lab on a Chip*, vol. 10, no. 7, pp. 824–827, 2010.
- [53] F. C. Van Delft, G. Ipolitti, D. V. Nicolau Jr, A. Sudalaiyadum Perumal, O. Kašpar, S. Kheireddine, S. Wachsmann-Hogiu, and D. V. Nicolau, “Something has to give: Scaling combinatorial computing by biological agents exploring physical networks encoding np-complete problems,” *Interface focus*, vol. 8, no. 6, p. 20 180 034, 2018.
- [54] D. N. Breslauer, R. N. Maamari, N. A. Switz, W. A. Lam, and D. A. Fletcher, “Mobile phone based clinical microscopy for global health applications,” *PloS one*, vol. 4, no. 7, e6320, 2009.
- [55] S. A. Sekula-Gibbs and M. A. Shearer, “Sentinel node biopsy should be offered in thin melanoma with mitotic rate greater than one,” *Dermatologic Surgery*, vol. 37, no. 8, pp. 1080–1088, 2011.
- [56] G. McConnell, J. Trägårdh, R. Amor, J. Dempster, E. Reid, and W. B. Amos, “A novel optical microscope for imaging large embryos and tissue volumes with sub-cellular resolution throughout,” *Elife*, vol. 5, e18659, 2016.
- [57] Z. Liu and P. J. Keller, “Emerging imaging and genomic tools for developmental systems biology,” *Developmental cell*, vol. 36, no. 6, pp. 597–610, 2016.
- [58] S. Pacheco, C. Wang, M. K. Chawla, M. Nguyen, B. K. Baggett, U. Utzinger, C. A. Barnes, and R. Liang, “High resolution, high speed, long working distance, large field of view confocal fluorescence microscope,” *Scientific reports*, vol. 7, no. 1, p. 13 349, 2017.
- [59] F. Legesse, O. Chernavskaiia, S. Heuke, T. Bocklitz, T. Meyer, J. Popp, and R. Heintzmann, “Seamless stitching of tile scan microscope images,” *Journal of microscopy*, vol. 258, no. 3, pp. 223–232, 2015.

- [60] Q. Lu, G. Liu, C. Xiao, C. Hu, S. Zhang, R. X. Xu, K. Chu, Q. Xu, and Z. J. Smith, “A modular, open-source, slide-scanning microscope for diagnostic applications in resource-constrained settings,” *PloS one*, vol. 13, no. 3, e0194063, 2018.
- [61] Z. Göröcs, Y. Ling, M. Dai Yu, D. Karahalios, K. Mogharabi, K. Lu, Q. Wei, and A. Ozcan, “Giga-pixel fluorescent imaging over an ultra-large field-of-view using a flatbed scanner,” *Lab on a Chip*, vol. 13, no. 22, pp. 4460–4466, 2013.
- [62] Z. Göröcs and A. Ozcan, “Biomedical imaging and sensing using flatbed scanners,” *Lab on a Chip*, vol. 14, no. 17, pp. 3248–3257, 2014.
- [63] X. Ou, G. Zheng, and C. Yang, “0.5 gigapixel microscopy using a flatbed scanner: Erratum,” *Biomedical optics express*, vol. 7, no. 2, p. 646, 2016.
- [64] T. Shimobaba, H. Yamanashi, T. Kakue, M. Oikawa, N. Okada, Y. Endo, R. Hirayama, N. Masuda, and T. Ito, “In-line digital holographic microscopy using a consumer scanner,” *Scientific reports*, vol. 3, p. 2664, 2013.
- [65] C. Zhang and K. S. Suslick, “A colorimetric sensor array for organics in water,” *Journal of the American Chemical Society*, vol. 127, no. 33, pp. 11 548–11 549, 2005.
- [66] G. Zheng, X. Ou, and C. Yang, “0.5 gigapixel microscopy using a flatbed scanner,” *Biomedical optics express*, vol. 5, no. 1, pp. 1–8, 2014.
- [67] K. Sullivan, J. Kloess, C. Qian, D. Bell, A. Hay, Y. P. Lin, and Y. Gu, “High throughput virus plaque quantitation using a flatbed scanner,” *Journal of virological methods*, vol. 179, no. 1, pp. 81–89, 2012.
- [68] A. Ozcan and E. McLeod, “Lensless imaging and sensing,” *Annual review of biomedical engineering*, vol. 18, pp. 77–102, 2016.
- [69] S. Seo, T.-W. Su, D. K. Tseng, A. Erlinger, and A. Ozcan, “Lensfree holographic imaging for on-chip cytometry and diagnostics,” *Lab on a Chip*, vol. 9, no. 6, pp. 777–787, 2009.
- [70] J. C. Contreras-Naranjo, Q. Wei, and A. Ozcan, “Mobile phone-based microscopy, sensing, and diagnostics,” *IEEE Journal of Selected Topics in Quantum Electronics*, vol. 22, no. 3, pp. 1–14, 2015.
- [71] Z. J. Smith, K. Chu, A. R. Espenson, M. Rahimzadeh, A. Gryshuk, M. Molinaro, D. M. Dwyre, S. Lane, D. Matthews, and S. Wachsmann-Hogiu, “Cell-phone-based platform for biomedical device development and education applications,” *PloS one*, vol. 6, no. 3, e17150, 2011.

- [72] T. Gao, Z. J. Smith, T.-y. Lin, D. Carrade Holt, S. M. Lane, D. L. Matthews, D. M. Dwyre, J. Hood, and S. Wachsmann-Hogiu, “Smart and fast blood counting of trace volumes of body fluids from various mammalian species using a compact, custom-built microscope cytometer,” *Analytical chemistry*, vol. 87, no. 23, pp. 11 854–11 862, 2015.
- [73] H. Zhu, O. Yaglidere, T.-W. Su, D. Tseng, and A. Ozcan, “Wide-field fluorescent microscopy on a cell-phone,” in *2011 Annual International Conference of the IEEE Engineering in Medicine and Biology Society*, IEEE, 2011, pp. 6801–6804.
- [74] I. I. Bogoch, J. R. Andrews, B. Speich, J. Utzinger, S. M. Ame, S. M. Ali, and J. Keiser, “Mobile phone microscopy for the diagnosis of soil-transmitted helminth infections: A proof-of-concept study,” *The American journal of tropical medicine and hygiene*, vol. 88, no. 4, pp. 626–629, 2013.
- [75] C. W. Pirnstill and G. L. Coté, “Malaria diagnosis using a mobile phone polarized microscope,” *Scientific reports*, vol. 5, p. 13 368, 2015.
- [76] R. R. Jahan-Tigh, G. M. Chinn, and R. P. Rapini, “A comparative study between smartphone-based microscopy and conventional light microscopy in 1021 dermatopathology specimens,” *Archives of pathology & laboratory medicine*, vol. 140, no. 1, pp. 86–90, 2016.
- [77] Q. Wei, R. Nagi, K. Sadeghi, S. Feng, E. Yan, S. J. Ki, R. Caire, D. Tseng, and A. Ozcan, “Detection and spatial mapping of mercury contamination in water samples using a smart-phone,” *ACS nano*, vol. 8, no. 2, pp. 1121–1129, 2014.
- [78] T. San Park, W. Li, K. E. McCracken, and J.-Y. Yoon, “Smartphone quantifies salmonella from paper microfluidics,” *Lab on a Chip*, vol. 13, no. 24, pp. 4832–4840, 2013.
- [79] A. Chen, R. Wang, C. R. Bever, S. Xing, B. D. Hammock, and T. Pan, “Smartphone-interfaced lab-on-a-chip devices for field-deployable enzyme-linked immunosorbent assay,” *Biomicrofluidics*, vol. 8, no. 6, p. 064 101, 2014.
- [80] G. Zheng, C. Kolner, and C. Yang, “Microscopy refocusing and dark-field imaging by using a simple led array,” *Optics letters*, vol. 36, no. 20, pp. 3987–3989, 2011.
- [81] Z. Liu, L. Tian, S. Liu, and L. Waller, “Real-time brightfield, darkfield, and phase contrast imaging in a light-emitting diode array microscope,” *Journal of biomedical optics*, vol. 19, no. 10, p. 106 002, 2014.

- [82] N. Lue, W. Choi, G. Popescu, T. Ikeda, R. R. Dasari, K. Badizadegan, and M. S. Feld, “Quantitative phase imaging of live cells using fast fourier phase microscopy,” *Applied Optics*, vol. 46, no. 10, pp. 1836–1842, 2007.
- [83] S. Dong, R. Shiradkar, P. Nanda, and G. Zheng, “Spectral multiplexing and coherent-state decomposition in fourier ptychographic imaging,” *Biomedical optics express*, vol. 5, no. 6, pp. 1757–1767, 2014.
- [84] S. Dong, Z. Bian, R. Shiradkar, and G. Zheng, “Sparsely sampled fourier ptychography,” *Optics express*, vol. 22, no. 5, pp. 5455–5464, 2014.
- [85] L. Tian, X. Li, K. Ramchandran, and L. Waller, “Multiplexed coded illumination for fourier ptychography with an led array microscope,” *Biomedical optics express*, vol. 5, no. 7, pp. 2376–2389, 2014.
- [86] G. Zheng, R. Horstmeyer, and C. Yang, “Wide-field, high-resolution fourier ptychographic microscopy,” *Nature photonics*, vol. 7, no. 9, p. 739, 2013.
- [87] L. Tian and L. Waller, “Quantitative differential phase contrast imaging in an led array microscope,” *Optics express*, vol. 23, no. 9, pp. 11 394–11 403, 2015.
- [88] D. V. Nicolau, M. Lard, T. Korten, F. C. van Delft, M. Persson, E. Bengtsson, A. Månsson, S. Diez, and H. Linke, “Parallel computation with molecular-motor-propelled agents in nanofabricated networks,” *Proceedings of the National Academy of Sciences*, vol. 113, no. 10, pp. 2591–2596, 2016.
- [89] M. H. Longair, D. A. Baker, and J. D. Armstrong, “Simple neurite tracer: Open source software for reconstruction, visualization and analysis of neuronal processes,” *Bioinformatics*, vol. 27, no. 17, pp. 2453–2454, 2011.
- [90] T. Ogawa, E. Shoji, N. J. Suematsu, H. Nishimori, S. Izumi, A. Awazu, and M. Iima, “The flux of euglena gracilis cells depends on the gradient of light intensity,” *PloS one*, vol. 11, no. 12, e0168114, 2016.
- [91] J. E. Corry, G. D. Curtis, and R. M. Baird, *Handbook of culture media for food and water microbiology*. Royal Society of Chemistry, 2011.
- [92] L. Shen, J. A. Hagen, and I. Papautsky, “Point-of-care colorimetric detection with a smartphone,” *Lab on a Chip*, vol. 12, no. 21, pp. 4240–4243, 2012.

## Chapter 3

# Simple adaptive mobile phone screen illumination for dual phone differential phase contrast (dpDPC) microscopy

### 3.1 Preface

This part of the work extends the capabilities of the dual-phone illumination-imaging system described in the previous chapter to include differential phase contrast imaging, resulting in so-called **dual-phone differential phase contrast (dpDPC) microscopy**. To achieve this, bright semicircles are displayed on the illumination phone screen, and images are taken with complementary semicircular illumination along a single axis, and then mathematically combined using a normalized difference to attain phase contrast images.

The following manuscript describes the process in detail, whereby the figures illustrate how dpDPC compares with DPC performed fully with a traditional microscope, and how screen illumination could be used for DPC with both a mobile phone-based imaging platform, as well as a traditional microscope, with impressive results, which attests to the adaptability of this illumination platform. They also showcase the capability of the system for extraction of qualitative and quantitative information from beads and various mammalian cell types, such as cell contrast and dimension measurements, cell counts, and distinguishing live and dead cells from morphology. This dual-phone setup also shows promise for quantitative phase imaging, but that would require further development in image referencing and analysis.

---

This chapter was taken in full from the following paper:

S. Kheireddine, Z. J. Smith, D. V. Nicolau, and S. Wachsmann-Hogiu, “**Simple adaptive mobile phone screen illumination for dual phone differential phase contrast (DPDPC) microscopy**,” *Biomedical Optics Express*, vol. 10, no. 9, p. 4369, 2019.

## 3.2 Manuscript details

Title: “**Simple adaptive mobile phone screen illumination for dual phone differential phase contrast (DPDPC) microscopy**”

Journal: *Biomedical Optics Express*

Published online: August 02, 2019

DOI: <https://doi.org/10.1364/BOE.10.004369>

URL: <https://www.osapublishing.org/boe/fulltext.cfm?uri=boe-10-9-4369&id=416424>

## 3.3 Authors and affiliations

Sara Kheireddine <sup>1</sup>, Zachary J. Smith <sup>2</sup>, Dan V. Nicolau <sup>1</sup> and Sebastian Wachsmann-Hogiu <sup>1,3,\*</sup>

<sup>1</sup> Department of Bioengineering, McGill University, Montreal, Quebec, H3A 0E9, Canada

<sup>2</sup> Department of Precision Machinery and Precision Instrumentation, University of Science and Technology of China, Hefei, China

<sup>3</sup> Department of Pathology and Laboratory Medicine, University of California Davis, Davis, CA 95616, USA

\* E-mail: [sebastian.wachsmannhogiu@mcgill.ca](mailto:sebastian.wachsmannhogiu@mcgill.ca)

## 3.4 Abstract

Phase contrast imaging is widely employed in the physical, biological, and medical sciences. However, typical implementations involve complex imaging systems that amount to in-line interferometers. We adapt differential phase contrast (DPC) to a dual-phone illumination-imaging system to obtain phase contrast images on a portable mobile phone platform. In this dual phone differential phase contrast (dpDPC) microscope, semicircles are projected

sequentially on the display of one phone, and images are captured using a low-cost, short focal length lens attached to the second phone. By numerically combining images obtained using these semicircle patterns, high quality DPC images with  $\approx 2$  micrometer resolution can be easily acquired with no specialized hardware, circuitry, or instrument control programs.

## 3.5 Introduction

In bright-field microscopy, when imaging pigmented or amplitude samples, the contrast in the resulting images is created due to greater light absorption in the denser regions of the sample, leading to absorption-based optical contrast. However, most biological specimens lack intrinsic absorption contrast and require exogenous staining for visualization. When imaging these transparent samples, light will simply pass through without any amplitude attenuation, which creates little to no contrast in the resulting images, making the sample difficult to observe. As staining is complex to perform in general, several optical methods have been developed to allow visualization of unstained, transparent samples, such as dark-field microscopy, polarized microscopy, and, most commonly, phase contrast (PC) microscopy.

First reported by Frits Zernike in the beginning of the 1930s [93], for which he was awarded the Nobel Prize in 1953, PC microscopy helped drastically improve biological imaging of unstained cells and thin tissue slices. PC microscopy works by interfering light paths that have not interacted with the specimen with those that have. Due to refractive index differences between the sample and the surrounding medium, phase shifts accrued by light passing through the sample are transformed into intensity differences due to this interference process, thus generating optical contrast. While classical PC microscopy requires the addition of annular illumination and conjugate phase rings in the back aperture of the objective, differential interference contrast microscopy [94], [95] requires the use of polarizers and prisms to be able to further highlight small differences in the refractive index within different parts of the sample. Additional exotic configurations exist, such as Hoffman modulation contrast microscopy [96], which uses oblique illumination to amplify contrast in the sample by employing an off-axis slit aperture as well as an optical amplitude spatial filter.

The above-mentioned techniques improve contrast, leading to a qualitative enhancement of the image. Yet, the phase information in the image is purely qualitative, because the interference as measured in these cases lacks a stable reference. However, the ability to obtain quantitative phase information could provide more meaningful criteria for image comparison, as well as useful information about the sample, such as sample height, or dry mass [97]. These potential benefits led to the development of quantitative phase contrast microscopy, or Quantitative Phase Imaging (QPI) [98]–[101], which not only provides contrast, but also

produces phase images, which depict the actual values of the phase shift variations at each pixel in the image. This, in turn, allows the user to extract refractive index values and spatial dimensions of the objects in the image, or to re-cast the data with controllable contrast a posteriori [102].

In the last decade or so, several groups have developed QPI methods, and demonstrated their application to practical problems, including cell-level drug resistance [103], cancer diagnostics and dynamics [104]–[106], red blood cell imaging and characterization [107]–[109], malaria diagnosis [110], [111], among many others. Several groups have extended QPI to compact measurement systems, such as mobile phone-based microscopes [112]–[114], or lab-on-chip devices [115]. While these systems have shown excellent utility, the optical setup for these techniques can be rather complex, bulky, and expensive, generally requiring careful alignment of the optical components, and exotic components such as spatial light modulators. Consequently, there has been increasing interest in simplifying these systems by combining controllable illumination with computational methods to reconstruct quantitative phase images without the need for a stable phase reference or phase shifting interferometry. In particular, recent studies have focused on using spatially variable illumination sources in QPI, such as LED arrays [81] or traditional microscope illuminators coupled to spatially addressable pixelated liquid crystal displays (LCDs) [116]. Using a controllable illumination system and acquiring several images in sequence, with the illumination changing between each image, allows for the computational reconstruction of qualitative [117] and quantitative phase images [87]. Further work has shown that in addition to QPI images, one can use this programmable illumination to recover 3D imaging volumes [118], perform Fourier ptychographic microscopy [85], and correct aberrations within the imaging system. As the illumination system is relatively low cost, such an approach naturally lends itself to small and portable imaging systems, including those built on single-board computing platforms such as mobile phones [119], [120] that can further include deep learning algorithms [121].

However, while the optical configuration in these systems can be quite simple, and thus vastly improve on traditional phase microscopes and QPI systems, a key drawback of the adoption of such methods by non-experts is the complex electronics needed to create and control these spatially variable illumination sources. Previously, we showed that a mobile phone-based microscope [71] could be placed to face a mobile phone screen, where the screen of the second phone is used as a controllable illumination source [122]. Such a dual-phone illumination-imaging microscope could easily mimic traditional microscope modalities such as bright-field, dark-field, and fluorescence, by controlling the color and spatial distribution of the illumination. It also showed the ability to easily obtain quite complex illumination schemes such as Rheinberg illumination. Critically, the illumination source does not require

specialized computer control, a microcontroller, or any associated electronics. A user simply draws the desired illumination pattern as an image, or as a “slide” in Microsoft PowerPoint or a similar presentation program, and the phone natively displays the correct illumination. Switching between illumination schemes is as simple as swiping a finger on the display. Thus, our dual-phone illumination-imaging system is extremely amenable to use by non-experts in field settings.

In this paper, we extend our prior work to phase contrast imaging, where we use one mobile phone for imaging, and another for illumination to generate semi-circular illumination patterns that can be used to compute differential phase contrast (DPC) images. Compared with prior systems [119], [120], our dual phone DPC (dpDPC) system is not only more compact and portable, but the use of a phone screen with densely packed RGB LEDs for illumination instead of an LED array or LCD allows for complex spatial patterns, intensity gradation, and color generation, as well as more pattern options to be explored. These benefits are all obtained without requiring specialized control software or utilizing complex electrical wiring. As detailed below, our system obtains good quality phase contrast images, with resolutions below 2 micrometers, of a wide variety of samples, including polystyrene beads, blood smears, and cell cultures.

## **3.6 Results and discussion**

### **3.6.1 Description of the imaging and illumination platforms**

To build an illumination-imaging platform capable of differential phase contrast (DPC), we adapted the dual-phone illumination-imaging system described in [122], and the asymmetrical illumination DPC generation concept described in [81] to produce images that can be later combined to generate DPC images. To demonstrate the generalizability of the illumination scheme, we performed imaging using a mobile phone microscope as shown in Fig. 3.1(a), as well as using a low-cost traditional microscope with on-board camera module (Fig. 3.1(b)). In both cases the illumination platform consists of the display of a mobile phone.

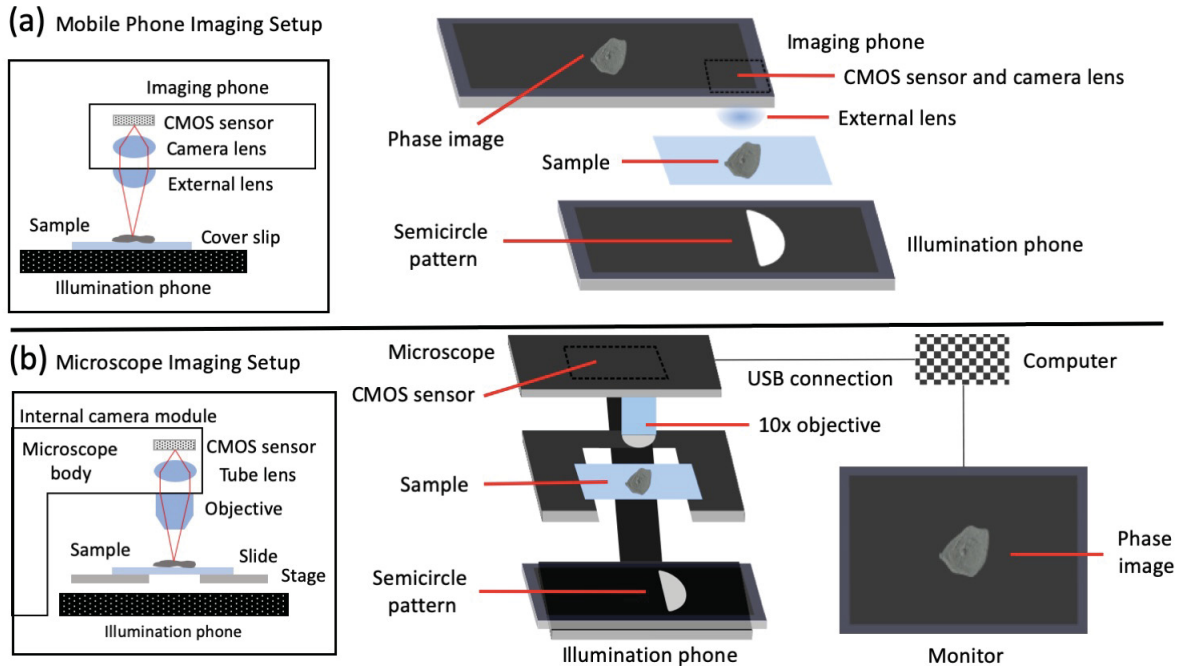


Figure 3.1: **Description of the system and components.** (a) Sketch of the overall optical (left) and physical (right) setup of the mobile phone-based imaging system and the illumination system. (b) Sketch of the overall optical (left) and physical (right) setup of the low-cost traditional microscope imaging system and the illumination system.

Figure 3.1(a) shows the optical setup of the mobile phone-based imaging system and the illumination system (left), as well the physical setup (right). The imaging system in this case consists of a Nokia mobile phone, with an attached external lens (iPhone 5 lens:  $NA = 0.23$ ,  $f2.2$ ), that provides a  $2x$  optical magnification, while the illumination system is a Retina display of an Apple iPhone 6. As shown in the figure, we projected semicircle patterns on the screen of the illumination phone to create asymmetrical illumination and produce the differential phase contrast images as described in Section 3.6.2. The sample was then mounted on top of the illumination screen (at a distance of  $25\text{ cm}$ ), and images were collected by the imaging phone. These images can then be displayed directly through the phone camera software, or transferred to a computer for further analysis using ImageJ.

Figure 3.1(b) shows the optical setup of the microscope-based imaging system and the illumination system (left), as well the physical setup (right). The imaging system in this case consists of a microscope with an on-board camera module, utilizing a  $10x$ ,  $0.25\text{ NA}$  objective. Once again, we projected semicircle patterns on the screen of the illumination phone (in this case a Xiaomi Redmi 3S), the sample was mounted on the sample stage, at a distance of  $\approx 20\text{ mm}$  from the illumination screen, and the imaging was performed by the camera module. The camera module is connected to the computer via USB. Image analysis

is then performed identically to the dual-phone setup.

### 3.6.2 Generation of differential phase contrast (DPC) images

Images taken with semicircle illumination patterns display phase information of the sample, with each semicircle orientation resulting in phase images along a specific axis. In order to acquire the differential phase contrast information along a single axis, a normalized difference of images taken with semicircle patterns of opposite orientations is performed, as shown in Eq. 3.1, to produce the final dpDPC image [87], [123].

$$I_{\text{DPC}} = \frac{I_1 - I_2}{I_1 + I_2} \quad (3.1)$$

where  $I_1$  and  $I_2$  represent either left and right or top and bottom images obtained with semicircle illumination. Example calculations are shown in Fig. 3.2, where images of human epithelial cheek cells (HECCs) taken with semicircle patterns with top-bottom, and left-right orientations, are combined to produce the final dpDPC image. The normalized difference of images taken with top-bottom semicircle orientations results in a DPC image with highest resolution along the vertical axis, and performing the same steps with images taken with left-right semicircle orientations results in a DPC image with highest resolution along the horizontal axis. These can be combined into a 4-axis DPC image with laterally isotropic resolution as described in [81], yet with the caveat that the reconstruction is no longer mathematically trivial, and is therefore not as amenable to non-experts.

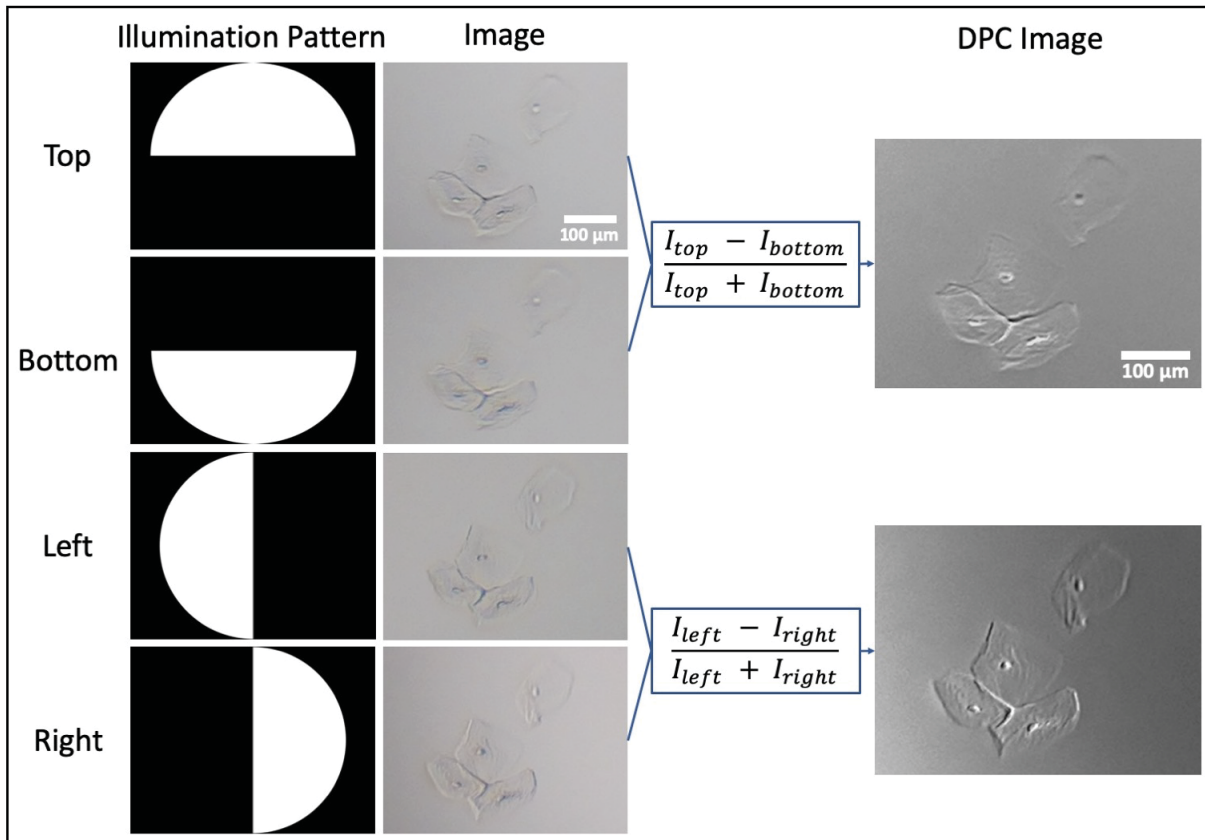


Figure 3.2: **Image computation for production of dual-phone differential phase contrast (dpDPC) images.** Successive images of human epithelial cheek cells (HECC) using top-, bottom-, left-, and right-semicircle illumination patterns:  $I_{top}$ ,  $I_{bottom}$ ,  $I_{left}$ , and  $I_{right}$ , respectively. The final DPC image shown on the top-right is obtained by using the normalized difference of  $I_{top}$  and  $I_{bottom}$  along the vertical axis. The final DPC image shown on the bottom-right is obtained by using the normalized difference of  $I_{left}$  and  $I_{right}$  along the horizontal axis.

For this to work, system alignment needs to be performed, as alignment issues can significantly alter the appearance of images. Misalignment can be caused by either the imaging system (external lens and phone camera) or by the illumination system. Typically, the external lens is hard mounted onto the phone and great care is taken that it is well aligned with the optical axis of the phone detector and camera-lens system. On the other hand, the illumination circle needs to be aligned with the optical axis of the imaging system in order to obtain high quality contrast images. This is performed by centering the illumination circle within the field of view (on the screen) of the imaging phone. Then, by maintaining this alignment, half circles of the original circle are produced, and images are collected as described earlier. When the circle is not well aligned with the optical axis of the imaging phone, the intensity gradient of the illumination for left-illumination and right-illumination images is different, which will lead to a composite DPC image that exhibits a high degree of

nonuniform illumination with poor quality of phase reconstruction.

The resulting DPC images were also compared with phase contrast images taken with a custom-made microscope that employs traditional phase contrast microscopy (10x, 0.25 NA objective), as shown in Fig. 3.3. The images show comparable phase contrast image quality using a much simpler setup. Changes in pixel intensity across individual cells were also plotted for both DPC images, and are shown as insets within the figure. As can be seen in the plots, a large number of fine intensity fluctuations can be observed across the cells that had been imaged using both the microscope and the dual-phone system, which corresponds to features present in the image.

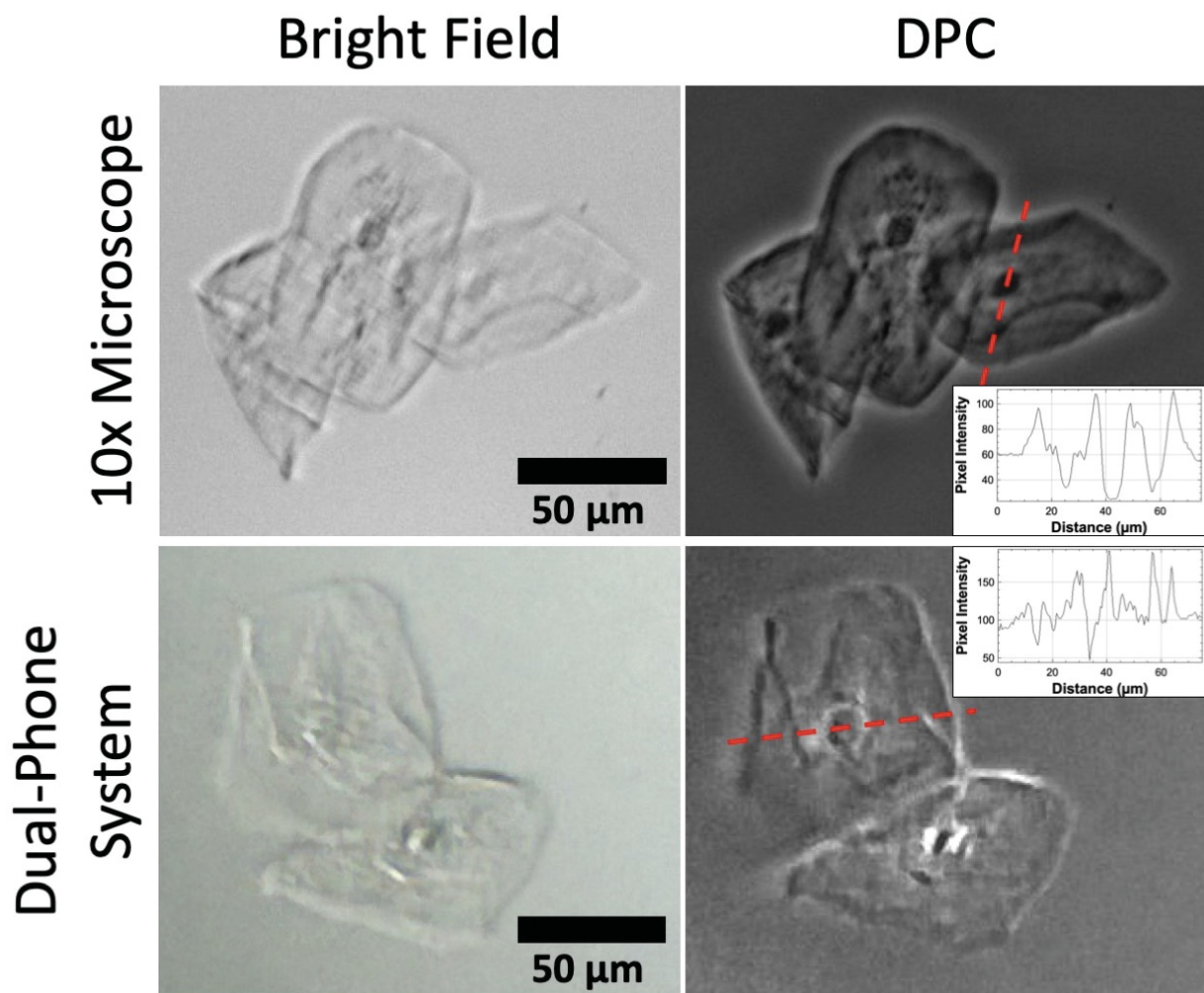


Figure 3.3: **Comparison of DPC images.** BF (top-left) and PC (top-right) images of HECC taken with a traditional microscope, using a 10x phase contrast objective with  $NA = 0.25$ . BF (bottom-left) and dpDPC (bottom-right) images of HECC taken using the dual-phone illumination-imaging system described in this paper. The insets on the right show pixel intensity plots generated across individual cells for both DPC images.

### 3.6.3 Application of the mobile phone-based imaging system to DPC microscopy of cells

Figure 3.4 shows both BF and dpDPC images of polystyrene beads, which are typically imaged for system calibration purposes (such as for determining resolution and image warping), mouse monocyte macrophage cells (J774A.1 cells), and mouse embryonic carcinoma cells (P19 cells). More specifically, we demonstrate the quantitative capabilities of the dual-phone system in terms of contrast and performing accurate cell measurements. First, an improvement in contrast of the dpDPC compared with BF is observed for all samples, as follows:

- i. for beads, 0.22 contrast for BF, and 0.26 contrast for dpDPC;
- ii. for monocytes, 0.11 contrast for BF, and 0.27 contrast for dpDPC;
- iii. and for P19 cells, 0.09 contrast for BF, and 0.26 contrast for dpDPC.

In addition, morphological parameters such as diameter, length measurements, and area are provided as well.

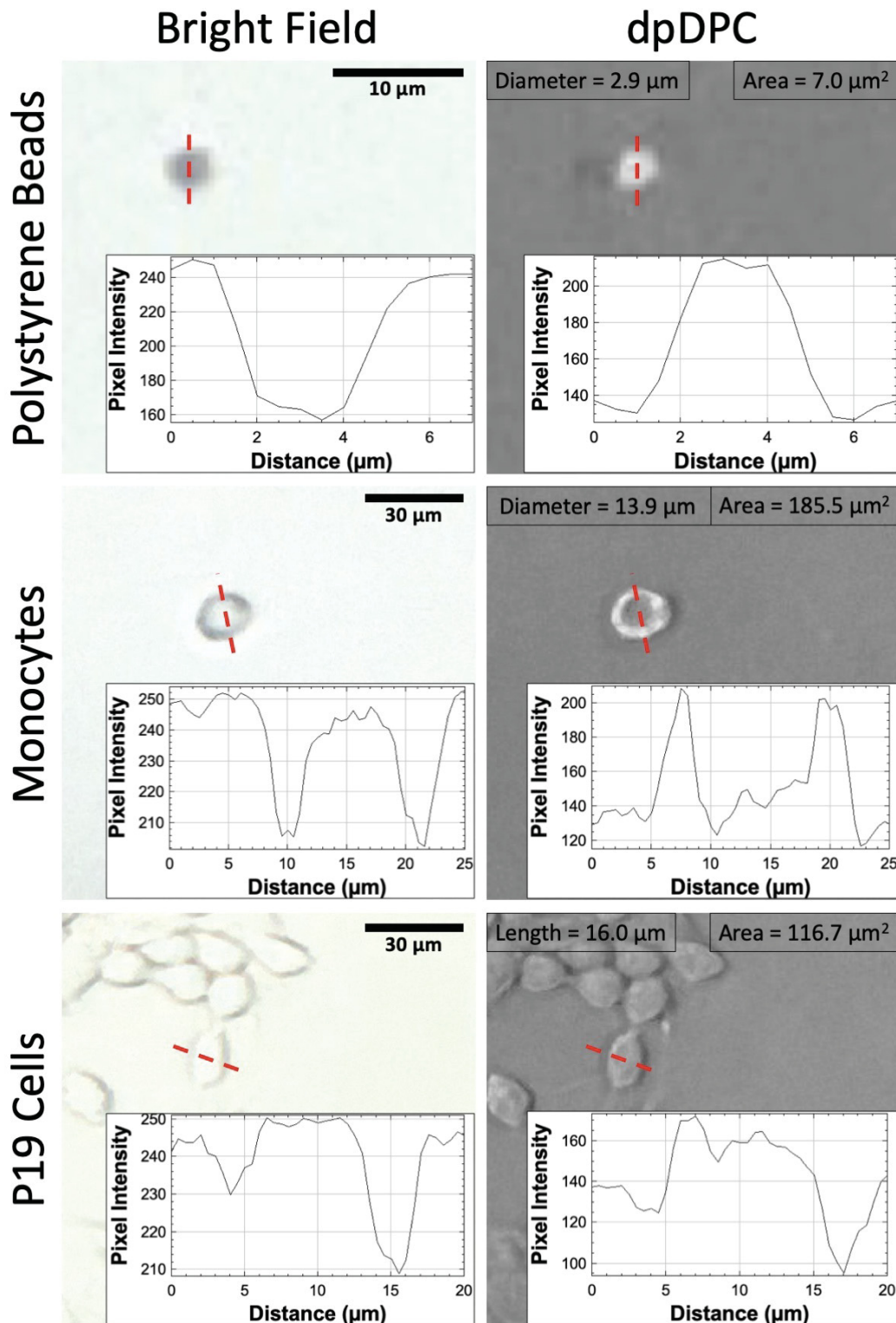


Figure 3.4: **Application of dpDPC microscopy to quantitative cell imaging.** Bright-field and dpDPC images of 3  $\mu\text{m}$  polystyrene beads, monocytes, and P19 cells. The respective insets show the pixel intensity profile across a single cell. dpDPC images also show cell dimension and area measurements.

In Fig. 3.5, we show dpDPC images of mouse neuroblastoma cells (N2a cells), and both live and dead mouse bone marrow-derived macrophages. These images provide a qualitative evaluation of the capabilities of the system, demonstrating that it can be used to image numerous samples of practical relevance, differentiate various cell types, and assess cell viability. Generally, bright-field (BF) images of such cells exhibit poor contrast, and consequently the overall cell structure is poorly defined. Moreover, obvious subcellular organelles, like the nucleus, as well as density variations along the cell area, are difficult to visualize. However, dpDPC images provide reasonable image quality over a wide field-of-view, with some ability to resolve subcellular detail. The enhanced contrast afforded by PC microscopy as shown in Figs. 3.4 and 3.5 could be utilized in future studies for identifying water-borne parasites [124], or simple monitoring of cell culture growth or confluence.

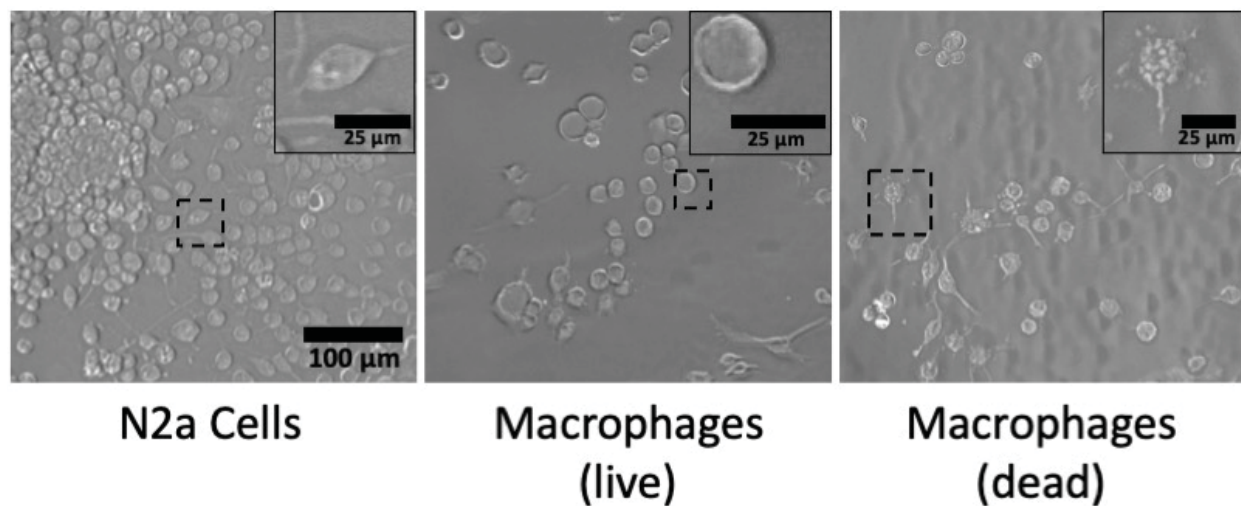


Figure 3.5: **Application of dpDPC microscopy to qualitative cell imaging.** dpDPC images of N2a cells, and both live and dead macrophage cells, with each respective inset showing a magnified image of an individual cell of that cell type.

### 3.6.4 Application of the phone illumination to DPC microscopy of cells using a low-cost microscope

To demonstrate the adaptability and versatility of this illumination-imaging system, we tested the same illumination setup with a different imaging platform, namely a traditional microscope imaging system. By placing the phone underneath the sample in a low cost, upright microscope, we acquired images of HECC (top) and a Wright-Giemsa-stained blood smear (bottom) (Fig. 3.6). In this figure we show a comparison between BF and DPC images obtained with this setup.

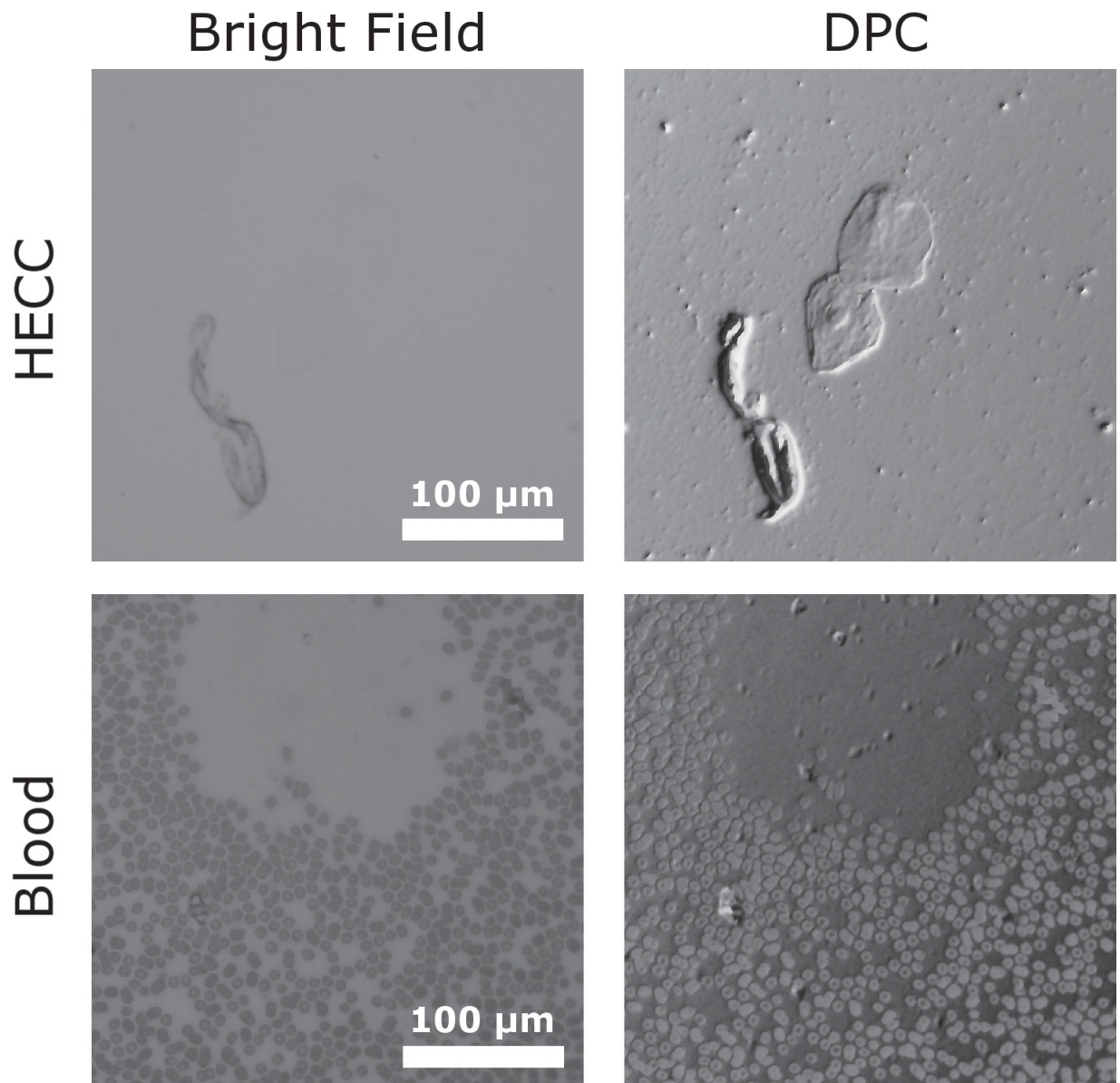


Figure 3.6: **Application of phone illumination to DPC microscopy of cells using a low-cost microscope.** BF and DPC images of HECC (top) and a WG-stained blood smear taken with a low-cost microscope that does not have PC capability, where the illumination has been replaced with a mobile phone screen exhibiting semicircle patterns for DPC microscopy.

As expected, due to the higher quality optics, the image quality using a traditional, low-cost microscope is slightly higher than that of the mobile phone system. However, the improved image quality comes at the cost of portability and the need for a separate computer. In this optical system, that does not have phase-contrast capability, by simply removing the condenser lens from the system and placing the phone on top of the condenser support structure, DPC images can easily be obtained. To further demonstrate the versatility of the

system, the Retina display screen of the iPhone was replaced in these experiments by that of a lower-cost Xiaomi Redmi 3 phone, with essentially identical results.

A comparison between BF and DPC images very clearly shows the marked improvement in contrast that can be achieved using a very simple and flexible illumination source, even on samples with their own absorption contrast, such as the stained blood smear. In this particular case, the DPC images are of higher quality than the BF images, which makes it easier to perform a cell count. A manual cell count of approximately 795 RBCs can be measured, highlighting the potential to provide clinically relevant information such as blood counts [71], [125]. Through the use of a mobile phone, rather than a more complex electronic system, DPC images can be acquired through simple manual positioning of the mobile phone, followed by swiping through various slides in a PowerPoint presentation. Thus, this illumination geometry completely eliminates the need for any expertise in system construction or electronic control.

### 3.7 Conclusion

In this paper, we demonstrate the ability of our multi-modal dual-phone illumination-imaging microscopy system [122] to perform differential phase microscopy (dpDPC). We demonstrate dpDPC images of multiple mammalian cell types, namely human epithelial cheek cells (HECC), a blood smear, mouse monocyte macrophage cells (J774A.1 cells), mouse neuroblastoma cells (N2a cells), mouse embryonic carcinoma cells (P19 cells), and mouse bone marrow-derived macrophages, as well as polystyrene beads. Critically, the illumination, image acquisition, and system control utilize familiar phone applications such as PowerPoint and the native Camera app, and do not require any specialized knowledge in microcontroller programming, or circuit design. Thus, the system is optimized for widespread adoption by users such as medical professionals and field workers who may not be highly trained in instrument control.

We also show that this setup can be generalized beyond mobile phone microscopy by utilizing our phone illumination with a traditional microscopy platform, demonstrating that by simply placing a phone in the illumination path of a low-cost microscope without phase contrast capability, high-contrast, high quality phase images can be obtained with no special system modifications or electronics expertise.

In this paper we focus only on the qualitative DPC imaging, as the emphasis is on an imaging system and analysis method that does not require a trained operator. However, in future studies quantitative phase information could be extracted, as described in [87], from images obtained with a similar or modified system. This quantitative phase information

could expand the potential application space to exploring cellular response to drugs [103], cell malignancy [106], and myriad other applications.

We finally highlight that while in this paper we describe using our dual-phone system for phase imaging, our system can at the same time acquire bright field, dark field, fluorescence, and Rheinberg illumination, all by simply changing the displayed image on the phone’s screen. Further, this flexible and intuitive illumination can be extended to traditional microscopy systems where illumination geometries such as Rheinberg illumination are typically too exotic to include on low-cost general purpose microscopes commonly available in educational or even clinical settings.

This system can thus serve as a portable, adaptable low-cost microscope or microscope add-on that is capable of multi-modal imaging at a much lower cost than traditional systems, without the need for specialized phase contrast objectives or addition of further hardware that could be difficult for non-experts to control. Moreover, the setup is quite versatile in terms of its components, where other phones, platforms, or combinations of both can be used, thus adding to its accessibility. We therefore believe that such a system will find widespread use among doctors, biologists, and others who may not be experts in hardware design, to solve challenges such as low-cost monitoring of cell cultures, water quality, or blood testing, among other potential applications.

## 3.8 Experimental

### 3.8.1 Imaging

For phone-based imaging, we used a Nokia phone (Lumia 1020 model), which has a 41.3-megapixel (MP) image sensor, and a sensor pixel size of 1.12  $\mu\text{m}$ . Furthermore, we attached an external lens (iPhone 5 lens: NA = 0.23, f2.2, 2x magnification) to the camera for enhanced focus. The imaging and illumination phones were clamped in place, and the sample was mounted onto an XYZ-translation stage (Thorlabs Inc.) for manipulation. The images were captured using the Lumia Camera application.

As for imaging with the low-cost microscope, we used a Jiangnan Electro-Optics DN-10B microscope (Nanjing, China), which comes equipped with a 3 MP image sensor, with a pixel size of 4.5  $\mu\text{m}$ . Images were acquired with a 10x, 0.25 NA objective.

### 3.8.2 Illumination

For illumination using the dpDPC system, we used a Retina display (12 cm diagonal) of an Apple mobile phone (iPhone 6), with a pixel density of 326 pixels per inch (PPI), which is equivalent to an RGB pixel size of  $\approx 78 \mu\text{m}$ . Moreover, the semicircle patterns projected onto the screen were designed using the Microsoft PowerPoint application for iOS. The illumination screen was placed approximately 25 cm below the sample, and was aligned in such a way that the center-line of the DPC semicircles was approximately centred beneath the external lens. For the microscope experiments, samples were illuminated from below by a Redmi 3S phone (Xiaomi, Beijing, China), with a  $720 \times 1280$  pixel screen and a pixel density of 294 PPI. The phone was placed approximately 2 cm below the sample, and was placed by hand such that the center-line of the DPC semicircles was approximately centred beneath the objective. Identical semicircle patterns as in the iPhone case were projected to the screen using the WPS Office application for Android (Kingsoft, Zhuhai, China).

### 3.8.3 Image analysis

In order to generate the final differential phase contrast (DPC) images, normalized image difference has to be performed. Image arithmetic was done using Fiji (ImageJ) software, as well as further image analysis.

### 3.8.4 Samples

Polystyrene beads with  $3 \mu\text{m}$  diameter were purchased from Corpuscular, Inc. and diluted in distilled water (1:1000 beads to water) before use. To image the beads,  $50 \mu\text{L}$  of the diluted suspension was pipetted onto a cover slip. Human epithelial cheek cell (HECC) samples were prepared for imaging by pipetting  $50 \mu\text{L}$  of 0.9% NaCl solution onto a cover slip, placing the cells into the water drop, then adding another cover slip on top. The HECC were originally collected by taking a tooth pick and swabbing the inside of the cheek. Mouse monocyte macrophage cells (J774A.1 cells) were generously gifted by Prof. Adam Hendricks' laboratory at McGill University. Mouse neuroblastoma cells (N2a cells), and mouse embryonic carcinoma cells (P19 cells) were generously gifted by Prof. Allen Ehrlicher's laboratory at McGill University. Mouse bone marrow-derived macrophages were generously gifted by Prof. Thomas Huser's laboratory at Bielefeld University. To prepare these cells for imaging, a few microliters of cells in suspension were pipetted onto a cover slip placed in a Petri dish, such that the cell suspension fully covers the bottom of the Petri dish and the cover slip. The Petri dish was then placed in an incubator overnight to allow for cell

adhesion onto the cover slip. To induce cell death (pyroptosis) in the macrophage cells, the cells were treated with 10  $\mu$ M Nigericin in PBS/HEPES buffer for 0.5 to 1 hour. The blood smear images were obtained from a commercially purchased slide used for teaching purposes.

### **3.9 Acknowledgements**

We would like to thank Ph.D. candidates Newsha Koushki (Allen Ehrlicher's lab) and Abdullah Chaudhary (Adam Hendricks' lab) at McGill, and Tung-Cheng Wang (Thomas Huser's lab) at Bielefeld University for providing us with cells for imaging. S.K. acknowledges the McGill Engineering Doctoral Award (MEDA).

### **3.10 Funding**

Natural Sciences and Engineering Research Council of Canada (NSERC) *10.13039/50110000-0038* (RGPIN-2018- 05675); Ministry of Science and Technology of the People's Republic of China (MOST) *10.13039/501100002855* (2016YFA0201300); Defense Advanced Research Projects Agency (DARPA) *10.13039/100000185* (HR0011-16-2-0028).

### **3.11 Disclosures**

The authors declare that there are no conflicts of interest related to this article.

## References

- [71] Z. J. Smith, K. Chu, A. R. Espenson, M. Rahimzadeh, A. Gryshuk, M. Molinaro, D. M. Dwyre, S. Lane, D. Matthews, and S. Wachsmann-Hogiu, “Cell-phone-based platform for biomedical device development and education applications,” *PloS one*, vol. 6, no. 3, e17150, 2011.
- [81] Z. Liu, L. Tian, S. Liu, and L. Waller, “Real-time brightfield, darkfield, and phase contrast imaging in a light-emitting diode array microscope,” *Journal of biomedical optics*, vol. 19, no. 10, p. 106 002, 2014.
- [85] L. Tian, X. Li, K. Ramchandran, and L. Waller, “Multiplexed coded illumination for fourier ptychography with an led array microscope,” *Biomedical optics express*, vol. 5, no. 7, pp. 2376–2389, 2014.
- [87] L. Tian and L. Waller, “Quantitative differential phase contrast imaging in an led array microscope,” *Optics express*, vol. 23, no. 9, pp. 11 394–11 403, 2015.
- [93] F. Zernike, “Phase contrast, a new method for the microscopic observation of transparent objects,” *Physica*, vol. 9, no. 7, pp. 686–698, 1942.
- [94] D. Hamilton and C. Sheppard, “Differential phase contrast in scanning optical microscopy,” *Journal of microscopy*, vol. 133, no. 1, pp. 27–39, 1984.
- [95] R. Allen and G. David, “The zeiss-nomarski differential interference equipment for transmitted-light microscopy,” *Zeitschrift für wissenschaftliche Mikroskopie und mikroskopische Technik*, vol. 69, no. 4, pp. 193–221, 1969.
- [96] R. Hoffman and L. Gross, “Modulation contrast microscope,” *Applied Optics*, vol. 14, no. 5, pp. 1169–1176, 1975.
- [97] L. Kastl, M. Isbach, D. Dirksen, J. Schnekenburger, and B. Kemper, “Quantitative phase imaging for cell culture quality control,” *Cytometry Part A*, vol. 91, no. 5, pp. 470–481, 2017.
- [98] P. Gleyzes, A. Boccara, and H. Saint-Jalmes, “Multichannel nomarski microscope with polarization modulation: Performance and applications,” *Optics letters*, vol. 22, no. 20, pp. 1529–1531, 1997.
- [99] A. Barty, K. Nugent, D. Paganin, and A. Roberts, “Quantitative optical phase microscopy,” *Optics Letters*, vol. 23, no. 11, pp. 817–819, 1998.

- [100] G. Popescu, T. Ikeda, R. R. Dasari, and M. S. Feld, “Diffraction phase microscopy for quantifying cell structure and dynamics,” *Optics letters*, vol. 31, no. 6, pp. 775–777, 2006.
- [101] Z. Wang, L. Millet, M. Mir, H. Ding, S. Unarunotai, J. Rogers, M. U. Gillette, and G. Popescu, “Spatial light interference microscopy (slim),” *Optics express*, vol. 19, no. 2, pp. 1016–1026, 2011.
- [102] L. Miccio, A. Finizio, R. Puglisi, D. Balduzzi, A. Galli, and P. Ferraro, “Dynamic DIC by digital holography microscopy for enhancing phase-contrast visualization,” *Biomedical optics express*, vol. 2, no. 2, pp. 331–344, 2011.
- [103] T. Yao, R. Cao, W. Xiao, F. Pan, and X. Li, “An optical study of drug resistance detection in endometrial cancer cells by dynamic and quantitative phase imaging,” *Journal of biophotonics*, e201800443, 2019.
- [104] M. Takabayashi, H. Majeed, A. Kajdacsy-Balla, and G. Popescu, “Disorder strength measured by quantitative phase imaging as intrinsic cancer marker in fixed tissue biopsies,” *PloS one*, vol. 13, no. 3, e0194320, 2018.
- [105] O. Tolde, A. Gandalovičová, A. Křížová, P. Veselý, R. Chmelík, D. Rosel, and J. Brábek, “Quantitative phase imaging unravels new insight into dynamics of mesenchymal and amoeboid cancer cell invasion,” *Scientific reports*, vol. 8, no. 1, pp. 1–13, 2018.
- [106] W. J. Eldridge, Z. A. Steelman, B. Loomis, and A. Wax, “Optical phase measurements of disorder strength link microstructure to cell stiffness,” *Biophysical journal*, vol. 112, no. 4, pp. 692–702, 2017.
- [107] J. Jung, L. E. Matemba, K. Lee, P. E. Kazyoba, J. Yoon, J. J. Massaga, K. Kim, D.-J. Kim, and Y. Park, “Optical characterization of red blood cells from individuals with sickle cell trait and disease in tanzania using quantitative phase imaging,” *Scientific reports*, vol. 6, p. 31698, 2016.
- [108] H. V. Pham, B. Bhaduri, K. Tangella, C. Best-Popescu, and G. Popescu, “Real time blood testing using quantitative phase imaging,” *PloS one*, vol. 8, no. 2, e55676, 2013.
- [109] Y. Park, C. A. Best, T. Auth, N. S. Gov, S. A. Safran, G. Popescu, S. Suresh, and M. S. Feld, “Metabolic remodeling of the human red blood cell membrane,” *Proceedings of the National Academy of Sciences*, vol. 107, no. 4, pp. 1289–1294, 2010.
- [110] H. S. Park, M. T. Rinehart, K. A. Walzer, J.-T. A. Chi, and A. Wax, “Automated detection of *p. falciparum* using machine learning algorithms with quantitative phase images of unstained cells,” *PloS one*, vol. 11, no. 9, e0163045, 2016.

- [111] Y. Park, M. Diez-Silva, G. Popescu, G. Lykotrafitis, W. Choi, M. S. Feld, and S. Suresh, “Refractive index maps and membrane dynamics of human red blood cells parasitized by plasmodium falciparum,” *Proceedings of the National Academy of Sciences*, vol. 105, no. 37, pp. 13 730–13 735, 2008.
- [112] Z. Yang and Q. Zhan, “Single-shot smartphone-based quantitative phase imaging using a distorted grating,” *PloS one*, vol. 11, no. 7, e0159596, 2016.
- [113] X. Meng, H. Huang, K. Yan, X. Tian, W. Yu, H. Cui, Y. Kong, L. Xue, C. Liu, and S. Wang, “Smartphone based hand-held quantitative phase microscope using the transport of intensity equation method,” *Lab on a Chip*, vol. 17, no. 1, pp. 104–109, 2017.
- [114] I. Hernández-Neuta, F. Neumann, J. Brightmeyer, T. Ba Tis, N. Madaboosi, Q. Wei, A. Ozcan, and M. Nilsson, “Smartphone-based clinical diagnostics: Towards democratization of evidence-based health care,” *Journal of internal medicine*, vol. 285, no. 1, pp. 19–39, 2019.
- [115] V. Bianco, B. Mandracchia, V. Marchesano, V. Pagliarulo, F. Olivieri, S. Coppola, M. Paturzo, and P. Ferraro, “Endowing a plain fluidic chip with micro-optics: A holographic microscope slide,” *Light: Science & Applications*, vol. 6, no. 9, e17055, 2017.
- [116] K. Guo, Z. Bian, S. Dong, P. Nanda, Y. M. Wang, and G. Zheng, “Microscopy illumination engineering using a low-cost liquid crystal display,” *Biomedical optics express*, vol. 6, no. 2, pp. 574–579, 2015.
- [117] Y. Ogasawara, R. Sugimoto, R. Maruyama, H. Arimoto, Y. Tamada, and W. Watanabe, “Mobile-phone-based rheinberg microscope with a light-emitting diode array,” *Journal of biomedical optics*, vol. 24, no. 3, p. 031 007, 2018.
- [118] L. Tian and L. Waller, “3d intensity and phase imaging from light field measurements in an led array microscope,” *optica*, vol. 2, no. 2, pp. 104–111, 2015.
- [119] Z. F. Phillips, M. V. D’Ambrosio, L. Tian, J. J. Rulison, H. S. Patel, N. Sadras, A. V. Gande, N. A. Switz, D. A. Fletcher, and L. Waller, “Multi-contrast imaging and digital refocusing on a mobile microscope with a domed led array,” *PloS one*, vol. 10, no. 5, e0124938, 2015.
- [120] D. Jung, J.-H. Choi, S. Kim, S. Ryu, W. Lee, J.-S. Lee, and C. Joo, “Smartphone-based multi-contrast microscope using color-multiplexed illumination,” *Scientific reports*, vol. 7, no. 1, p. 7564, 2017.

- [121] Y. Rivenson, H. Ceylan Koydemir, H. Wang, Z. Wei, Z. Ren, H. Günaydın, Y. Zhang, Z. Gorocs, K. Liang, D. Tseng, *et al.*, “Deep learning enhanced mobile-phone microscopy,” *ACS Photonics*, vol. 5, no. 6, pp. 2354–2364, 2018.
- [122] S. Kheireddine, A. S. Perumal, Z. J. Smith, D. V. Nicolau, and S. Wachsmann-Hogiu, “Dual-phone illumination-imaging system for high resolution and large field of view multi-modal microscopy,” *Lab on a Chip*, vol. 19, no. 5, pp. 825–836, 2019.
- [123] S. B. Mehta and C. J. Sheppard, “Quantitative phase-gradient imaging at high resolution with asymmetric illumination-based differential phase contrast,” *Optics letters*, vol. 34, no. 13, pp. 1924–1926, 2009.
- [124] E. C. Nieminski, F. Schaefer, and J. E. Ongerth, “Comparison of two methods for detection of giardia cysts and cryptosporidium oocysts in water.,” *Appl. Environ. Microbiol.*, vol. 61, no. 5, pp. 1714–1719, 1995.
- [125] Z. J. Smith, T. Gao, K. Chu, S. M. Lane, D. L. Matthews, D. M. Dwyre, J. Hood, K. Tatsukawa, L. Heifetz, and S. Wachsmann-Hogiu, “Single-step preparation and image-based counting of minute volumes of human blood,” *Lab on a Chip*, vol. 14, no. 16, pp. 3029–3036, 2014.

# Chapter 4

## Discussion

This thesis aims to address and optimize the trade-off between spatial resolution and field-of-view (FOV) imposed by lens-based, and to a lesser extent, lens-free microscopy approaches, via construction, assembly, and integration of existing technologies into novel, multi-modal microscopy platforms for imaging of cells and microorganisms within open and confined spaces. Biological and biomedical imaging requires simultaneously high spatial resolution and large FOV for numerous applications, and as such, it is vital to minimize this imperative compromise, and maximize the specimen area that can be imaged with a particular resolving power.

Through the course of this dissertation, chapter 1 gives a theoretical introduction to microscopy in the biological and biomedical fields, and important parameters and system specifications to consider as well as relevant applications. Section 1.3 within chapter 1 describes the process for identification of usable imaging platforms based on sample and system considerations. Chapter 2 introduces a compact mobile phone-based illumination-imaging system capable of multi-modal microscopy, and chapter 3 expands on that work via adaptation of the dual-phone system for differential phase contrast (DPC) microscopy.

### 4.1 Identification of system requirements

In section 1.3 of chapter 1, a biocomputational microfluidic device, modelling the Subset Sum Problem (SSP), is proposed as a particularly challenging biological application for imaging. Not only does the imaging need to be performed at a spatial resolution high enough to discern individual microorganisms within the microfluidic network, but also with a FOV large enough to encompass the full chip area, in order for agent tracking from device entry to exit to be possible. Since chip size is dependent on SSP cardinality and biological agent size used, multiple device areas are possible, and given that there is no one-size-fits-all solution

to such a problem, different technology options would be needed to cater for different size ranges. As such, the problem was elucidated in terms of current imaging technologies and their corresponding spatial resolution and FOV parameters.

Figure 1.2 sums up elegantly the resolution and FOV capabilities of each technology, at the time of writing, and could be used as a reference point for other applications, whereby the pre-known problem parameters could be fitted into the boundaries of the various imaging platforms, to see which would be the most feasible. This simplifies application-imaging platform pairing by displaying all the practical possibilities in one graphic, and should be used as a first step for assessment of the imaging application at hand. In the case where an appropriate system is not directly found, and image stitching is necessary to bridge the required resolution-FOV gap, an analysis similar to what is described in section 1.3.3 should be done. For applications where observations are time-independent, stitching would only result in loss of some spatial information, but in case of time-dependent problems, both spatial and temporal information could be lost, and further compromises would have to be factored in. Overall, this chapter presents a straightforward approach for satisfying complex imaging requirements.

## **4.2 Dual-phone illumination-imaging system for high resolution and large field of view multi-modal microscopy**

In chapter 2, a compact mobile phone-based illumination-imaging system is introduced as a suitable platform for imaging applications that require parameters bounded by the region marked in Figure 1.4. This system offers a spatial resolution close to  $2\ \mu\text{m}$  and a FOV of approximately  $10\ \text{mm}^2$ , with the possibility of multiple microscopy modalities such as bright-field (BF), dark-field (DF), Rheinberg and point illumination, and fluorescence imaging. Illumination patterns are projected onto a mobile phone Retina display using a PowerPoint application, thus simplifying the design and testing of different modalities, without the need for specialized microscope add-ons or objectives, which can be bulky, expensive, and time-consuming to set up. A similar approach to simple illumination pattern generation had been established using LED arrays [83]–[87], but since these require programming and control with an external computer, phone screen illumination is even more straightforward, and allows for more possibilities.

This illumination-imaging system has demonstrated its ability to visualize individual *E. coli* bacteria within plaza regions of microfluidic devices as well as *E. gracilis* inside channels

and open areas with pillars, thus verifying its high spatial resolution, and image quality from a qualitative perspective for detection of organism morphology. The same obtained images could also be used for extraction of quantitative information such as cell counts, and cell dimensions as well as microorganism velocity calculations through observation of their motility behaviour in recorded videos. Moreover, the system was used for imaging diatoms, *E. gracilis*, and human epithelial cheek cells (HECC) using BF, DF, and Rheinberg illumination. Multiple rings and varying ring thickness in DF allow for enhanced contrast, and generation of embossing effects, depending on the sample at hand, which further enhances visualization of translucent cells. Furthermore, the ability to easily manipulate colour combinations for Rheinberg illumination, without the need for additional filters, allows for better system adaptability to the specimen at hand, whereby the colours would be chosen based on the optical properties of the sample.

One major problem with microorganism velocity measurements is that it requires acquisition of image sequences or videos, as opposed to still images, and agent tracking would need to be performed, which is a computationally heavy and time consuming process, and can be particularly problematic in regions where there is agent overlap. To overcome this, the mobile phone-based system was used to capture long-exposure still DF images of live *E. gracilis*. After some relatively minor post-processing and analysis, the average agent speed was found, and the trajectories were easily visible for further analysis. Last but not least, through simple insertion of excitation and emission filters into the imaging platform, and without the need for complex or coherent illumination, fluorescence images of fluorescein-filled microfluidic devices and fluorescently labelled HEK 293 cells were successfully imaged, further attesting to the extensive capabilities of the system.

### **4.3 Simple adaptive mobile phone screen illumination for dual phone differential phase contrast (dpDPC) microscopy**

In chapter 3, the same mobile phone-based microscope was adapted for dual-phone differential phase contrast (dpDPC) imaging, where multiple semicircular patterns are generated on the illumination phone screen, images of the sample are taken with each asymmetric illumination configuration, and these images are mathematically combined to form differential phase contrast images. This modality was tested with several sample types, such as polystyrene beads, HECC, blood smears as well as mouse monocyte, neuroblastoma, carcinoma, and macrophage cells, and allows for qualitative assessment of cell morphology, and

viability, along with visualization of density gradients across the cell that highlight subcellular structures. Besides, the enhanced specimen-background contrast this modality yields, permits facile extraction of quantitative image data, like cell dimension measurements and counts.

Given the hardware and operation complexity of traditional DPC microscopes, this platform simplifies DPC imaging both in terms of the required setup, in addition to making this modality more amenable to microscopy non-experts, which makes it more user-friendly, not to mention portable and more adaptable, whereby pairing DPC phone screen illumination with a classic microscope without phase contrast components allows for generation and recording of DPC images. Whereas not demonstrated in the relevant manuscript [126], this apparatus could be further adapted for quantitative phase contrast (QPC) imaging [87], such that differences in the refractive index within the sample could be utilized for determination of cell dry mass [127], diagnosis of sickle cell anaemia [107], classification of cancer cells [128], and for many other biomedical applications [129].

## **4.4 Translation of phone screen illumination to lens-free microscopy**

The adaptability of phone screen illumination implies that it can be used in conjunction with various imaging platforms. As shown in Fig. 3.6.4, standard illumination was replaced by phone screen illumination in a conventional microscope setup, and was used to successfully generate DPC images, without the need for objectives specialized for phase contrast imaging. Moreover, phone screen illumination could also be applied to lens-free imaging. A research paper, to which I made a contribution as a co-author, introduces a reflection-based, dark-field, lens-free system for imaging of micron-sized objects, which uses a pragmatic LED platform to change the illumination angle quickly and accurately [130]. In order to simplify oblique illumination further, the LED setup was replaced with phone screen illumination, and the screen was used to generate rings of different diameters, each pertaining to a different illumination angle. This combination setup and the relevant preliminary results are not part of the published manuscript.

Subsequently, two elegant imaging and illumination systems were merged: a lens-free, CMOS-based, direct on-chip imaging system, and a mobile phone-based screen illumination system, respectively, which together form an inexpensive, portable, practical, and versatile imaging-illumination microscopy construct. A white ring was projected onto the phone screen to achieve oblique illumination, where different illumination angles can be achieved

by using rings of different radii, or by altering the distance between the screen and the sample. This setup was used to characterize the contrast across HECC samples, and results showed an improvement in sample contrast when imaging at larger illumination angles, which allows for ease of visualization of unstained, transparent, and translucent samples. Further experiments should be conducted to explore changes in sample contrast for angles  $> 87^\circ$ , but improvements to the setup such as using a larger screen would need to be made for simpler angle adjustment, or using a screen with organic LEDs (OLEDs), such as that of the iPhone X, instead of a Retina display, to achieve higher brightness and larger viewing angles [131], which would provide better contrast for oblique illumination at larger angles of incidence.

As a whole, this system would be useful for visualization of beads, cells, microorganisms at high resolution and large FOV, depending on the specifications of the CMOS sensor in use. In the published manuscript, the image sensor used was that of the Raspberry Pi camera V1.3, which provides a pixel-limited spatial resolution corresponding to the pixel size ( $\approx 1.4 \mu\text{m}$ ) and a FOV corresponding to the active sensor area ( $3.6 \times 2.73 \text{ mm}$ ). At the present time, the smallest pixel size achievable for CMOS technologies is  $1.12 \mu\text{m}$ , so any further enhancement to spatial resolution using such a lens-free system can only be achieved via the application of relevant illumination manipulation techniques. In terms of enlarging the FOV, CMOS sensors with larger areas can be custom-made for this purpose; however, the subsequent increase in price would be a deterrent for adoption. Given the current state of the art, a spatial resolution of  $1.12 \mu\text{m}$  and a FOV of  $3.6 \times 2.73 \text{ mm}$  is the best that can be expected for similarly constructed microscopy systems to be used in their native state.

Lastly, while such a system could be used in a laboratory setting, it would be especially beneficial for applications in low-resource environments, where expensive instruments are unavailable, or for on-field measurements, since this platform configuration allows for rapid experiment performance. However, the method has several limitations that could be improved by applying more advanced engineering approaches. One such limitation is the increase of the sensor surface temperature during imaging, which restricts the use of this method for live biological samples. However, this issue could be potentially resolved by the addition of a heat sink that can reduce the temperature of the sensor. Another limitation of the system is that, at this point of development, it allows measurements of only fixed/dry samples. In order to perform dark field imaging of liquid samples, further improvements to the system are necessary for refractive index matching. Overall, further work needs to be done if this system is to be available for commercial use, but it is promising even in its current form for the range of applications and user-friendliness it offers.

## 4.5 Outlook and future perspectives

Broadly speaking, whereas mobile phone-based microscopes are not novel in and of themselves, the phone imaging platform used in chapters 2 and 3 provides, at the time of publication, the best possible spatial resolution-FOV trade-off for commercially available mobile phones. Of course, a larger CMOS chip built with the smallest-available pixel size would provide an even larger FOV at high resolution, but would be expensive to custom-make, and is not readily available for purchase. Some of the many advantages of using mobile phones for imaging are their ubiquity and affordability, where inexpensive alternatives could almost always be found, where necessary, making this an ideal platform for use in low-resource environments. Moreover, different phone cameras could be used for different applications, depending on the required specifications, and external optical components, such as lenses, could be appended if need be.

Furthermore, illumination for microscopy is typically complex, and requires bulky, specialized, and expensive components for certain modalities. Screen illumination introduces a novel, compact, economical, user-friendly, simple-to-design, and viable multi-modal alternative that works with multiple imaging platforms, and could be easily adapted accordingly. Put together with a portable imaging system, this results in an all-in-one, miniaturized approach to imaging in the field, in medical, or environmental settings as well as for educational purposes, where no special skills, expertise, or training would be required for use, and a simple accompanying user manual would suffice. The system could be used for a preliminary look at specimen found on-site, which could then be transferred to a facility with high-end microscopes for more in-depth, quality imaging. This mobile phone-based illumination-imaging system could be even further improved by a supplementary phone application that processes images directly on-phone as necessary, resulting in effortless integration of illumination, imaging, post-processing, and analysis.

## References

- [83] S. Dong, R. Shiradkar, P. Nanda, and G. Zheng, “Spectral multiplexing and coherent-state decomposition in fourier ptychographic imaging,” *Biomedical optics express*, vol. 5, no. 6, pp. 1757–1767, 2014.
- [84] S. Dong, Z. Bian, R. Shiradkar, and G. Zheng, “Sparsely sampled fourier ptychography,” *Optics express*, vol. 22, no. 5, pp. 5455–5464, 2014.
- [85] L. Tian, X. Li, K. Ramchandran, and L. Waller, “Multiplexed coded illumination for fourier ptychography with an led array microscope,” *Biomedical optics express*, vol. 5, no. 7, pp. 2376–2389, 2014.
- [86] G. Zheng, R. Horstmeyer, and C. Yang, “Wide-field, high-resolution fourier ptychographic microscopy,” *Nature photonics*, vol. 7, no. 9, p. 739, 2013.
- [87] L. Tian and L. Waller, “Quantitative differential phase contrast imaging in an led array microscope,” *Optics express*, vol. 23, no. 9, pp. 11 394–11 403, 2015.
- [107] J. Jung, L. E. Matemba, K. Lee, P. E. Kazyoba, J. Yoon, J. J. Massaga, K. Kim, D.-J. Kim, and Y. Park, “Optical characterization of red blood cells from individuals with sickle cell trait and disease in tanzania using quantitative phase imaging,” *Scientific reports*, vol. 6, p. 31 698, 2016.
- [126] S. Kheireddine, Z. J. Smith, D. V. Nicolau, and S. Wachsmann-Hogiu, “Simple adaptive mobile phone screen illumination for dual phone differential phase contrast (dpdpc) microscopy,” *Biomedical optics express*, vol. 10, no. 9, pp. 4369–4380, 2019.
- [127] R. Barer, “Interference microscopy and mass determination,” *Nature*, vol. 169, no. 42-96, pp. 366–367, 1952.
- [128] D. Roitshtain, L. Wolbromsky, E. Bal, H. Greenspan, L. L. Satterwhite, and N. T. Shaked, “Quantitative phase microscopy spatial signatures of cancer cells,” *Cytometry Part A*, vol. 91, no. 5, pp. 482–493, 2017.
- [129] Y. Park, C. Depeursinge, and G. Popescu, “Quantitative phase imaging in biomedicine,” *Nature Photonics*, vol. 12, no. 10, pp. 578–589, 2018.
- [130] M. Imanbekova, A. S. Perumal, S. Kheireddine, D. V. Nicolau, and S. Wachsmann-Hogiu, “Lensless, reflection-based dark-field microscopy (rdfm) on a cmos chip,” *Biomedical Optics Express*, vol. 11, no. 9, pp. 4942–4959, 2020.

- [131] W. Ding, Y. Wang, H. Chen, and S. Y. Chou, “Plasmonic nanocavity organic light-emitting diode with significantly enhanced light extraction, contrast, viewing angle, brightness, and low-glare,” *Advanced Functional Materials*, vol. 24, no. 40, pp. 6329–6339, 2014.

# Chapter 5

## Conclusion

To recapitulate, the objective of this thesis has been to address and minimize the requisite trade-off between spatial resolution and field-of-view, and it does so via integration of available technologies, primarily mobile phones, to create an inexpensive, compact, portable, and versatile microscope. The dual-phone illumination-imaging system uses one phone for imaging and another for illumination. The novelty of this setup lies in phone screen illumination, whereby different shapes and colours could be simply designed and projected onto the screen to generate various illumination modalities, such as bright-field, dark-field, Rheinberg illumination, point illumination, fluorescence, and differential phase contrast. Moreover, phone screen ring illumination was applied to a lens-free imaging platform to attain reflection-based dark-field microscopy via sensor illumination at large oblique angles. This further corroborates the adaptability of phone screen illumination, which could also be integrated into a traditional microscope as a versatile light source.

As described elaborately throughout this work, there is a general need for high spatial resolution and large field-of-view imaging in the biological and biomedical fields. Multiple applications in areas of cytology, histology, developmental biology, neuronal mapping, and cell tracking require pairing with a microscopy system capable of discerning individual biological agents while capturing large areas in one shot, for maximal and accurate extraction of qualitative and quantitative information about the sample. The dual-phone illumination-imaging system has been used for observation of cells and microorganisms within open and confined spaces, specifically glass slides and microfluidic devices, performing cell dimension measurements, and cell counts, and for facile extraction of their movement trajectories for speed calculations using long exposure images and basic image post-processing. It has also been used for distinguishing different cell types, live and dead cells, and prominent intracellular features, namely nuclei and chloroplasts, and for generation of 3D-like cellular effects for enhanced contrast.

Whereas traditional microscopes generally have higher quality optics than mobile phones or other imaging platforms, that typically comes at the expense of bulky equipment, high cost, and the need for expert training. Not only does screen illumination simplify multi-modal illumination generation, but it also allows for ease of switching between modalities, by simple swiping between slides on the screen, which otherwise would not have been as straightforward with a regular microscope, where objectives, annuli, prisms, or light sources might need to be added or exchanged, or a different system altogether might need to be used. Overall, this phone-based illumination-imaging platform offers portability and user-friendliness, whereby microscopy non-experts could use this system for multi-modal imaging of micron-sized objects, biological or otherwise, live or fixed. Imaging could be performed in the field, or for initial examination of a sample, before transporting it to an imaging facility for further analysis. Such a system would be useful in the medical, educational, and environmental domains, and could be made even more accessible if a phone application were to be developed for direct, on-phone image post-processing, thereby rendering this system fully standalone.

Once the required microscopy specifications for a particular application are defined, and suitable mobile phones have been chosen accordingly, the illumination and imaging components need to be integrated into a single functional unit for subsequent commercial use. An accompanying phone application would present a graphical user interface that allows the operator to verify system alignment, and choose imaging parameters as well as illumination modalities. Moreover, in-app image computation and analysis would result in further system cohesion from the software side, whereby image arithmetic, as in the case of background subtraction, image corrections (e.g. flat-field correction), and DPC image generation (see section 3.6.2) could be directly performed on the imaging phone. Given the steady development in computational power and graphics processing unit (GPU) capabilities of new-generation mobile phones, this integrated phone-based microscope could be further enhanced through employment of artificial intelligence for image post-processing and analysis. This would enable the system to perform image deconvolution, which aims to reduce noise-related elements or aberrations in the final image, further improving spatial resolution, and pattern recognition, which would allow for automatic cell classification based on morphology assessment, distinction of cell viability, performance of cell counts, and cell tracking via trajectory tracing (see section 2.6.6).

In conclusion, consolidation of this phone-based illumination-imaging system into an elegant microscope with incorporated image processing capabilities renders it operable by non-experts, where the user would only need to load the sample into a designated slot, and operate the system using instructions provided within the interactive phone application.

Having a compact, automated microscope would not only reduce potential user system handling errors, but would also maintain long-term component alignment. In terms of future perspectives, advancement of the spatial resolution and field-of-view specifications of phone-based microscopes will depend on the growth of phone camera and processor technologies, and will scale up accordingly. Apart from the aforementioned applications in the biological and biomedical fields, this microscope could be used for observation of microorganism motility, biocomputations, and biologically guided simulations. Furthermore, this system naturally lends itself for use in low-resource environments, where it could be useful in rural or inaccessible communities. Similarly, it can serve as a handy microscope for field work or even in laboratory settings, where preliminary sample assessment before further analysis is possible. Lastly, it can be used as a low-cost classroom microscope in the education domain, and in numerous comparable settings.

# Bibliography

- [1] W. J. Croft, *Under the microscope: a brief history of microscopy*. World Scientific, 2006, vol. 5.
- [2] Y. D. Ivanov, T. O. Pleshakova, I. D. Shumov, A. F. Kozlov, I. A. Ivanova, A. A. Valueva, V. Y. Tatur, M. V. Smelov, N. D. Ivanova, and V. S. Ziborov, “Afm imaging of protein aggregation in studying the impact of knotted electromagnetic field on a peroxidase,” *Scientific Reports*, vol. 10, no. 1, pp. 1–9, 2020.
- [3] J. Sanderson, *Understanding light microscopy*. John Wiley & Sons, 2019.
- [4] D. B. Murphy, *Fundamentals of light microscopy and electronic imaging*. John Wiley & Sons, 2002.
- [5] H. Nyquist, “Certain topics in telegraph transmission theory,” *Transactions of the American Institute of Electrical Engineers*, vol. 47, no. 2, pp. 617–644, 1928.
- [6] R. W. Cole, T. Jinadasa, and C. M. Brown, “Measuring and interpreting point spread functions to determine confocal microscope resolution and ensure quality control,” *Nature protocols*, vol. 6, no. 12, pp. 1929–1941, 2011.
- [7] R. P. Nieuwenhuizen, K. A. Lidke, M. Bates, D. L. Puig, D. Grünwald, S. Stallinga, and B. Rieger, “Measuring image resolution in optical nanoscopy,” *Nature methods*, vol. 10, no. 6, pp. 557–562, 2013.
- [8] A. C. Descloux, K. S. Grussmayer, and A. Radenovic, “Parameter-free image resolution estimation based on decorrelation analysis,” *Nature Methods*, vol. 16, no. ARTICLE, pp. 918–924, 2019.
- [9] I. de Kernier, A. Ali-Cherif, N. Rongeat, O. Cioni, S. Morales, J. Savatier, S. Monneret, and P. Blandin, “Large field-of-view phase and fluorescence mesoscope with microscopic resolution,” *Journal of biomedical optics*, vol. 24, no. 3, p. 036501, 2019.
- [10] Y. Wan, K. McDole, and P. J. Keller, “Light-sheet microscopy and its potential for understanding developmental processes,” *Annual review of cell and developmental biology*, vol. 35, pp. 655–681, 2019.

- [11] J. N. Stirman, I. T. Smith, M. W. Kudenov, and S. L. Smith, “Wide field-of-view, multi-region, two-photon imaging of neuronal activity in the mammalian brain,” *Nature biotechnology*, vol. 34, no. 8, pp. 857–862, 2016.
- [12] S. Eom, S. Sanami, R. Bise, C. Pascale, Z. Yin, S.-i. Huh, E. Osuna-Highley, S. N. Junkers, C. J. Helfrich, P. Y. Liang, *et al.*, “Phase contrast time-lapse microscopy datasets with automated and manual cell tracking annotations,” *Scientific data*, vol. 5, no. 1, pp. 1–12, 2018.
- [13] J. Chalfoun, M. Majurski, T. Blattner, K. Bhadriraju, W. Keyrouz, P. Bajcsy, and M. Brady, “Mist: Accurate and scalable microscopy image stitching tool with stage modeling and error minimization,” *Scientific reports*, vol. 7, no. 1, pp. 1–10, 2017.
- [14] P. Kask, K. Palo, C. Hinnah, and T. Pommerencke, “Flat field correction for high-throughput imaging of fluorescent samples,” *Journal of microscopy*, vol. 263, no. 3, pp. 328–340, 2016.
- [15] A. Greenbaum, W. Luo, T.-W. Su, Z. Göröcs, L. Xue, S. O. Isikman, A. F. Coskun, O. Mudanyali, and A. Ozcan, “Imaging without lenses: Achievements and remaining challenges of wide-field on-chip microscopy,” *Nature methods*, vol. 9, no. 9, pp. 889–895, 2012.
- [16] Z. Göröcs and A. Ozcan, “On-chip biomedical imaging,” *IEEE reviews in biomedical engineering*, vol. 6, pp. 29–46, 2012.
- [17] T.-W. Su, S. O. Isikman, W. Bishara, D. Tseng, A. Erlinger, and A. Ozcan, “Multi-angle lensless digital holography for depth resolved imaging on a chip,” *Optics express*, vol. 18, no. 9, pp. 9690–9711, 2010.
- [18] J. Kun, M. Smieja, B. Xiong, L. Soleymani, and Q. Fang, “The use of motion analysis as particle biomarkers in lensless optofluidic projection imaging for point of care urine analysis,” *Scientific reports*, vol. 9, no. 1, pp. 1–12, 2019.
- [19] X. Cui, L. M. Lee, X. Heng, W. Zhong, P. W. Sternberg, D. Psaltis, and C. Yang, “Lensless high-resolution on-chip optofluidic microscopes for caenorhabditis elegans and cell imaging,” *Proceedings of the National Academy of Sciences*, vol. 105, no. 31, pp. 10 670–10 675, 2008.
- [20] T. Tanaka, T. Saeki, Y. Sunaga, and T. Matsunaga, “High-content analysis of single cells directly assembled on cmos sensor based on color imaging,” *Biosensors and Bioelectronics*, vol. 26, no. 4, pp. 1460–1465, 2010.

- [21] J. Garcia-Sucerquia, W. Xu, S. K. Jericho, P. Klages, M. H. Jericho, and H. J. Kreuzer, “Digital in-line holographic microscopy,” *Applied optics*, vol. 45, no. 5, pp. 836–850, 2006.
- [22] M. Kanka, R. Riesenberger, and H. Kreuzer, “Reconstruction of high-resolution holographic microscopic images,” *Optics letters*, vol. 34, no. 8, pp. 1162–1164, 2009.
- [23] A. Ozcan and U. Demirci, “Ultra wide-field lens-free monitoring of cells on-chip,” *Lab on a Chip*, vol. 8, no. 1, pp. 98–106, 2008.
- [24] G. Stybayeva, O. Mudanyali, S. Seo, J. Silangcruz, M. Macal, E. Ramanculov, S. Dandekar, A. Erlinger, A. Ozcan, and A. Revzin, “Lensfree holographic imaging of antibody microarrays for high-throughput detection of leukocyte numbers and function,” *Analytical chemistry*, vol. 82, no. 9, pp. 3736–3744, 2010.
- [25] Y. Zhang, H. C. Koydemir, M. M. Shimogawa, S. Yalcin, A. Guziak, T. Liu, I. Oguz, Y. Huang, B. Bai, Y. Luo, *et al.*, “Motility-based label-free detection of parasites in bodily fluids using holographic speckle analysis and deep learning,” *Light: Science & Applications*, vol. 7, no. 1, pp. 1–18, 2018.
- [26] T.-W. Su, A. Erlinger, D. Tseng, and A. Ozcan, “Compact and light-weight automated semen analysis platform using lensfree on-chip microscopy,” *Analytical chemistry*, vol. 82, no. 19, pp. 8307–8312, 2010.
- [27] R. Delacroix, S. N. A. Morel, L. Hervé, T. Bordy, J.-M. Dinten, M. Drancourt, and C. Allier, “Cerebrospinal fluid lens-free microscopy: A new tool for the laboratory diagnosis of meningitis,” *Scientific reports*, vol. 7, no. 1, pp. 1–8, 2017.
- [28] W. Xu, M. Jericho, I. Meinertzhagen, and H. Kreuzer, “Digital in-line holography for biological applications,” *Proceedings of the National Academy of Sciences*, vol. 98, no. 20, pp. 11 301–11 305, 2001.
- [29] A. F. Coskun, T.-W. Su, and A. Ozcan, “Wide field-of-view lens-free fluorescent imaging on a chip,” *Lab on a Chip*, vol. 10, no. 7, pp. 824–827, 2010.
- [30] O. Mudanyali, E. McLeod, W. Luo, A. Greenbaum, A. F. Coskun, Y. Hennequin, C. P. Allier, and A. Ozcan, “Wide-field optical detection of nanoparticles using on-chip microscopy and self-assembled nanolenses,” *Nature photonics*, vol. 7, no. 3, p. 247, 2013.
- [31] F. Kazemzadeh and A. Wong, “Laser light-field fusion for wide-field lensfree on-chip phase contrast microscopy of nanoparticles,” *Scientific reports*, vol. 6, no. 1, pp. 1–6, 2016.

- [32] T. Aidukas, R. Eckert, A. R. Harvey, L. Waller, and P. C. Konda, “Low-cost, sub-micron resolution, wide-field computational microscopy using opensource hardware,” *Scientific reports*, vol. 9, no. 1, pp. 1–12, 2019.
- [33] G. Jin, I.-H. Yoo, S. P. Pack, J.-W. Yang, U.-H. Ha, S.-H. Paek, and S. Seo, “Lens-free shadow image based high-throughput continuous cell monitoring technique,” *Biosensors and Bioelectronics*, vol. 38, no. 1, pp. 126–131, 2012.
- [34] A. Greenbaum, Y. Zhang, A. Feizi, P.-L. Chung, W. Luo, S. R. Kandukuri, and A. Ozcan, “Wide-field computational imaging of pathology slides using lens-free on-chip microscopy,” *Science translational medicine*, vol. 6, no. 267, 267ra175–267ra175, 2014.
- [35] M. Roy, D. Seo, C.-H. Oh, M.-H. Nam, Y. J. Kim, and S. Seo, “Low-cost telemedicine device performing cell and particle size measurement based on lens-free shadow imaging technology,” *Biosensors and Bioelectronics*, vol. 67, pp. 715–723, 2015.
- [36] A. Shanmugam and C. D. Salthouse, “Lensless fluorescence imaging with height calculation,” *Journal of Biomedical Optics*, vol. 19, no. 1, p. 016 002, 2014.
- [37] M. Roy, D. Seo, S. Oh, J.-W. Yang, and S. Seo, “A review of recent progress in lens-free imaging and sensing,” *Biosensors and Bioelectronics*, vol. 88, pp. 130–143, 2017.
- [38] W. Bishara, T.-W. Su, A. F. Coskun, and A. Ozcan, “Lensfree on-chip microscopy over a wide field-of-view using pixel super-resolution,” *Optics express*, vol. 18, no. 11, pp. 11 181–11 191, 2010.
- [39] W. Bishara, U. Sikora, O. Mudanyali, T.-W. Su, O. Yaglidere, S. Luckhart, and A. Ozcan, “Holographic pixel super-resolution in portable lensless on-chip microscopy using a fiber-optic array,” *Lab on a Chip*, vol. 11, no. 7, pp. 1276–1279, 2011.
- [40] G. Zheng, S. A. Lee, Y. Antebi, M. B. Elowitz, and C. Yang, “The epetri dish, an on-chip cell imaging platform based on subpixel perspective sweeping microscopy (spsm),” *Proceedings of the National Academy of Sciences*, vol. 108, no. 41, pp. 16 889–16 894, 2011.
- [41] A. C. Sobieranski, F. Inci, H. C. Tekin, M. Yuksekkaya, E. Comunello, D. Cobra, A. Von Wangenheim, and U. Demirci, “Portable lensless wide-field microscopy imaging platform based on digital inline holography and multi-frame pixel super-resolution,” *Light: Science & Applications*, vol. 4, no. 10, e346, 2015.
- [42] C. S. Williams and O. A. Becklund, *Introduction to the optical transfer function*. SPIE Press, 2002, vol. 112.

- [43] H.-C. Shih, T.-A. Lee, H.-M. Wu, P.-L. Ko, W.-H. Liao, and Y.-C. Tung, “Microfluidic collective cell migration assay for study of endothelial cell proliferation and migration under combinations of oxygen gradients, tensions, and drug treatments,” *Scientific reports*, vol. 9, no. 1, pp. 1–10, 2019.
- [44] R. Rusconi, M. Garren, and R. Stocker, “Microfluidics expanding the frontiers of microbial ecology,” *Annual review of biophysics*, vol. 43, pp. 65–91, 2014.
- [45] M. Binz, A. P. Lee, C. Edwards, and D. V. Nicolau, “Motility of bacteria in microfluidic structures,” *Microelectronic Engineering*, vol. 87, no. 5-8, pp. 810–813, 2010.
- [46] J. Taktikos, H. Stark, and V. Zaburdaev, “How the motility pattern of bacteria affects their dispersal and chemotaxis,” *PloS one*, vol. 8, no. 12, e81936, 2013.
- [47] H. C. Berg, *Random walks in biology*. Princeton University Press, 1993.
- [48] G. Saxena, R. N. Bharagava, G. Kaithwas, and A. Raj, “Microbial indicators, pathogens and methods for their monitoring in water environment,” *Journal of water and health*, vol. 13, no. 2, pp. 319–339, 2015.
- [49] D. V. Nicolau, M. Lard, T. Korten, F. C. van Delft, M. Persson, E. Bengtsson, A. Månsson, S. Diez, and H. Linke, “Parallel computation with molecular-motor-propelled agents in nanofabricated networks,” *Proceedings of the National Academy of Sciences*, vol. 113, no. 10, pp. 2591–2596, 2016.
- [50] A. Tero, S. Takagi, T. Saigusa, K. Ito, D. P. Bebbler, M. D. Fricker, K. Yumiki, R. Kobayashi, and T. Nakagaki, “Rules for biologically inspired adaptive network design,” *Science*, vol. 327, no. 5964, pp. 439–442, 2010.
- [51] G. Du, Q. Fang, and J. M. den Toonder, “Microfluidics for cell-based high throughput screening platforms—a review,” *Analytica chimica acta*, vol. 903, pp. 36–50, 2016.
- [52] L. Eamer, R. Nosrati, M. Vollmer, A. Zini, and D. Sinton, “Microfluidic assessment of swimming media for motility-based sperm selection,” *Biomicrofluidics*, vol. 9, no. 4, p. 044 113, 2015.
- [53] F. C. Van Delft, G. Ipolitti, D. V. Nicolau Jr, A. Sudalayadum Perumal, O. Kašpar, S. Kheireddine, S. Wachsmann-Hogiu, and D. V. Nicolau, “Something has to give: Scaling combinatorial computing by biological agents exploring physical networks encoding np-complete problems,” *Interface focus*, vol. 8, no. 6, p. 20 180 034, 2018.
- [54] D. N. Breslauer, R. N. Maamari, N. A. Switz, W. A. Lam, and D. A. Fletcher, “Mobile phone based clinical microscopy for global health applications,” *PloS one*, vol. 4, no. 7, e6320, 2009.

- [55] S. A. Sekula-Gibbs and M. A. Shearer, “Sentinel node biopsy should be offered in thin melanoma with mitotic rate greater than one,” *Dermatologic Surgery*, vol. 37, no. 8, pp. 1080–1088, 2011.
- [56] G. McConnell, J. Trägårdh, R. Amor, J. Dempster, E. Reid, and W. B. Amos, “A novel optical microscope for imaging large embryos and tissue volumes with sub-cellular resolution throughout,” *Elife*, vol. 5, e18659, 2016.
- [57] Z. Liu and P. J. Keller, “Emerging imaging and genomic tools for developmental systems biology,” *Developmental cell*, vol. 36, no. 6, pp. 597–610, 2016.
- [58] S. Pacheco, C. Wang, M. K. Chawla, M. Nguyen, B. K. Baggett, U. Utzinger, C. A. Barnes, and R. Liang, “High resolution, high speed, long working distance, large field of view confocal fluorescence microscope,” *Scientific reports*, vol. 7, no. 1, p. 13 349, 2017.
- [59] F. Legesse, O. Chernavskaiia, S. Heuke, T. Bocklitz, T. Meyer, J. Popp, and R. Heintzmann, “Seamless stitching of tile scan microscope images,” *Journal of microscopy*, vol. 258, no. 3, pp. 223–232, 2015.
- [60] Q. Lu, G. Liu, C. Xiao, C. Hu, S. Zhang, R. X. Xu, K. Chu, Q. Xu, and Z. J. Smith, “A modular, open-source, slide-scanning microscope for diagnostic applications in resource-constrained settings,” *PloS one*, vol. 13, no. 3, e0194063, 2018.
- [61] Z. Göröcs, Y. Ling, M. Dai Yu, D. Karahalios, K. Mogharabi, K. Lu, Q. Wei, and A. Ozcan, “Giga-pixel fluorescent imaging over an ultra-large field-of-view using a flatbed scanner,” *Lab on a Chip*, vol. 13, no. 22, pp. 4460–4466, 2013.
- [62] Z. Göröcs and A. Ozcan, “Biomedical imaging and sensing using flatbed scanners,” *Lab on a Chip*, vol. 14, no. 17, pp. 3248–3257, 2014.
- [63] X. Ou, G. Zheng, and C. Yang, “0.5 gigapixel microscopy using a flatbed scanner: Erratum,” *Biomedical optics express*, vol. 7, no. 2, p. 646, 2016.
- [64] T. Shimobaba, H. Yamanashi, T. Kakue, M. Oikawa, N. Okada, Y. Endo, R. Hirayama, N. Masuda, and T. Ito, “In-line digital holographic microscopy using a consumer scanner,” *Scientific reports*, vol. 3, p. 2664, 2013.
- [65] C. Zhang and K. S. Suslick, “A colorimetric sensor array for organics in water,” *Journal of the American Chemical Society*, vol. 127, no. 33, pp. 11 548–11 549, 2005.
- [66] G. Zheng, X. Ou, and C. Yang, “0.5 gigapixel microscopy using a flatbed scanner,” *Biomedical optics express*, vol. 5, no. 1, pp. 1–8, 2014.

- [67] K. Sullivan, J. Kloess, C. Qian, D. Bell, A. Hay, Y. P. Lin, and Y. Gu, "High throughput virus plaque quantitation using a flatbed scanner," *Journal of virological methods*, vol. 179, no. 1, pp. 81–89, 2012.
- [68] A. Ozcan and E. McLeod, "Lensless imaging and sensing," *Annual review of biomedical engineering*, vol. 18, pp. 77–102, 2016.
- [69] S. Seo, T.-W. Su, D. K. Tseng, A. Erlinger, and A. Ozcan, "Lensfree holographic imaging for on-chip cytometry and diagnostics," *Lab on a Chip*, vol. 9, no. 6, pp. 777–787, 2009.
- [70] J. C. Contreras-Naranjo, Q. Wei, and A. Ozcan, "Mobile phone-based microscopy, sensing, and diagnostics," *IEEE Journal of Selected Topics in Quantum Electronics*, vol. 22, no. 3, pp. 1–14, 2015.
- [71] Z. J. Smith, K. Chu, A. R. Espenson, M. Rahimzadeh, A. Gryshuk, M. Molinaro, D. M. Dwyre, S. Lane, D. Matthews, and S. Wachsmann-Hogiu, "Cell-phone-based platform for biomedical device development and education applications," *PloS one*, vol. 6, no. 3, e17150, 2011.
- [72] T. Gao, Z. J. Smith, T.-y. Lin, D. Carrade Holt, S. M. Lane, D. L. Matthews, D. M. Dwyre, J. Hood, and S. Wachsmann-Hogiu, "Smart and fast blood counting of trace volumes of body fluids from various mammalian species using a compact, custom-built microscope cytometer," *Analytical chemistry*, vol. 87, no. 23, pp. 11 854–11 862, 2015.
- [73] H. Zhu, O. Yaglidere, T.-W. Su, D. Tseng, and A. Ozcan, "Wide-field fluorescent microscopy on a cell-phone," in *2011 Annual International Conference of the IEEE Engineering in Medicine and Biology Society*, IEEE, 2011, pp. 6801–6804.
- [74] I. I. Bogoch, J. R. Andrews, B. Speich, J. Utzinger, S. M. Ame, S. M. Ali, and J. Keiser, "Mobile phone microscopy for the diagnosis of soil-transmitted helminth infections: A proof-of-concept study," *The American journal of tropical medicine and hygiene*, vol. 88, no. 4, pp. 626–629, 2013.
- [75] C. W. Pirnstill and G. L. Coté, "Malaria diagnosis using a mobile phone polarized microscope," *Scientific reports*, vol. 5, p. 13 368, 2015.
- [76] R. R. Jahan-Tigh, G. M. Chinn, and R. P. Rapini, "A comparative study between smartphone-based microscopy and conventional light microscopy in 1021 dermatopathology specimens," *Archives of pathology & laboratory medicine*, vol. 140, no. 1, pp. 86–90, 2016.

- [77] Q. Wei, R. Nagi, K. Sadeghi, S. Feng, E. Yan, S. J. Ki, R. Caire, D. Tseng, and A. Ozcan, "Detection and spatial mapping of mercury contamination in water samples using a smart-phone," *ACS nano*, vol. 8, no. 2, pp. 1121–1129, 2014.
- [78] T. San Park, W. Li, K. E. McCracken, and J.-Y. Yoon, "Smartphone quantifies salmonella from paper microfluidics," *Lab on a Chip*, vol. 13, no. 24, pp. 4832–4840, 2013.
- [79] A. Chen, R. Wang, C. R. Bever, S. Xing, B. D. Hammock, and T. Pan, "Smartphone-interfaced lab-on-a-chip devices for field-deployable enzyme-linked immunosorbent assay," *Biomicrofluidics*, vol. 8, no. 6, p. 064 101, 2014.
- [80] G. Zheng, C. Kolner, and C. Yang, "Microscopy refocusing and dark-field imaging by using a simple led array," *Optics letters*, vol. 36, no. 20, pp. 3987–3989, 2011.
- [81] Z. Liu, L. Tian, S. Liu, and L. Waller, "Real-time brightfield, darkfield, and phase contrast imaging in a light-emitting diode array microscope," *Journal of biomedical optics*, vol. 19, no. 10, p. 106 002, 2014.
- [82] N. Lue, W. Choi, G. Popescu, T. Ikeda, R. R. Dasari, K. Badizadegan, and M. S. Feld, "Quantitative phase imaging of live cells using fast fourier phase microscopy," *Applied Optics*, vol. 46, no. 10, pp. 1836–1842, 2007.
- [83] S. Dong, R. Shiradkar, P. Nanda, and G. Zheng, "Spectral multiplexing and coherent-state decomposition in fourier ptychographic imaging," *Biomedical optics express*, vol. 5, no. 6, pp. 1757–1767, 2014.
- [84] S. Dong, Z. Bian, R. Shiradkar, and G. Zheng, "Sparsely sampled fourier ptychography," *Optics express*, vol. 22, no. 5, pp. 5455–5464, 2014.
- [85] L. Tian, X. Li, K. Ramchandran, and L. Waller, "Multiplexed coded illumination for fourier ptychography with an led array microscope," *Biomedical optics express*, vol. 5, no. 7, pp. 2376–2389, 2014.
- [86] G. Zheng, R. Horstmeyer, and C. Yang, "Wide-field, high-resolution fourier ptychographic microscopy," *Nature photonics*, vol. 7, no. 9, p. 739, 2013.
- [87] L. Tian and L. Waller, "Quantitative differential phase contrast imaging in an led array microscope," *Optics express*, vol. 23, no. 9, pp. 11 394–11 403, 2015.
- [88] D. V. Nicolau, M. Lard, T. Korten, F. C. van Delft, M. Persson, E. Bengtsson, A. Månsson, S. Diez, and H. Linke, "Parallel computation with molecular-motor-propelled agents in nanofabricated networks," *Proceedings of the National Academy of Sciences*, vol. 113, no. 10, pp. 2591–2596, 2016.

- [89] M. H. Longair, D. A. Baker, and J. D. Armstrong, “Simple neurite tracer: Open source software for reconstruction, visualization and analysis of neuronal processes,” *Bioinformatics*, vol. 27, no. 17, pp. 2453–2454, 2011.
- [90] T. Ogawa, E. Shoji, N. J. Suematsu, H. Nishimori, S. Izumi, A. Awazu, and M. Iima, “The flux of euglena gracilis cells depends on the gradient of light intensity,” *PloS one*, vol. 11, no. 12, e0168114, 2016.
- [91] J. E. Corry, G. D. Curtis, and R. M. Baird, *Handbook of culture media for food and water microbiology*. Royal Society of Chemistry, 2011.
- [92] L. Shen, J. A. Hagen, and I. Papautsky, “Point-of-care colorimetric detection with a smartphone,” *Lab on a Chip*, vol. 12, no. 21, pp. 4240–4243, 2012.
- [93] F. Zernike, “Phase contrast, a new method for the microscopic observation of transparent objects,” *Physica*, vol. 9, no. 7, pp. 686–698, 1942.
- [94] D. Hamilton and C. Sheppard, “Differential phase contrast in scanning optical microscopy,” *Journal of microscopy*, vol. 133, no. 1, pp. 27–39, 1984.
- [95] R. Allen and G. David, “The zeiss-nomarski differential interference equipment for transmitted-light microscopy,” *Zeitschrift für wissenschaftliche Mikroskopie und mikroskopische Technik*, vol. 69, no. 4, pp. 193–221, 1969.
- [96] R. Hoffman and L. Gross, “Modulation contrast microscope,” *Applied Optics*, vol. 14, no. 5, pp. 1169–1176, 1975.
- [97] L. Kastl, M. Isbach, D. Dirksen, J. Schnekenburger, and B. Kemper, “Quantitative phase imaging for cell culture quality control,” *Cytometry Part A*, vol. 91, no. 5, pp. 470–481, 2017.
- [98] P. Gleyzes, A. Boccara, and H. Saint-Jalmes, “Multichannel nomarski microscope with polarization modulation: Performance and applications,” *Optics letters*, vol. 22, no. 20, pp. 1529–1531, 1997.
- [99] A. Barty, K. Nugent, D. Paganin, and A. Roberts, “Quantitative optical phase microscopy,” *Optics Letters*, vol. 23, no. 11, pp. 817–819, 1998.
- [100] G. Popescu, T. Ikeda, R. R. Dasari, and M. S. Feld, “Diffraction phase microscopy for quantifying cell structure and dynamics,” *Optics letters*, vol. 31, no. 6, pp. 775–777, 2006.
- [101] Z. Wang, L. Millet, M. Mir, H. Ding, S. Unarunotai, J. Rogers, M. U. Gillette, and G. Popescu, “Spatial light interference microscopy (slim),” *Optics express*, vol. 19, no. 2, pp. 1016–1026, 2011.

- [102] L. Miccio, A. Finizio, R. Puglisi, D. Balduzzi, A. Galli, and P. Ferraro, “Dynamic DIC by digital holography microscopy for enhancing phase-contrast visualization,” *Biomedical optics express*, vol. 2, no. 2, pp. 331–344, 2011.
- [103] T. Yao, R. Cao, W. Xiao, F. Pan, and X. Li, “An optical study of drug resistance detection in endometrial cancer cells by dynamic and quantitative phase imaging,” *Journal of biophotonics*, e201800443, 2019.
- [104] M. Takabayashi, H. Majeed, A. Kajdacsy-Balla, and G. Popescu, “Disorder strength measured by quantitative phase imaging as intrinsic cancer marker in fixed tissue biopsies,” *PloS one*, vol. 13, no. 3, e0194320, 2018.
- [105] O. Tolde, A. Gandalovičová, A. Křížová, P. Veselý, R. Chmelík, D. Rosel, and J. Brábek, “Quantitative phase imaging unravels new insight into dynamics of mesenchymal and amoeboid cancer cell invasion,” *Scientific reports*, vol. 8, no. 1, pp. 1–13, 2018.
- [106] W. J. Eldridge, Z. A. Steelman, B. Loomis, and A. Wax, “Optical phase measurements of disorder strength link microstructure to cell stiffness,” *Biophysical journal*, vol. 112, no. 4, pp. 692–702, 2017.
- [107] J. Jung, L. E. Matemba, K. Lee, P. E. Kazyoba, J. Yoon, J. J. Massaga, K. Kim, D.-J. Kim, and Y. Park, “Optical characterization of red blood cells from individuals with sickle cell trait and disease in tanzania using quantitative phase imaging,” *Scientific reports*, vol. 6, p. 31 698, 2016.
- [108] H. V. Pham, B. Bhaduri, K. Tangella, C. Best-Popescu, and G. Popescu, “Real time blood testing using quantitative phase imaging,” *PloS one*, vol. 8, no. 2, e55676, 2013.
- [109] Y. Park, C. A. Best, T. Auth, N. S. Gov, S. A. Safran, G. Popescu, S. Suresh, and M. S. Feld, “Metabolic remodeling of the human red blood cell membrane,” *Proceedings of the National Academy of Sciences*, vol. 107, no. 4, pp. 1289–1294, 2010.
- [110] H. S. Park, M. T. Rinehart, K. A. Walzer, J.-T. A. Chi, and A. Wax, “Automated detection of *p. falciparum* using machine learning algorithms with quantitative phase images of unstained cells,” *PloS one*, vol. 11, no. 9, e0163045, 2016.
- [111] Y. Park, M. Diez-Silva, G. Popescu, G. Lykotrafitis, W. Choi, M. S. Feld, and S. Suresh, “Refractive index maps and membrane dynamics of human red blood cells parasitized by *plasmodium falciparum*,” *Proceedings of the National Academy of Sciences*, vol. 105, no. 37, pp. 13 730–13 735, 2008.
- [112] Z. Yang and Q. Zhan, “Single-shot smartphone-based quantitative phase imaging using a distorted grating,” *PloS one*, vol. 11, no. 7, e0159596, 2016.

- [113] X. Meng, H. Huang, K. Yan, X. Tian, W. Yu, H. Cui, Y. Kong, L. Xue, C. Liu, and S. Wang, “Smartphone based hand-held quantitative phase microscope using the transport of intensity equation method,” *Lab on a Chip*, vol. 17, no. 1, pp. 104–109, 2017.
- [114] I. Hernández-Neuta, F. Neumann, J. Brightmeyer, T. Ba Tis, N. Madaboosi, Q. Wei, A. Ozcan, and M. Nilsson, “Smartphone-based clinical diagnostics: Towards democratization of evidence-based health care,” *Journal of internal medicine*, vol. 285, no. 1, pp. 19–39, 2019.
- [115] V. Bianco, B. Mandracchia, V. Marchesano, V. Pagliarulo, F. Olivieri, S. Coppola, M. Paturzo, and P. Ferraro, “Endowing a plain fluidic chip with micro-optics: A holographic microscope slide,” *Light: Science & Applications*, vol. 6, no. 9, e17055, 2017.
- [116] K. Guo, Z. Bian, S. Dong, P. Nanda, Y. M. Wang, and G. Zheng, “Microscopy illumination engineering using a low-cost liquid crystal display,” *Biomedical optics express*, vol. 6, no. 2, pp. 574–579, 2015.
- [117] Y. Ogasawara, R. Sugimoto, R. Maruyama, H. Arimoto, Y. Tamada, and W. Watanabe, “Mobile-phone-based rheinberg microscope with a light-emitting diode array,” *Journal of biomedical optics*, vol. 24, no. 3, p. 031 007, 2018.
- [118] L. Tian and L. Waller, “3d intensity and phase imaging from light field measurements in an led array microscope,” *optica*, vol. 2, no. 2, pp. 104–111, 2015.
- [119] Z. F. Phillips, M. V. D’Ambrosio, L. Tian, J. J. Rulison, H. S. Patel, N. Sadras, A. V. Gande, N. A. Switz, D. A. Fletcher, and L. Waller, “Multi-contrast imaging and digital refocusing on a mobile microscope with a domed led array,” *PloS one*, vol. 10, no. 5, e0124938, 2015.
- [120] D. Jung, J.-H. Choi, S. Kim, S. Ryu, W. Lee, J.-S. Lee, and C. Joo, “Smartphone-based multi-contrast microscope using color-multiplexed illumination,” *Scientific reports*, vol. 7, no. 1, p. 7564, 2017.
- [121] Y. Rivenson, H. Ceylan Koydemir, H. Wang, Z. Wei, Z. Ren, H. Günaydın, Y. Zhang, Z. Gorocs, K. Liang, D. Tseng, *et al.*, “Deep learning enhanced mobile-phone microscopy,” *ACS Photonics*, vol. 5, no. 6, pp. 2354–2364, 2018.
- [122] S. Kheireddine, A. S. Perumal, Z. J. Smith, D. V. Nicolau, and S. Wachsmann-Hogiu, “Dual-phone illumination-imaging system for high resolution and large field of view multi-modal microscopy,” *Lab on a Chip*, vol. 19, no. 5, pp. 825–836, 2019.

- [123] S. B. Mehta and C. J. Sheppard, “Quantitative phase-gradient imaging at high resolution with asymmetric illumination-based differential phase contrast,” *Optics letters*, vol. 34, no. 13, pp. 1924–1926, 2009.
- [124] E. C. Nieminski, F. Schaefer, and J. E. Ongerth, “Comparison of two methods for detection of giardia cysts and cryptosporidium oocysts in water.,” *Appl. Environ. Microbiol.*, vol. 61, no. 5, pp. 1714–1719, 1995.
- [125] Z. J. Smith, T. Gao, K. Chu, S. M. Lane, D. L. Matthews, D. M. Dwyre, J. Hood, K. Tatsukawa, L. Heifetz, and S. Wachsmann-Hogiu, “Single-step preparation and image-based counting of minute volumes of human blood,” *Lab on a Chip*, vol. 14, no. 16, pp. 3029–3036, 2014.
- [126] S. Kheireddine, Z. J. Smith, D. V. Nicolau, and S. Wachsmann-Hogiu, “Simple adaptive mobile phone screen illumination for dual phone differential phase contrast (dpdpc) microscopy,” *Biomedical optics express*, vol. 10, no. 9, pp. 4369–4380, 2019.
- [127] R. Barer, “Interference microscopy and mass determination,” *Nature*, vol. 169, no. 4296, pp. 366–367, 1952.
- [128] D. Roitshtain, L. Wolbromsky, E. Bal, H. Greenspan, L. L. Satterwhite, and N. T. Shaked, “Quantitative phase microscopy spatial signatures of cancer cells,” *Cytometry Part A*, vol. 91, no. 5, pp. 482–493, 2017.
- [129] Y. Park, C. Depeursinge, and G. Popescu, “Quantitative phase imaging in biomedicine,” *Nature Photonics*, vol. 12, no. 10, pp. 578–589, 2018.
- [130] M. Imanbekova, A. S. Perumal, S. Kheireddine, D. V. Nicolau, and S. Wachsmann-Hogiu, “Lensless, reflection-based dark-field microscopy (rdfm) on a cmos chip,” *Biomedical Optics Express*, vol. 11, no. 9, pp. 4942–4959, 2020.
- [131] W. Ding, Y. Wang, H. Chen, and S. Y. Chou, “Plasmonic nanocavity organic light-emitting diode with significantly enhanced light extraction, contrast, viewing angle, brightness, and low-glare,” *Advanced Functional Materials*, vol. 24, no. 40, pp. 6329–6339, 2014.

# Appendix A

## Addendum to chapter 2 following thesis review

In this section, I will make some clarifications regarding the operation, performance, and limitations of the dual-phone illumination-imaging system. In order to align the camera with the illumination screen, we first determine the center of the imaging system field-of-view, which corresponds to the central region of the imaging mobile phone screen, via establishing the midpoints along the length and width of the screen. We then move the illumination screen using an XYZ-translation stage and visually align the displayed illumination pattern to the predetermined central region of the imaging screen.

For further accuracy, one could instead project a calibration image onto the illumination screen, where the image would be the Fourier transform of the original illumination pattern, and visually align it with the center of the field-of-view. To ensure repeatability and robustness, instead of performing this alignment every time before using the system, one could build an apparatus to permanently hold the illumination-imaging phones in the correct alignment position, which would have the added advantage of minimizing disturbances to the system alignment during microscope operation.

Misalignment of the illumination and imaging systems can certainly result in image non-uniformities. However, concerning the detectable non-uniformities within the shown images, more specifically as can be observed in Fig. 2.3(c) and (d), and Fig. 2.7(a), these artefacts manifest themselves primarily due to field curvature aberrations brought about by the external lens attached to the camera, which lead to vignetting or light fall-off effects close to the image edges, resulting in non-uniform intensities throughout the image. This can be rectified by using a higher quality external lens or lens assembly, as well as performing flat-field correction on the resulting images, as is described in sections 1.1.2.4 and 1.1.5.

Apart from imaging system optics, illumination plays a substantial role in image quality,

as is explained in detail in chapter 1. Phone screen illumination simplifies the generation of classical illumination patterns and allows for virtually endless creative possibilities, where the small screen pixel size and tight pixel packing enables finer control of pattern design, such that shapes can be drawn with higher accuracy and uniformity, which is particularly important for patterns that include curves and vertices. However, compared to conventional light-emitting diode (LED) illuminators, phone screen illumination suffers from some limitations. The LEDs (pixels) comprising the phone screen are typically smaller than those of LED arrays, which results in lower light intensity per pixel. On the other hand, the aforementioned tight pixel packing on the screen offers more LEDs per unit area, which could counteract the reduced individual LED intensity, but this is naturally dependent on the used illumination pattern, and as such the number of pixels it constitutes.

Moreover, the use of colour-specific LEDs allows LED illuminators to provide a narrower spectrum per wavelength. In the case of mobile phone screen displays, the backlight typically consists of white LEDs which are then filtered to generate different colours, thus resulting in broader, less precise spectra. For applications where specific wavelengths are required for illumination, this could be critical. Overall, despite offering higher colour fidelity, traditional LED arrays have larger LEDs that are relatively widely spaced apart compared to phone displays, and thus provide lower pattern control and precision. As such, the choice of illumination platform is application-dependent. Lastly, whereas at face value it may seem that using a mobile phone for illumination is more expensive than using an LED array, when one factors in the fact that an LED array is not a standalone device, and needs to be controlled using a microcontroller such as an Arduino Uno, which in turn requires programming via a computer, the price no longer plays a significant role, and the phone screen compactness and utility are highlighted.

# Appendix B

## Addendum to chapter 3 following thesis review

In this section, I will highlight certain aspects of differential phase contrast (DPC) image reconstruction, as well as emphasize the advantages of using the dual-phone illumination-imaging system for DPC microscopy. In principle, asymmetric illumination creates an illumination intensity gradient along the sample, which in turn underscores the phase gradients due to differences in the refractive index within different parts of the sample. These phase gradients translate into asymmetry in the Fourier space of the image, which corresponds to intensity differences in real space. By taking the normalized difference of phase images obtained with complementary asymmetric illumination patterns, one can generate a DPC image.

As shown in 3.6.2, each DPC image was generated along one of two axes of asymmetry - namely, the horizontal, and the vertical, whereby asymmetrical illumination was provided via complementary left-right, and top-bottom semicircular patterns, respectively. A semi-circular illumination pattern is optimal, because in conventional microscopes, asymmetrical illumination is typically produced using a physical barrier that covers half the condenser diaphragm, such as a half stop, or by aligning the filament image such that it covers exactly half the condenser diaphragm. In the case of the dual-phone illumination imaging system, a circle in the center of the illumination phone screen is visually aligned to the center of the field-of-view of the imaging phone, and then semicircles are displayed along the same central axis of the calibration circle.

Whereas complementary asymmetric illumination images along a single axis are sufficient to produce a DPC image, any spatial frequencies that lie along the axis of asymmetry cancel out during the subsequent image computation, resulting in apparent phase artefacts in the reconstructed image, as can be observed in Fig. 3.3. These aberrations in the single-axis

DPC image could be improved via image deconvolution; however, to eliminate them, multi-axis DPC images should be generated instead. To achieve this, complementary asymmetric illumination images should be captured along multiple axes, and phone screen illumination allows for simple design of and switching between these patterns.

In general, as the number of axes used for DPC image generation increases, fidelity of phase reconstruction in the final image increases, but so does image computational complexity. Moreover, since the phase accuracy only increases marginally with the number of axes beyond a certain point, one must weigh the cost of increased data acquisition, longer imaging times, and demanding mathematical image reconstruction against the benefit of added DPC image accuracy, and find a suitable trade-off for the application at hand. In the seminal paper by Tian and Waller [87], 2-axis DPC was found to be an acceptable compromise.

In addition to simplifying illumination, the dual-phone illumination-imaging system reduces the complexity of phase contrast image generation by eliminating the need for additional bulky, and expensive optics, such as condenser annuli, phase rings, and beam splitters. Moreover, through employing asymmetrical illumination as a means for DPC image generation, this microscope potentially allows for quantitative phase imaging (QPI). However, the system would need to be made more robust, and a stable phase reference would need to be used for accurate extraction of quantitative phase information via deconvolution of DPC images.